The Journal of Gemmology

Volume 26 No. 8 October 1999

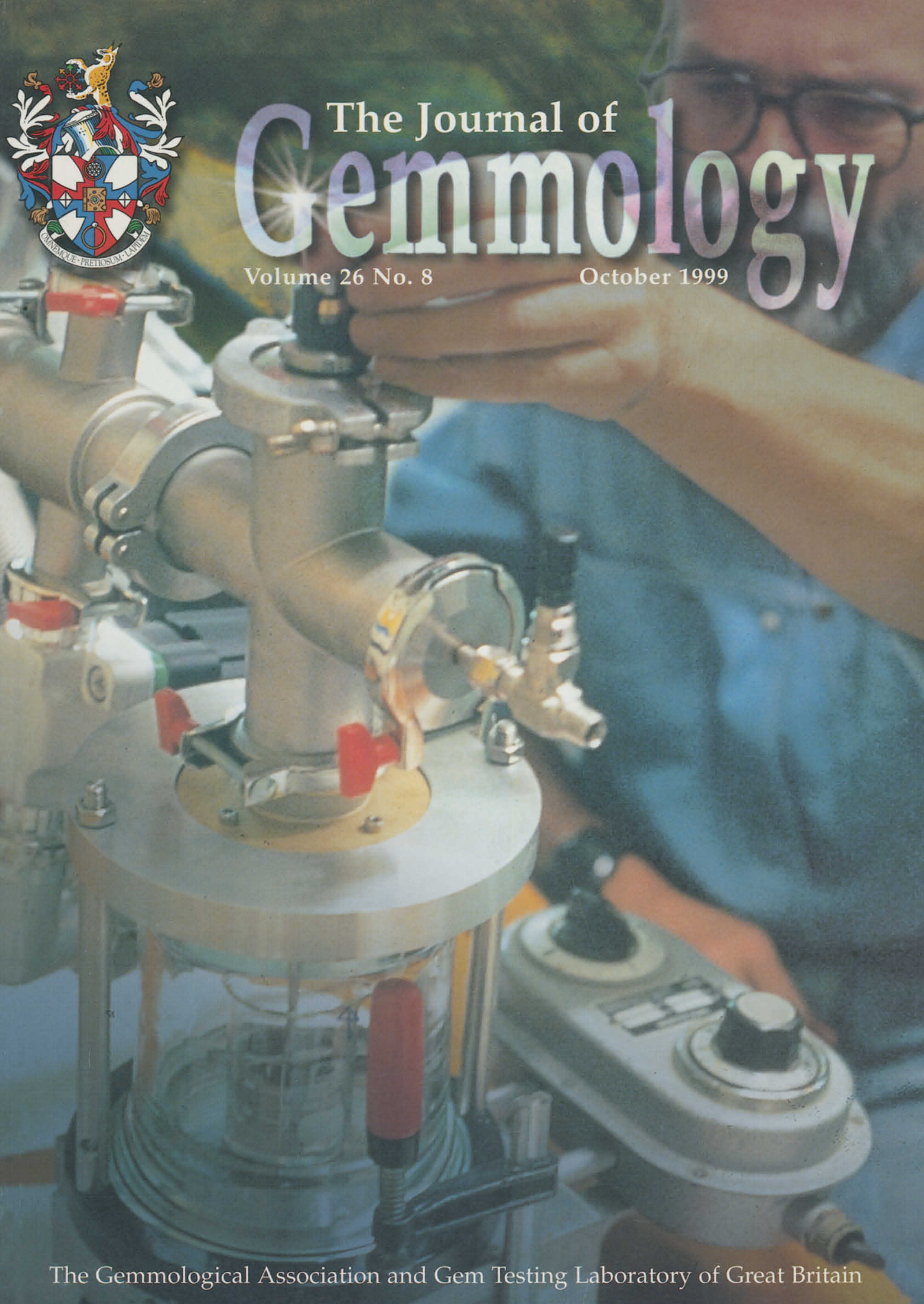

The Gemmological Association and Gem Testing Laboratory of Great Britain

Gemmological Association and Gem Testing Laboratory of Great Britain

27 Greville Street, London EC1N 8TN
Tel: 020 7404 3334 Fax: 020 7404 8843
e-mail: gagtl@btinternet.com Website: www.gagtl.ac.uk/gagtl

President:
Professor R.A. Howie

Vice-Presidents:
E.M. Bruton, A.E. Farn, D.G. Kent, R.K. Mitchell

Honorary Fellows:
Chen Zhonghui, R.A. Howie, R.T. Liddicoat Jnr, K. Nassau

Honorary Life Members:
H. Bank, D.J. Callaghan, E.A. Jobbins, H. Tillander

Council of Management:
T.J. Davidson, N.W. Deeks, R.R. Harding, I. Mercer, J. Monnickendam,
M.J. O'Donoghue, E. Stern, I. Thomson, V.P. Watson

Members' Council:
A.J. Allnutt, P. Dwyer-Hickey, S.A. Everitt, A.G. Good, J. Greatwood,
B. Jackson, L. Music, J.B. Nelson, P.G. Read, R. Shepherd, P.J. Wates, C.H. Winter

Branch Chairmen:
Midlands – G.M. Green, North West – I. Knight, Scottish – B. Jackson

Examiners:
A.J. Allnutt, M.Sc., Ph.D., FGA, L. Bartlett, B.Sc., M.Phil., FGA, DGA,
E.M. Bruton, FGA, DGA, S. Coelho, B.Sc., FGA, DGA, Prof. A.T. Collins, B.Sc., Ph.D,
A.G. Good, FGA, DGA, J. Greatwood, FGA, G.M. Howe, FGA, DGA,
B. Jackson, FGA, DGA, G.H. Jones, B.Sc., Ph.D., FGA, M. Newton, B.Sc., D.Phil.,
C.J.E. Oldershaw, B.Sc. (Hons), FGA, H.L. Plumb, B.Sc., FGA, DGA,
R.D. Ross, B.Sc., FGA, DGA, P.A. Sadler, B.Sc., FGA, DGA,
E. Stern, FGA, DGA, S.M. Stocklmayer, B.Sc. (Hons), FGA, Prof. I. Sunagawa, D.Sc.,
M. Tilley, GG, FGA, C.M. Woodward, B.Sc., FGA, DGA

The Journal of Gemmology
Editor: Dr R.R. Harding
Assistant Editors: M.J. O'Donoghue, P.G. Read
Associate Editors: Dr C.E.S. Arps (Leiden),
G. Bosshart (Zurich), Prof. A.T. Collins (London), Dr J.W. Harris (Glasgow),
Prof. R.A. Howie (Derbyshire), Dr J.M. Ogden (Cambridge),
Prof. A.H. Rankin (Kingston upon Thames), Dr J.E. Shigley (Carlsbad),
Prof. D.C. Smith (Paris), E. Stern (London), S.M. Stocklmayer (Perth),
Prof. I. Sunagawa (Tokyo), Dr M. Superchi (Milan), C.M. Woodward (London)
Production Editor: M.A. Burland

Vol 26, No. 8, October 1999 ISSN: 1355-4565

Synthetic red beryl from Russia

Ulrich Henn[1] and Claudio C. Milisenda[2]

1. *German Gemmological Association (DGemG), Idar-Oberstein, Germany*
2. *German Foundation for Gemstone Research (DSEF), Idar-Oberstein, Germany*

ABSTRACT: The present study is a result of an examination of synthetic red beryls recently produced in Russia. The standard gemmological properties correspond to the known range for synthetic beryls of Russian production. Chemical analyses showed distinct cobalt contents in addition to iron and manganese. Divalent cobalt dominates the absorption spectra and is responsible for the red colour. The low Na_2O concentrations are typical for synthetic beryls produced hydrothermally. An overall low alkali content can also be concluded from the IR spectra which showed a predominance of H_2O-type I, i.e. water molecules not bound to alkali ions. Inhomogeneous growth structure formed a typical inclusion pattern.

Keywords: synthetic red beryl, hydrothermal growth, Russian production, physico-chemical properties, internal characteristics

Introduction

Commercial quantities of synthetic emeralds have been available since the 1930s and it was in the 1960s when large amounts of that material entered the trade. Although it is well known that in Japan and particularly in Russia various other synthetic beryl varieties had been produced, these specimens did not gain commercial importance, firstly because natural beryls are present in quite large amounts and in very good qualities, and secondly, except for synthetic emeralds, the price differences between synthetic beryls and their natural counterparts is too low.

During the development of the growth of synthetic emeralds a number of colouring agents have been used for research purposes which have resulted in a number of synthetic beryl varieties.

Emel'yanova *et al.* (1965) first mentioned synthetic beryls which were doped with vanadium, manganese, cobalt and nickel. A few samples of synthetic pink beryls were first observed in the trade in 1981 (Bank & Becker, 1981). In the same year Dillon (1981) mentioned synthetic pink to reddish beryls produced by Regency Created Emeralds Co. in the USA. Since 1979 various synthetic beryls including green, reddish, pale blue, pink and violet varieties have been produced in Japan by Adachi New Industrial Ltd. of Osaka (Chikayama and Miyata, 1987; Scarratt, 1987; Chikayama, 1992) which are known under the trade name 'ANICS'. These specimens have been produced by chemical vapour deposition, i.e. crystallization from a vapour phase. As a speciality this Japanese company also produced bicoloured, 'watermelon' type synthetic beryls which consist of a synthetic pinkish beryl core and a synthetic emerald overgrowth (Koivula and Misiorowski, 1986).

Both Solntsev *et al.* (1978) and Ilyin *et al.* (1980) reported on synthetic beryl varieties

ISSN: 1355–4565

***Table I:** Gemmological properties of synthetic beryl*

	Refractive index				*Fluorescence*	
Synthetic beryl source and colour	n_e	n_o	Δn	*Specific gravity*	*UVL (long wave)*	*UVS (short wave)*
ANICS (Japan)						
reddish	1.563	1.566	0.003	2.66	weak red-violet	dull red
violet	1.563	1.567	0.004	2.65	red-violet	strong violet
pale blue	1.566	1.571	0.005	2.67	milky green-blue	violet
'watermelon'	1.562	1.566	0.004	2.64	core: red rim: violet	core: inert rim: violet
Biron (Australia)						
pinkish	1.571	1.578	0.007	2.69	orange-pink	
Novosibirsk (Russia)						
pinkish	1.570	1.576	0.006	2.67	weak violet	
orangy-red	1.574	1.580	0.006	2.69		
blue (Cu)	1.570	1.576	0.006	2.69	violet	
blue (Fe)	1.571	1.579	0.008	2.68		
	1.575	1.583	0.008	2.69*		
green (V)	1.570	1.578	0.008	2.69		
Russia, this study						
red	1.570–72	1.578–80	0.008	2.63–65	inert	inert

* data after Schmetzer (1989). All other data obtained by the authors.

including cobalt-bearing synthetic red beryls manufactured in Novosibirsk, Russia. Various facetable synthetic beryls produced in Russia were mentioned by Koivula and Kammerling (1988) and include purple (coloured by chromium and manganese), pinkish (manganese), blue (copper) and orangy-red (cobalt) varieties. The production technique is analogous to that used to grow hydrothermal synthetic emeralds in Novosibirsk. However, the resulting crystals were only a few centimetres long and relatively flat so that only small stones could be cut. The synthetic crystals weighed between 11 and 25 ct. In contrast the same producer grew synthetic emeralds that weighed on average between 50 and 100 ct, sometimes even more. Blue synthetic aquamarines from Russia coloured by iron like the natural specimens were described by Schmetzer (1990). In addition, other synthetic beryl varieties of Russian production were briefly mentioned by Koivula and Kammerling (1991) and Koivula *et al.* (1992).

Pinkish synthetic beryls are also produced in Australia by Biron International Ltd., which are well known as a major producer of hydrothermally grown synthetic emeralds. The synthetic rough is coloured by trivalent titanium and allows the faceting of stones with a weight up to 20 ct (Brown, 1993). Overall, the occurrence of faceted non-green synthetic beryls is rare.

Recently, the German Gemmological Association received from one of its fellows both rough and cut synthetic red beryls which were produced in Russia. The faceted round stones measure 6.5 x 5 mm and weigh between 0.98 and 1.08 ct (*Figure 1*). The colour is reminiscent of the natural red beryls from Utah, USA (see Henn and Becker, 1995).

The physico-chemical properties and the microscopic characteristics of the samples investigated are given below.

Standard gemmological properties

The refractive indices, maximum birefringences and specific gravity are given in *Table I* and the measured values were: $n_e = 1.570 - 1.572$, $n_o = 1.578 - 1.580$ with $\Delta_n = 0.008$ and $SG = 2.63 - 2.65$. Except for SG, these data are within the known range for hydrothermally grown synthetic beryls from Russia which are also shown in *Table I* for comparison, along with data obtained on a number of synthetic beryls produced in Japan and Australia. The recent red beryls show strong pleochroism with cinnamon-brown and violet colours and they are inert to both long- and short-wave UV radiation.

Figure 1: *Two faceted synthetic red beryls produced in Russia each weighing approximately 1 ct.*

Spectroscopic analysis

The UV/VIS absorption spectrum is plotted in *Figure 2*, and the absorption maxima and their assignments are given in *Table II*. The spectrum of the ordinary ray (o) is characterized by absorption maxima in the green and blue and that of the extraordinary ray (e) by absorption in the yellow-green and blue. The broad absorption in the green and yellow-green part of the polarized spectra is responsible for the red colour of the samples.

Figure 2: *Polarized absorption spectra of a representative sample of synthetic red beryl of Russian production.*

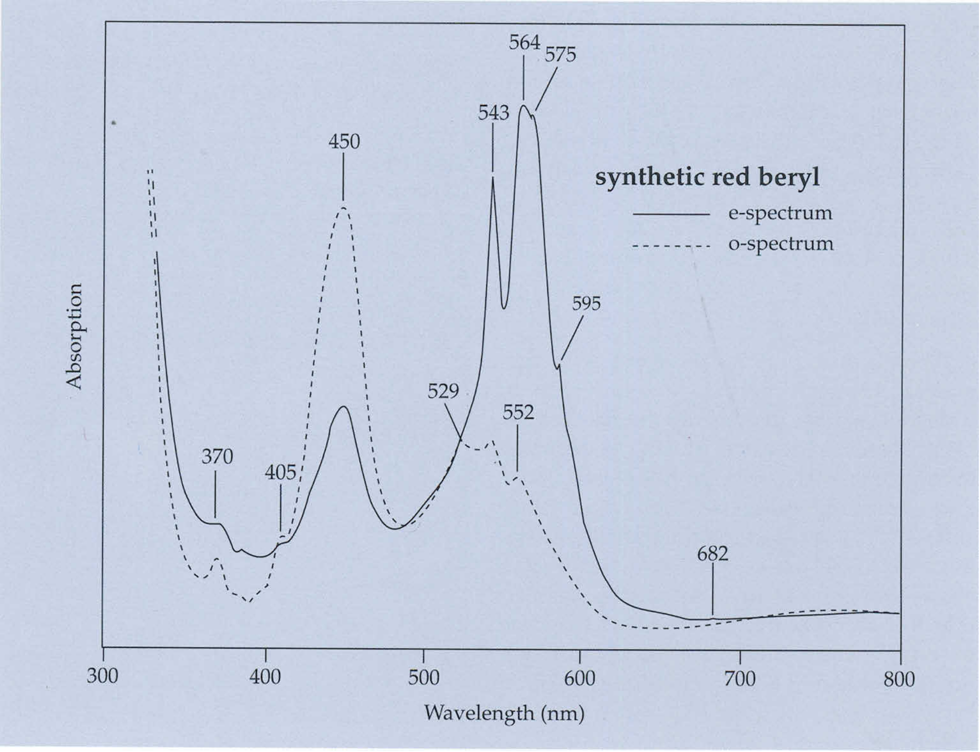

***Table II:** UV/VIS absorption maxima and assignments*

Absorption maxima (nm)	*(cm^{-1})*	*Assignment*	*Polarization o = ordinary ray e = extraordinary ray*
370	27000	Fe^{3+}	e < o
405	24700	Fe^{3+}	e ≈ o
450	22200	Co^{2+}, Co^{3+}	e < o
529	18900	Co^{2+}	o
543	18400	Co^{2+}	e > o
552	18100	Co^{2+}	o
564	17700	Co^{2+}	e
575	17400	Co^{2+}	e
595	16800	Co^{2+}	e
682	14600	Cr^{3+}	e

In both cases this absorption is a combination of several maxima. In the o-spectrum the maxima occur at 552, 543 and 529 nm and are caused by Co^{2+} (Solntsev *et al.*, 1978; Ilyin *et al.*, 1980; Platonov, pers. comm., 1999). This trace element also produces the absorption maxima at 595, 575, 564 and 543 nm in the e-spectrum. The non-pleochroic broad absorption in the blue with a maximum at 450 nm is also attributed to Co^{2+} and possibly Co^{3+} (Platonov, pers. comm., 1999). Two additional absorption maxima at 370 and 405 nm in the ultraviolet and violet part of the spectrum are caused by trivalent iron. A weak chromium (Cr^{3+}) absorption line at 682 nm is visible in the e-spectrum.

The IR spectrum is consistent with the general pattern found in low alkali hydrothermally grown synthetic beryls (Schmetzer and Kiefert, 1990). The samples tested showed H_2O-vibrations between 3500 and 4000 cm^{-1} and between 5000 and 5600 cm^{-1}. The most distinct maxima are those at 3694 and 3592 cm^{-1}, with the absorption band at 3694 cm^{-1} being stronger than that at 3592 cm^{-1}. The former is assigned to type-I water molecules which are not bound to adjacent alkali ions and the weaker band is caused by type-II water molecules which are bound to alkali ions.

Chemical analysis

The chemical composition of a representative sample was obtained by electron microprobe analysis and is given in *Table III*. Aluminium and silicon oxides form the major components. Beryllium oxide cannot be measured with the electron microprobe. The analyses revealed iron, cobalt and manganese as the most significant trace constituents and this is consistent with conclusions drawn from the absorption spectra. The low Na_2O-content of 0.06 wt.% and even lower K_2O content confirm the conclusion drawn from the IR-spectrum that the synthetic red beryl is a low alkali type.

Microscopic features

Under an immersion microscope the faceted samples showed a step-like growth structure. A distinct inhomogeneous growth in the form of irregularly changing subgrain boundaries is visible almost perpendicular to the step-like growth (*Figures 3 to 5*). These growth characteristics are also typically found in Russian hydrothermally grown synthetic emeralds (cf. Henn *et al.*, 1988; Schmetzer, 1988). Planar and veil-like feathers consisting of liquid and two-phase inclusions form

***Table III:** Electron microprobe analysis of a Russian synthetic red beryl*

wt.%	*Range (7 analyses)*	*mean*
SiO_2	65.55–66.77	66.08
TiO_2	0.03–0.08	0.05
Al_2O_3	16.75–17.38	16.96
Cr_2O_3	0.00–0.03	0.02
FeO	1.45–1.73	1.62
MnO	0.15–0.21	0.18
CoO	0.17–0.47	0.31
MgO	0.02–0.05	0.03
Na_2O	0.00–0.14	0.06
K_2O	0.00–0.03	0.01
Total		85.32

NB: BeO and H_2O not determined

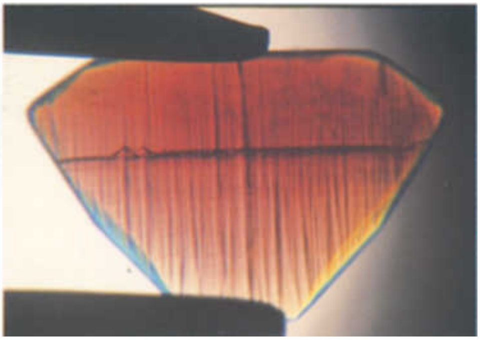

Figure 3: Faceted synthetic red beryl. Step-like growth structure parallel to the table and inhomogeneous growth almost perpendicular to the table. Immersion, magnified 6x.

inclusion patterns also typical of such emeralds, and black platelets (*Figure 6*) may well be hematite (cf. Schmetzer, 1990).

Conclusions

The standard gemmological properties and the microscopic characteristics of synthetic red beryls of recent Russian production correspond to the known properties for hydrothermally grown synthetic beryls manufactured in Russia. The absorption spectra of the synthetic red beryl showed that the colour is caused by divalent cobalt. Based on the IR-spectra the samples can be classified as hydrothermally grown low alkali-type synthetic beryls. The spectroscopic characteristics are confirmed by chemical analyses which show significant amounts of cobalt and manganese oxides and low sodium concentrations.

Figure 4: Subgrain boundaries, variably oriented in detail, almost perpendicular to the step-like growth structure. Immersion, magnified 30x.

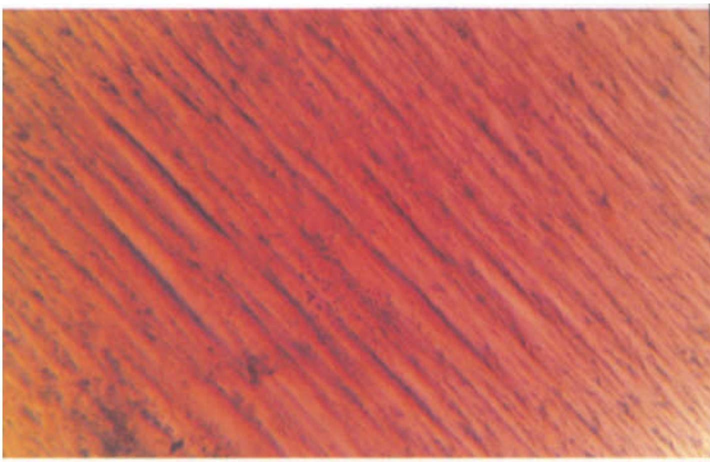

Figure 5: A distinct inhomogeneous growth in the form of irregularly oriented subgrain boundaries is one of the most diagnostic identification features of Russian synthetic red beryls. Immersion, magnified 40x.

As with synthetic emeralds hydrothermally grown in Russia, inhomogeneous growth patterns in synthetic red beryls are diagnostic in distinguishing them from natural red beryls.

Figure 6: Feathers with liquid and two-phase inclusions and hexagonal black platelets also form a typical inclusion pattern. Immersion, magnified 30x.

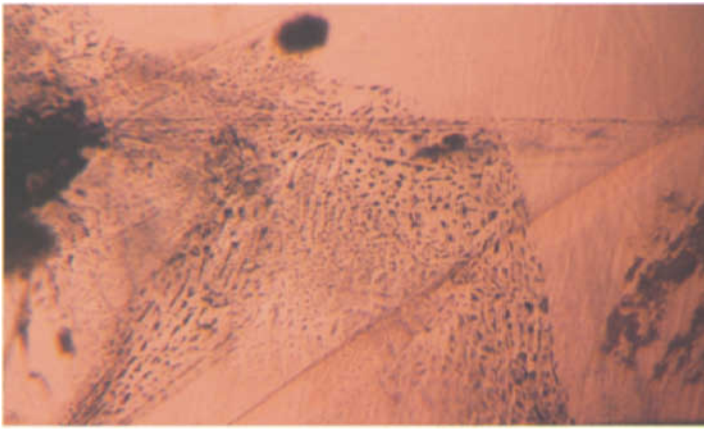

References

Bank, H., and Becker, G., 1981. Synthetischer rosafarbener Beryll. *Z. Dt. Gemmol. Ges.*, **30**, 112–13

Brown, G., 1993. Australian titaniferous synthetic beryl. *J. Gemmol. Ass. Hong Kong*, **16**, 5–6

Chikayama, A., 1992. Japanese synthetic stones by various methods. Z. Dt. Gemmol. Ges., 41, 145–6

Chikayama, A., and Miyata, T., 1987. Synthetic gemstones from Japan. *Transactions of the XXI International Gemmological Conference*, Brazil 1987

Dillon, S., 1981. Gem news: synthetic red beryl. *Gems & Gemology*, **17**, 57

Emel'yanova, E.N., Grum-Grzhimailo, S.V., Boksha, O.N., Varina, T.M., 1965. Artificial beryl containing V, Mn, Co and Ni. *Sov. Phys.-Cryst.*, **10**, 46–9

Henn, U., Lind, Th., and Bank, H., 1988. Hydrothermally grown synthetic emeralds from USSR. *Can. Gemmol.*, **9**, 66–72

Henn, U., and Becker, G., 1995. Rote Berylle aus Utah, USA. Neue Beobachtungen. *Z. Dt. Gemmol. Ges.*, **44**, 55–60

Ilyin, A.G., Klyakhin, V.A., Pavluchenko, V.S., and Chepurnova, G.A., 1980. Physical properties of monocrystals of some beryl varieties grown in hydrothermal conditions. *The growing of the beryllium minerals' crystals and study of their properties.* Novosibirsk, 3–10 (in Russian)

Koivula, J.I., and Misiorowski, E., 1986. Gem news: synthetic 'watermelon' beryl. *Gems & Gemology*, **22**, 55

Koivula, J.I., and Kammerling, R.C., 1988. Gem news: unusual synthetic beryls from the Soviet Union. *Gems & Gemology*, **24**, 252

Koivula, J.I., and Kammerling, R.C., 1991. Gem news: more Soviet synthetics. *Gems & Gemology*, **27**, 55

Koivula, J.I., Kammerling, R.C., and Fritsch, E.,1992. Gem news: more on hydrothermal synthetic beryls. *Gems & Gemology*, **28**, 63–4

Scarratt, K., 1987. Notes from the laboratory – 12: ANICS, synthetically grown beryl. *J. Gemm.*, **21**, 135

Schmetzer, K., 1988. Characterization of Russian hydrothermally-grown synthetic emeralds. *J. Gemm.*, **21**, 145–64

Schmetzer, K., 1990. Hydrothermally grown synthetic aquamarine manufactured in Novosibirsk, USSR. *Gems & Gemology*, **26**, 206–11

Schmetzer, K., and Kiefert, L., 1990. Water in beryl – a contribution to the separability of natural and synthetic emeralds by infrared spectroscopy. *J. Gemm.*, **22**, 215–23

Solntsev, V.P., Kharchenko, E.J., Bukin, G.V., Klyakhin, V.A., Lebedev, A.S., Lokhova, G.G., and Ripinen, D.J., 1978. A study of isomorphic substitutions in natural and synthetic beryls. *Investigations on experimental mineralogy.* Novosibirsk, 39–53 (in Russian)

Multicomponent inclusions in Nacken synthetic emeralds

Dr Karl Schmetzer[1], Dr Lore Kiefert[2] and Dr Heinz-Jürgen Bernhardt[3]

1. Marbacher Strasse 22b, D-85238 Petershausen, Germany
2. SSEF Swiss Gemmological Institute, Falknerstr. 9, CH-4001 Basel, Switzerland
3. Institut für Mineralogie, Ruhr-Universität, D-44780 Bochum, Germany

ABSTRACT: Multicomponent inclusions in Nacken synthetic emeralds were examined by a combination of microscopy, electron microprobe analysis and micro-Raman spectroscopy. The tiny crystals at the widest ends of nailhead spicules are most probably beryl. Various forms of cavities contain single component and multicomponent fillings, which were determined as a solidified melt consisting of the ingredients of beryl and residues of a molybdenum- and vanadium-bearing flux. The residual slightly inhomogeneous melt trapped in elongated cavities is partly unmixed and contains polymerized and non-polymerized molybdates as well as Si–O–Si networks and isolated SiO_4 tetrahedra. Similar inclusions in Chatham synthetic emeralds are also characterized.

Keywords: Chatham, crystal growth, electron microprobe analyses, multi-component inclusions, Nacken, nailhead spicules, Raman spectra, synthetic emerald

Introduction

Nacken synthetic emeralds were grown in the 1920s by Professor R. Nacken of Frankfurt, Germany, and were regarded as hydrothermally grown synthetic emeralds for almost half a century (Van Praagh, 1946, 1947; Webster, 1955, 1958; Eppler, 1958; Espig, 1962; Landais, 1971; see also Schmetzer and Kiefert, 1998). This view was also confirmed by the examination with modern analytical techniques such as infrared spectroscopy which revealed the presence of characteristic water absorption bands of hydrothermally-grown synthetic emeralds (Landais, 1971). A detailed study by Nassau (1976, 1978, 1980), however, showed that two different types of Nacken synthetic emeralds were grown, both by the flux method. The first type of crystal contained irregularly shaped seeds of natural, colourless beryl, and the second type was grown without natural seeds.

The examination of both types of Nacken synthetic emerald by Nassau (1976, 1978, 1980) revealed the presence of water absorption bands in the spectra of the first type samples, which are caused by the water content of the natural beryl seed. In contrast, infrared spectra of samples of the second type of Nacken synthetic emeralds showed an absorption spectrum without any water related absorption bands, which is typical for flux-grown synthetic emeralds. These results are also useful to understand the earlier examinations by Landais (1971) using infrared spectroscopy, who, most probably, investigated samples of the first type with a natural beryl seed (Landais, 1998).

ISSN: 1355–4565

Chemical investigations by Nassau (1978, 1980) proved that the flux used by Nacken was a molybdenum- and vanadium-bearing compound, most probably a lithium-containing oxide of a general formula MoO_3–V_2O_5–Li_2O, whose exact composition is still unknown. The X-ray fluorescence spectrum of characteristic inclusions was examined in the scanning electron microscope (SEM-EDXRF). With this technique, however, the presence of light elements such as lithium and beryllium cannot be determined. The experimental conditions applied by Nassau (1978, 1980) allowed the examination of the material trapped within various cavities alone, i.e. the X-ray fluorescence spectra represented only substances trapped in cavities without any contributions of the synthetic emerald host to the X-ray fluorescence patterns obtained (Nassau, 1998).

Two types of patterns were described consisting of the characteristic X-ray lines of (a) an Al–Si–V–Mo-bearing compound and (b) an Al–Si–V–Cr–Mo-bearing compound.

These results indicate that the material trapped within the cavities consists of a mixture of the components of beryl (BeO, Al_2O_3, SiO_2) with different percentages of chromium and of components of the flux (most probably MoO_3, V_2O_5, Li_2O). The material in the cavities was assumed to be in the vitreous state (Nassau, 1978, 1980, 1998).

Occasionally, inclusions that form elongated spicules with a tiny crystal at their widest ends are present in Nacken synthetic emeralds. These tiny crystals were described as phenakite by Nassau (1978), which is not consistent with the description of Eppler (1958), who assumed tiny beryl crystals being present as nailheads in Nacken synthetic emeralds. Both determinations, however, were based on visual appearance only and not on direct analytical measurements.

Tiny crystals at the base of nailhead spicules are common in hydrothermal synthetic emeralds, but may also form in flux-grown synthetic emerald when growth is started on a seed plate inclined at an angle to the *c*-axis (Flanigen *et al.*, 1967). In hydrothermal synthetic emeralds, these tiny crystals at the widest ends of elongated spicules were regarded exclusively as phenakite crystals for a long time. It was proven by micro-Raman spectroscopy, however, that not only phenakite but beryl and chrysoberyl crystals could also be present at the ends of elongated spicules in hydrothermal synthetic emerald from different producers (Schmetzer *et al.*, 1997). Continuing the study of nailhead spicules in synthetic emeralds, the authors have tried to determine experimentally the identity of the nailhead crystals present in these typical inclusions of Nacken synthetic emeralds and

Figure 1a,b: *Nacken synthetic emerald crystals with natural seeds (a) and without natural seeds (b). The largest crystals of both types measure about 5.5 x 4 mm (photos: M. Glas).*

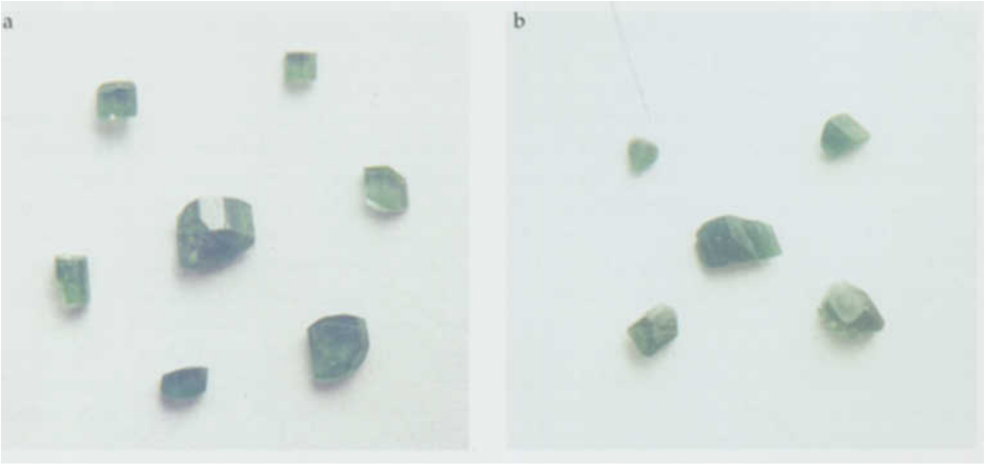

to evaluate the discrepancy between the papers of Eppler (1958) and Nassau (1978). In addition, the identification of various substances present in the cavities of Nacken synthetic emeralds has been attempted.

Materials and methods

The present study is based on the examination of 14 individual samples (*Figures 1a, b*) ranging from 5.5 to 2 mm in size. The synthetic emeralds originated from the following collections: E. Gübelin, Lucerne, Switzerland (5); F.H. Pough, Reno, Nevada, USA (8); M. Schaeffer, Detmold, Germany (1).

For assessing the study of Eppler (1958), Nacken synthetic emeralds of the Gübelin collection have been available. The papers of Nassau (1976, 1978, 1980) were based on samples of the Pough collection and on synthetic emeralds from the British Museum (Natural History), London. The present authors tried to obtain the Nacken synthetic emeralds kept in the British Museum for comparison, but these samples were not made available.

For the examination of chemical properties of the substances trapped in elongated spicules and/or channels parallel to the *c*-axis, one sample without a microscopically visible colourless seed was sawn into two parts along the *c*-axis and subsequently polished down step by step. In some of these steps several elongated cavities were carefully opened and the inclusions exposed to the surface were examined by electron microprobe.

To determine the compositions of nailhead crystals at the widest ends of elongated spicules as well as individual components or phases trapped in different cavities of Nacken synthetic emeralds, numerous inclusions in both types of samples (with and without colourless seeds) were examained by micro-Raman spectroscopy. This technique, which is useful for the determination of inclusions in natural and synthetic emeralds (Schmetzer *et al.*, 1997; Schmetzer and Kiefert, 1998; Zwaan and Burke, 1998), is also a very sensitive tool for determining the substances present in artificially filled fissures of natural emeralds (Hänni *et al.*, 1997). Micro-Raman spectroscopy has been used by Delé-Dubois *et al.* (1986) as well as Delé-Dubois and Poirot (1989) for the determination of residual substances in synthetic emeralds. In these papers, the materials trapped in various cavities of flux-grown synthetic emeralds were determined as polymolybdates and molybdenum oxides.

Figure 2: *Prismatic crystal of Nacken synthetic emerald which contains a colourless, natural irregularly-shaped seed; the* c*-axis runs vertically, melt filled channels and spicules are oriented parallel to* c. *Immersion, length of crystal 2 mm.*

Microscopic properties

The microscopic examination confirmed the results of Nassau (1976, 1978, 1980), who classified the 19 synthetic emeralds available for his study into two groups with and without natural seeds.

In our 14 samples, colourless, natural irregularly shaped seeds were observed in eight synthetic emeralds (*Figures 2 and 3*). In two of these crystals, thin, flat cavities oriented on planes parallel to the basal pinacoid were observed (*Figure 3*). These

Figure 3: *Prismatic crystal of Nacken synthetic emerald which contains a colourless, natural irregularly shaped seed; the c-axis runs vertically, melt filled channels and spicules are oriented parallel to c, flat cavities with primary liquid and two-phase inclusions are oriented perpendicular to c. Immersion, length of crystal. 3.4 mm.*

cavities contain primary liquid and/or two-phase inclusions, which is a typical microscopic feature for natural beryl or natural emerald from certain localities, e.g. Russian Uralian emeralds (see Schmetzer *et al.*, 1991).

In the remaining six of our Nacken samples, no colourless irregularly shaped seeds were observable by microscopic examination. One larger synthetic emerald crystal of this group was examined by infrared spectroscopy, which showed the absence of water-related absorption bands. Again, these results are consistent with the findings described by Nassau (1978, 1980).

All Nacken synthetic emeralds revealed numerous channels or spicules oriented parallel to the *c*-axis (*Figures 2 and 3*), which are more or less opaque in transmitted light (*Figure 4a*). Nailhead spicules, i.e. elongated spicules with tiny crystals at their widest ends, are common in samples with colourless seeds, but rare in the second group of synthetic emeralds without colourless natural seeds. The tiny birefringent crystals have a refractive index close to that of the host synthetic emerald, so they can be difficult to observe without crossed polarizers (*Figure 4a, b*). In samples with colourless seeds, most of these tiny birefringent crystals were in direct contact with the irregularly shaped surface of the seed. The narrower ends of the spicules always pointed in the direction of growth parallel to the *c*-axis of the synthetic emerald crystals. Occasionally, nailhead spicules were seen on two opposite surfaces of the seed with their tips pointing in opposite directions up and down along the *c*-axis (*Figure 5*).

The material trapped in the channels and spicules appeared inhomogeneous under the microscope. In addition to a shrinking bubble, which was frequently oberved, several yellow, yellowish or whitish, transparent or translucent substances were

Figure 4a, b: *Nailhead spicules in Nacken synthetic emerald: the tiny beryl crystals at the wider ends of the spicules display a low relief in plane polarized light (a), the birefringent crystals are clearly visible with crossed polarizers (b; right), Immersion 100x.*

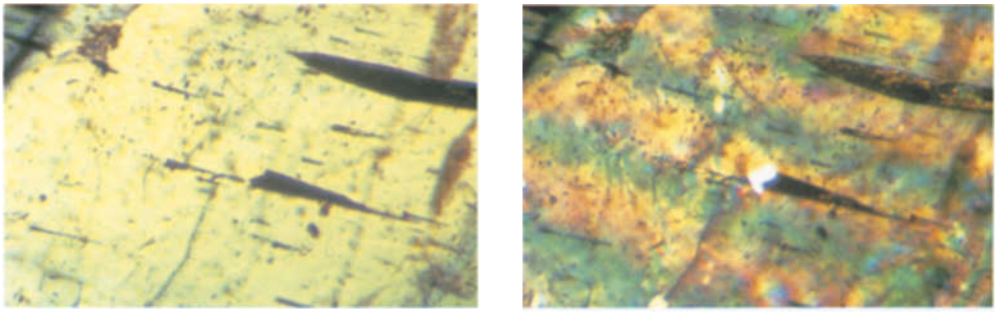

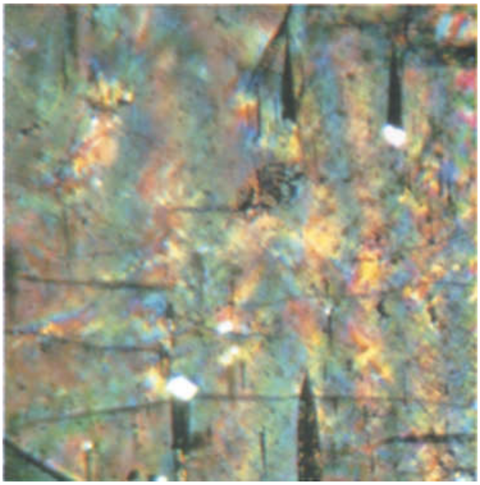

Figure 5: *Nailhead spicules in Nacken synthetic emerald: the* c*-axis runs vertically, the narrower ends of the spicules point towards the directions of growth up and down along the* c*-axis, the tiny beryl crystals at the wider ends of the spicules are in direct contact with two irregularly-shaped surfaces of a colourless beryl seed in the centre of the crystal. Immersion, crossed polarizers. 60x.*

often present (*Figures 6, 7 and 8*). Only in a few cases did a single cavity appear to be homogeneously filled with one single phase or component.

Determination of birefringent crystals at the widest ends of cone-shaped spicules

Numerous nailheads at the widest ends of elongated spicules (*Figures 4, 5 and 6*) in different samples were examined by micro-Raman spectroscopy. In all cases, we obtained Raman spectra of beryl only; no spectra indicating phenakite were recorded. The authors have identified nailhead spicules in hydrothermal synthetic emeralds from various producers (Schmetzer *et al.*, 1997) and have used the same experimental conditions in the present investigation; they are confident that if the spicules had been anything other than beryl they would have been detected by the Raman microprobe. Consequently, the birefringent crystals at the ends of cone-shaped spicules are most

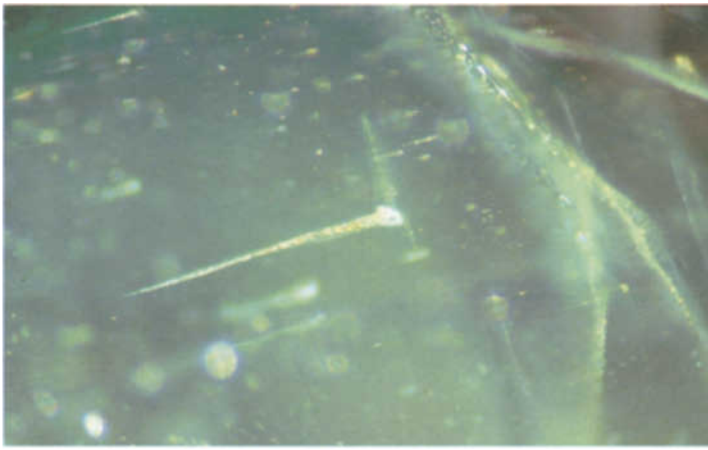

Figure 6: *Nailhead spicule with multicomponent filling in Nacken synthetic emerald. 100x.*

Figure 7: *Elongated spicule with multicomponent filling in Nacken synthetic emerald. 100x.*

Figure 8: *Elongated channel parallel to the* c*-axis with multicomponent filling and shrinking bubble. Renishaw Raman microscope. 200x.*

probably tiny beryl crystals whose orientation is different from that of the host synthetic emerald.

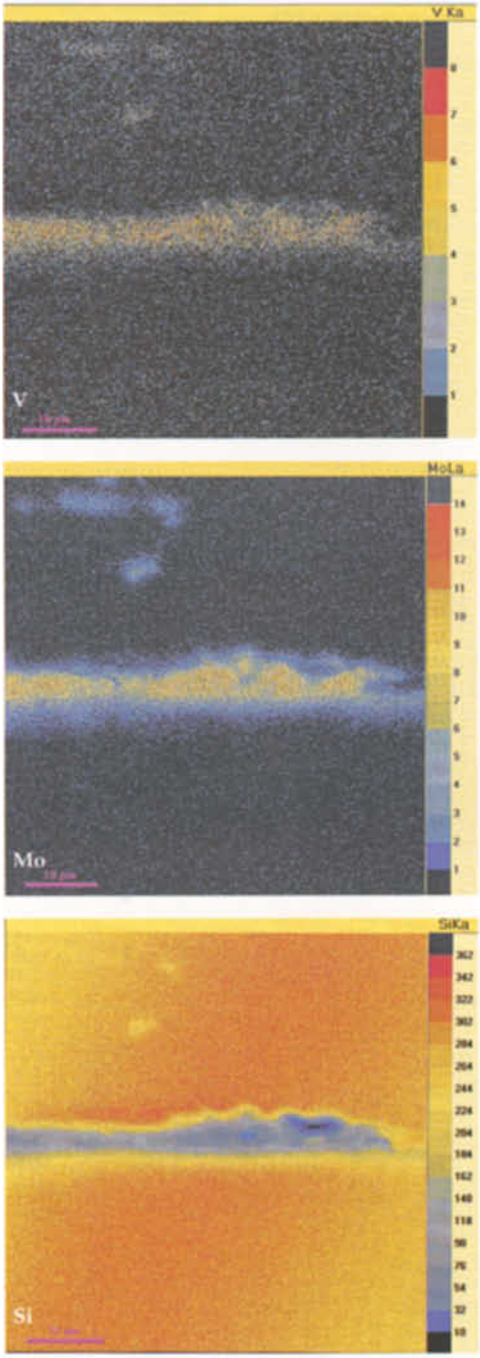

Figure 9a, b, c: *Element distribution maps obtained by electron microprobe analysis showing a slightly inhomogeneous distribution of Si, Mo and V as components of residual melt trapped in a channel parallel to the* c*-axis.*

Examination of multicomponent inclusions in elongated cavities

Microprobe analyses showed that the substances trapped in various cavities (*Figures 6, 7 and 8*) revealed the characteristic X-ray lines of Al, Si, V, Cr and Mo. Consequently, these cavities contain the ingredients of emerald (Al, Si, Cr) and residual quantities of the flux (Mo, V). Furthermore, neither sodium nor potassium was found in the cavities. These chemical data are consistent with the analytical results of Nassau (1978, 1980).

Although element distribution maps for some cavities (*Figure 9a, b and c*) revealed various inhomogeneities, no different phases or distinct phase boundaries between different chemical compounds were seen. No individual areas which consisted only of clearly resolved silicates without components of the flux (molybdenum and vanadium) or which consisted of only molybdenum and/or vanadium without any silicon were observed.

In Nacken synthetic emeralds, several basic types of Raman spectra were obtained from the material trapped in various cavities. No differences were observed relating specifically to sample type. For individual areas of different cavities, similar spectra were observed in some cases, but varying types of spectra were commonly obtained from different areas within one single cavity.

The most simple and frequently measured spectrum consisted of a single Raman line at about 956 cm^{-1} with a shoulder at about 871 cm^{-1} (*Figure 10a*). Other parts of the inclusions gave more complex spectra containing two additional lines at 830 cm^{-1} and in the 425 to 435 cm^{-1} range (*Figure 10b*) and in most cases, a line at about 714 cm^{-1} was also present (*Figure 10c, d and e*). Less commonly, two lines at 894 cm^{-1} and in the 313 to 320 cm^{-1} range were observed.

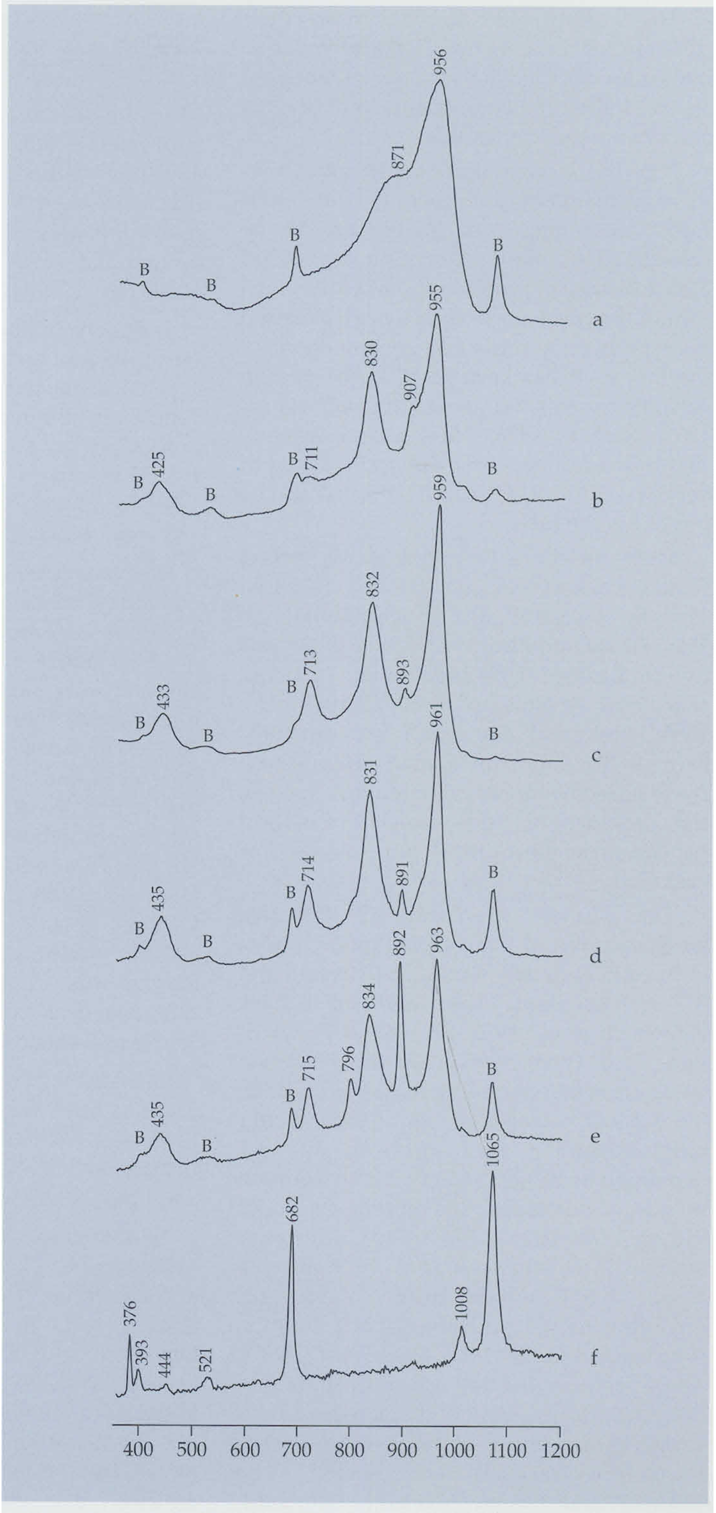

Figure 10: *Typical Raman spectra obtained from multicomponent inclusions in spicules or channels parallel to the c-axis of Nacken synthetic emerald crystals; the inclusions consist of residues of a molybdenum- and vanadium-bearing flux and the ingredients of beryl; in spectra 10a to 10e the positions of Raman lines of the host beryl are indicated by B: 10f is a Raman spectrum of the beryl host alone.*

The variation in Raman lines, their possible overlaps and their relative intensities, indicate that the spectra represent several individual components in cavities in Nacken synthetic emeralds.

For the assignment of Raman lines measured, major amounts of MoO_3 and minor percentages of V_2O_5 have to be considered as components of the flux. It has also to be taken into account that Li_2O, which cannot be measured directly by electron microprobe, could also be a component of the flux as it has been used in the past in solvents for emerald growth (Flanigen *et al.*, 1967; Nassau, 1976; Nassau and Nassau, 1980). In addition, the main components of beryl, i.e. SiO_2, Al_2O_3 and BeO could also be present in the melt.

MoO_3 is characterized by two strong Raman lines at 996 and 826 cm^{-1} (Krasser, 1969; Py *et al.*, 1977; Mohan and Ravikumar, 1984; Hirata and Zhu, 1992) and V_2O_5 reveals two strong lines at 994 and 701 cm^{-1} (Sanchez *et al.*, 1982; Abello *et al.*, 1983; Clauws *et al.*, 1985; Hirata and Zhu, 1992). Consequently, because the dominant Raman lines of both oxide phases were not present in our spectra, the presence of both molybdenum and vanadium in the form of pure oxides was excluded.

The Raman spectrum of the free molybdate ion in aqueous solution consists of three lines at 897 (strong), 837 (weak) and 317 cm^{-1} (medium) (Busey and Keller, 1964; Weinstock *et al.*, 1973; Schwab *et al.*, 1985; Pope and West, 1995). A similar Raman spectrum was reported for a melt of Li_2MoO_4 in K_2MoO_4 (Cape *et al.*, 1976). After polymerization, the spectrum of the heptamolybdate ion ($Mo_7O_{24}^{6-}$) in solution reveals a dominant Raman line at about 940 cm^{-1} (Aveston *et al.*, 1964; Griffith and Lesniak, 1969; Johansson *et al.*, 1979; Schwab *et al.*, 1985), which shifts to 960 cm^{-1} according to the pH-value of the solution (Murtaa and Ikeda, 1983; Ozeki *et al.*, 1987). The spectrum of the octomolybdate ion ($Mo_8O_{26}^{4-}$) in solution is characterized by a strong Raman line at about 960 to 970 cm^{-1}, in solids several lines were observed in the 920 to 970 cm^{-1} range (Aveston *et al.*, 1964; Griffith and Lesniak, 1969; Johansson *et al.*, 1979; Murata and Ikeda, 1983; Ozeki *et al.*, 1987).

In lithium borate molybdate glasses, the strongest Mo-related Raman line is observed at 940 cm^{-1} with a shoulder at about 880 cm^{-1} (Maaß *et al.*, 1993). In lithium phosphate molybdate glasses similar Raman lines were observed at about 940 cm^{-1} with a shoulder at 880 cm^{-1} (Chowdari *et al.*, 1993).

For crystalline lithium molybdates, especially for Li_2MoO_4, no Raman spectrum is available to the present authors from literature data. Only infrared spectra are reported for Li_2MoO_4 (Clark and Doyle, 1966; Spoliti *et al.*, 1981; Kurilenko *et al.*, 1988; Badilescu *et al.*, 1993), for $Li_2Mo_2O_7$ (Goel and Mehrotra, 1985) and for Li_2MoO_3 (Badilescu *et al.*, 1993).

To evaluate a possible presence of lithium molybdate in cavities of Nacken synthetic emeralds, we examined the Raman spectrum of Li_2MoO_4, a compound which is commercially available from ALFA (a Johnson Matthey company), Catalog-No. 48115. The substance was checked by X-ray powder diffraction and revealed a powder diagram consistent with rhombohedral lithium molybdate, Li_2MoO_4 (JCPDS file No. 12-0763) with some weak additional lines. The Raman spectrum of crystalline Li_2MoO_4 consisted of a dominant line at 904 cm^{-1} with some weaker additional Raman lines. Consequently, the presence of rhombohedral Li_2MoO_4 in the cavities of Nacken synthetic emeralds can be excluded.

In addition, it is worth mentioning that no Raman lines of lithium vanadate (see Feigelson *et al.*, 1972; Ghorai and Bhattacharya, 1995; Tang *et al.*, 1995; Zhang and Frech, 1997) were observed.

Silicate glasses that contain large amounts of BeO and Al_2O_3 and especially glasses with a composition close to that of beryl are known (e.g. Riebling and Duke, 1967; Dmitriev and Khan, 1971), but Raman spectra are lacking. Raman spectra of glasses in the silica-alumina system, however, reveal one dominant Raman line at about 430 cm^{-1} (McMillan and Piriou, 1982; Poe *et al.*, 1992), which is also observed in vitreous silica

Chatham flux grown synthetic emeralds

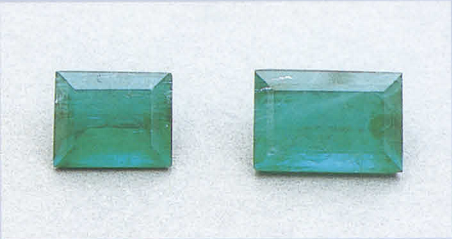

Figure 11: *Two faceted Chatham synthetic emeralds; sizes of the samples 9.1 x 7.3 mm and 11.4 x 7.7 mm (photo: H.A. Hänni).*

During the examination of nailhead spicules in hydrothermal synthetic emeralds (Schmetzer *et al.*, 1997) and Nacken synthetic emeralds (this article), similar inclusions in two Chatham flux grown synthetic emeralds were also observed. These two faceted stones of 3.31 and 2.08 ct (*Figure 11*) from the Gübelin research collection are remarkable because they contain tiny crystals at the ends of elongate spicules without any contact to a special seed plate or to an irregularly shaped core.

Figure 12: *Growth pattern of Chatham synthetic emerald consisting of growth sectors related to the basal pinacoid (right) and to a prism face (left); nailhead spicules occur in the basal growth sector. The c-axis runs vertically, immersion, 50x.*

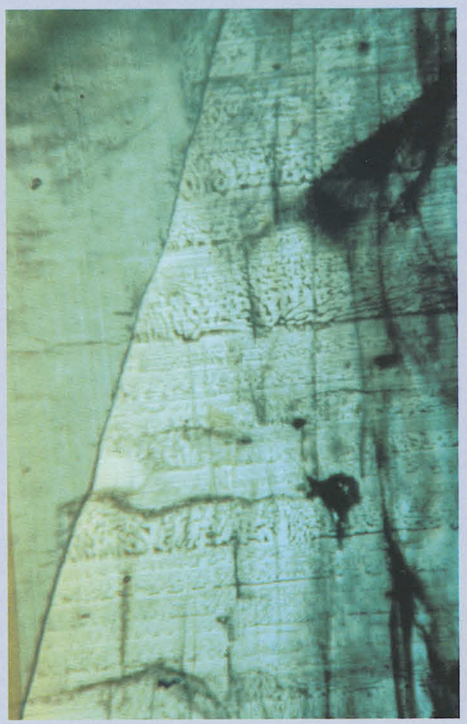

In both synthetic emeralds, the microscopic examination in an immersion liquid revealed a pattern consisting of two distinct growth sectors which are related to the basal pinacoid and to a prism face (*Figure 12*). Numerous nailhead spicules were found as inclusions only in those growth sectors related to the basal pinacoid. The multicomponent inclusions consist of a birefringent tiny crystal at the widest ends of the elongate cone-shaped spicules, and colourless or yellowish, transparent or translucent substances within the cones; the spicules are oriented parallel to the *c*-axis (*Figure 13*).

The examination of numerous birefringent crystals at the widest ends of the spicules by micro-Raman spectroscopy consistently indicated that they were phenakite. The spectra of the material trapped within the cones (*Figure 14*) consisted of several sharp Raman lines with the most intense and dominant lines

Figure 13: *Nailhead spicule with multi-component filling in Chatham synthetic emerald. 50x.*

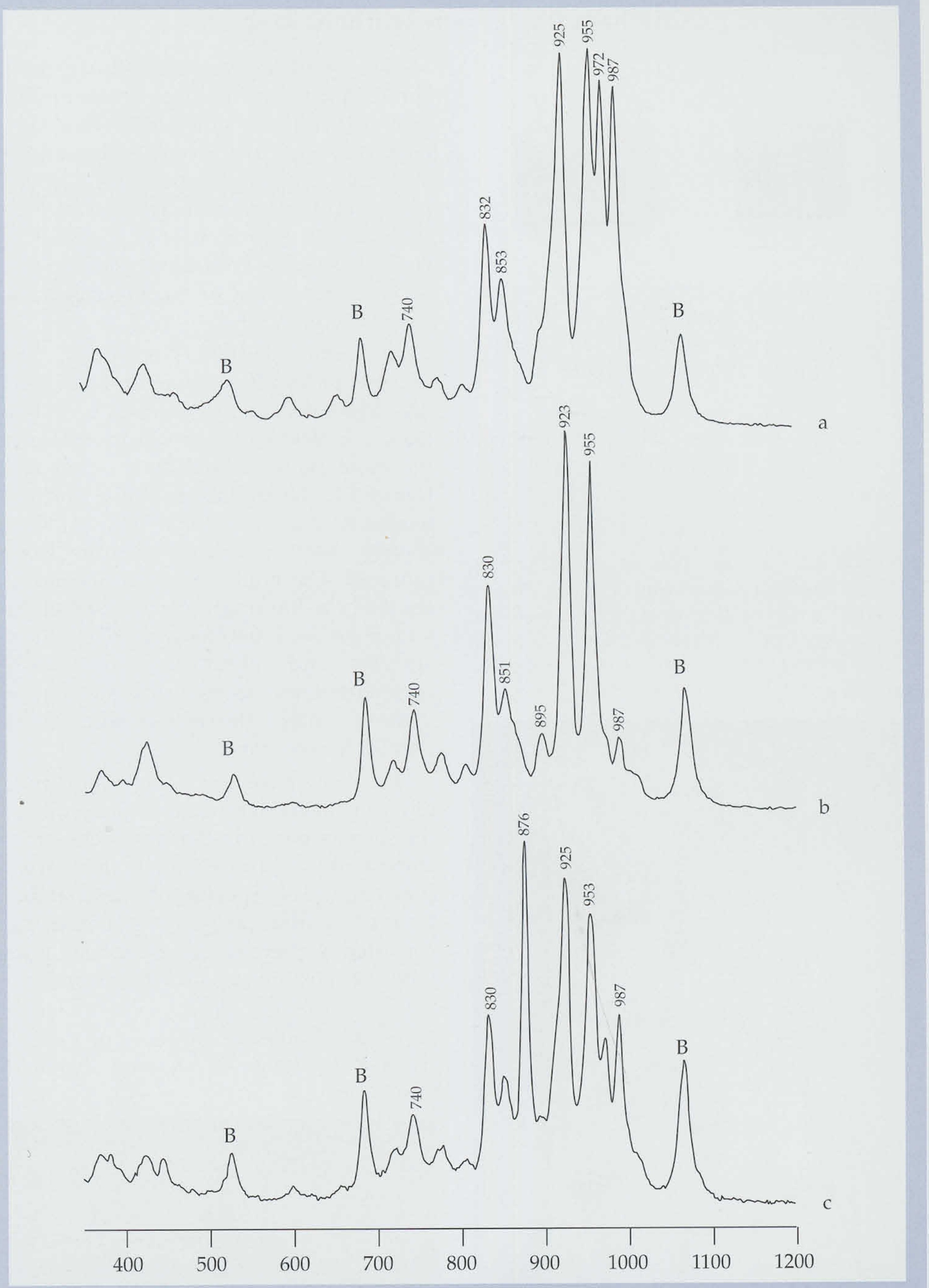

Figure 14: *Typical Raman spectra obtained from multiphase inclusions in spicules parallel to the c-axis of Chatham synthetic emerald crystals; the inclusions comprise residues of a molybdenum-bearing flux and components of beryl; the position of Raman lines of the host beryl is indicated by B, spectrum c shows the dominant Raman line of a phenakite nailhead at 876 cm^{-1}.*

always in the 900 to 1000 cm^{-1} range. In particular, four Raman lines at 925, 957, 972 and 989 cm^{-1} were frequently found in our spectra. Raman lines in the 430 and 830 cm^{-1} range were also present. Due to variable intensities of these dominant lines, probably different substances are trapped in the cone-shaped spicules of the two Chatham synthetic emeralds but some variation could be due to differences in orientation. This confirms conclusions drawn from microscopic examination (*Figure 13*). In both samples, the presence of molybdenum as a residual ingredient of the flux was proven by X-ray fluorescence (EDXRF).

At present, we are unable to present a complete and detailed interpretation of all Raman lines observed. However, comparing our measured Raman lines with literature data (Aveston *et al.*, 1964; Griffith and Lesniak, 1969; Johansson *et al.*, 1979; Kasprzak *et al.*, 1982; Murata and Ikeda, 1983, Schwab *et al.*, 1985; Ozeki *et al.*, 1987), we may conclude that several polymolybdates are present, especially the octomolybdate ion ($Mo_8O_{26}^{4-}$). In addition, the bands in the 830 and 430 cm^{-1} range are assigned to a polymerized network of SiO_4 tetrahedra and to isolated SiO_4 tetrahedra with non-bridging oxygen atoms.

(McMillan *et al.*, 1982; Xu *et al.*, 1989; Poe *et al.*, 1992). This strong Raman line is assigned to a three dimensional, polymerized Si–O–Si network or to six-membered Si–O–Si rings (McMillan *et al.*, 1982; Matson *et al.*, 1983; Xu *et al.*, 1989).

Raman spectra of Li_2O–SiO_2 and Li_2O–Al_2O_3–SiO_2 glasses have been examined by various authors. Glasses with lower Li_2O contents reveal strong Raman lines in the 490, 570, 950 and 1100 cm^{-1} ranges (Sharma and Simons, 1981; Matson *et al.*, 1983; Xu *et al.*, 1989; Fukumi *et al.*, 1990; Mysen, 1990; Mysen and Frantz, 1992); these were not observed in our spectra. Crystalline spodumene has two strong lines at 707 and 356 cm^{-1} (Sharma and Simons, 1981; Dowty, 1987), the 356 cm^{-1} line was not observed in our spectra. In Li_2O–SiO_2 glasses with higher Li_2O contents, however, a strong Raman line at 830 cm^{-1} is characteristic and is assigned to isolated SiO_4^{4-} tetrahedra (Iwamoto *et al.*, 1987; Tatsumisago *et al.*, 1987; Umesaki *et al.*, 1988). In these glasses, the SiO_4 tetrahedra contain non-bridging oxygen atoms. This assignment is confirmed by White and Minser (1984) for sodium silicate glasses.

Raman spectra of amorphous BeO show a strong line at 683 cm^{-1} and one weaker line at 723 cm^{-1} (Walrafen and Samanta, 1979). These two lines were also obtained from crystalline BeO, bromellite (Loh, 1968; Hofmeister *et al.*, 1987). Because the 683 cm^{-1} line is absent from some of our spectra showing a distinct 714 cm^{-1} line (see e.g. *Figure 10c*), an assignment of this line to BeO is rather uncertain.

According to the above data, a possible assignment of our Raman spectra obtained from trapped residual melt in Nacken synthetic emerald is as follows (see again *Figures 10a to f*):

component A, line at 956 cm^{-1} with a shoulder at about 871 cm^{-1} – polymerized polymolybdate, especially heptamolybdate;

component B, lines at 894 and about 317 cm^{-1} – non-polymerized molybdate;

component C, line at 430 cm^{-1} – polymerized Si–O–Si network or ring;

component D, line at 830 cm^{-1} – non-polymerized SiO_4 tetrahedra;

component E, line at 714 cm^{-1} – unknown component of the solidified (Li–Be)–Al–Si–V–Cr–Mo melt.

Most probably, the vanadium content of the residual melt is incorporated in components A to E, as has been already described for various hexamolybdates or molybdovanadophosphates (Kasprzak *et al.*, 1982; Buckley and Clark, 1985).

Consequently, the residual melt trapped in cavities of Nacken synthetic emerald consists of several components, the main ones of which were identified as polymerized and non-polymerized molybdates, Si–O–Si networks and isolated SiO_4 tetrahedra. All components of the solidified melt are in the vitreous state and no crystalline phases have so far been identified. It is interesting to note that similar (Li–V–Mo) – (Be–Al–Si–Cr) – glasses were prepared as intermediate substances for the growth of synthetic emeralds (Kasuga, 1985 a, b, c, d, e). The variation of Raman spectra obtained from different parts of a single inclusion indicates that the melt trapped within such channels and spicules has partly unmixed during the cooling process. Similar observations,. i.e. phase separations in beryl glasses, have also been described by Riebling and Duke (1967).

At present, we are unable to assign the Raman line at 714 cm^{-1} to a specific crystalline or amorphous (vitreous) compound. Additional research is needed, and synthesis experiments should be performed to prepare specific compounds with known chemical compositions until one is found with this feature.

Conclusion

Nailhead spicules in Nacken synthetic emeralds consist of cone-shaped cavities with tiny crystals, most probably beryl, at the widest end and are partially filled with multicomponent inclusions. These inclusions derive from residual melt and consist of vanadium-bearing polymerized polymolybdate and non-polymerized molybdate from vanadium- and molybdenum-bearing fluxes. Additional components of the solidified melt are isolated SiO_4 groups and polymerized aluminous silicates. It has been shown by optical, chemical and spectroscopic means that various cavities in Nacken synthetic emeralds contain single or multicomponent, partly inhomogeneous vitreous fillings. The fillings have partly unmixed during the final stage of emerald growth and subsequent cooling.

Acknowledgements

The authors are grateful to the following for supplying samples used in this study: Professor Dr E. Gübelin of Lucerne, Switzerland, Dr F.H. Pough of Reno, Nevada, USA, and M. Schaeffer of Detmold, Germany. Professor H.A. Hänni of Basel, Switzerland, kindly reviewed the manuscript.

References

Abello, L., Husson, E., Repelin, Y., and Lucazeau, G., 1983. Vibrational spectra and valence force field of crystalline V_2O_5. *Spectrochimica Acta*, **39A**(7), 641–51

Aveston, J., Anacker, E.W., and Johnson, J.S., 1964. Hydrolysis of molybdenum (VI). Ultracentrifugation, acidity measurements, and Raman spectra of polymolybdates. *Inorganic Chemistry*, **3**(5), 735–46

Badilescu, S., Boufker, K., Ashrit, P.V., Girouard, F.E., and Truong, V.-V., 1993. FT-IR/ATR study of lithium intercalation into molybdenum oxide thin film. *Applied Spectroscopy*, **47**(6), 749–52

Buckley, R.I., and Clark, R.J.H., 1985. Structural and electronic properties of some polymolybdates reducible to molybdenum blues. *Coordination Chemistry Reviews*, **65**, 167–218

Busey, R.H., and Keller, O.L., 1964. Structure of the aqueous pertechnetate ion by Raman and infrared spectroscopy. Raman and infrared spectra of crystalline $KTcO_4$, $KReO_4$, Na_2MoO_4, Na_2WO_4, $Na_2MoO_4.2H_2O$, and $Na_2WO_4.2H_2O$. *Journal of Chemical Physics*, **41**(1), 215–25

Cape, T.W., Maroni, V.A., Cunningham, P.T., and Bates, J.B., 1976. Raman and i.r.-emission studies of some tungstate- and molybdate-containing melts. *Spectrochimica Acta*, **32A**(5), 1219–23

Chowdari, B.V.R., Tan, K.L., and Chia, W.T., 1993. Structural and physical characterization of Li_2O:P_2O_5:MO_3 (M = Cr_2, Mo, W) ion conducting glasses. *Materials Research Symposium Proceedings*, **293**, 325–36

Clark, G.M., and Doyle, W.P., 1966. Infra-red spectra of anhydrous molybdates and tungstates. *Spectrochimica Acta*, **22**, 1441–7

Clauws, P., Broeckx, J., and Vennik, J., 1985. Lattice vibrations of V_2O_5. *Physica status solidi (b)*, **131**(2), 459–73

Delé-Dubois, M.-L., and Poirot, J.-P., 1989. Nature des inclusions dans les émeraudes suivant leurs origines. Georaman-89: Contributions, Symposium Université de Toulouse, France, Mai 1989, 8

Delé-Dubois, M.-L., Poirot, J.-P., and Schubnel, H.-J., 1986. Identification de micro-inclusions dans des rubis et émeraudes de synthèse par spectroscopie Raman. *Revue de Gemmologie a.f.g.*, **88**, 15–17

Dmitriev, I.A., and Khan, V.P., 1971. Formation of beryl structure in glasses of the BeO–Al_2O_3–SiO_2–MgO system. *Soviet Physics Crystallography*, 15(6), 1093–4

Dowty, E., 1987. Vibrational interactions of tetrahedra in silicate glasses and crystals: II. Calculations on melilites, pyroxenes, silica polymorphs and feldspars. *Physics and Chemistry of Minerals*, **14**, 128–38

Eppler, W.F., 1958. Synthetischer Smaragd. *Deutsche Goldschmiede-Zeitung*, **56**(4), 193–7

Espig, H., 1962. Die Synthese des Smaragdes und einiger anderer Minerale. *Berichte der Geologischen Gesellschaft der DDR*, **7**, 464–75

Feigelson, R.S., Martin, G.W., and Johnson, B.C., 1972. Crystal growth and properties of some alkali metal metavanadates. *Journal of Crystal Growth*, **13/14**, 686–92

Flanigen, E.M., Breck, D.W., Mumbach, N.R., and Taylor, A.M., 1967. Characteristics of synthetic emeralds. *American Mineralogist*, **52**(5–6), 744–72

Fukumi, K., Hayakawa, J., and Komiyama, T., 1990. Intensity of Raman band in silicate glasses. *Journal of Non-Crystalline Solids*, **119**(3), 297–302

Ghorai, A.K., and Bhattacharya, D.P., 1995. Mobility characteristics of non-equilibrium carriers in III–V compounds at low lattice temperatures. *Journal of the Physics and Chemistry of Solids*, **56**(2), 165–71

Goel, S.P., and Mehrotra, P.N., 1985. IR and thermal studies on lithium oxomolybdenum (VI) oxalate. *Journal of Thermal Analysis*, **30**, 145–51

Griffith, W.P., and Lesniak, P.J.B., 1969. Raman studies on species in aqueous solutions. Part III. Vanadates, molybdates, and tungstates. *Journal of the Chemical Society (a)*, **1969**, 1066–71

Hänni, H.A., Kiefert, L., Chalain, J.-P., and Wilcock, I.C., 1997. A Raman microscope in the gemmological laboratory: first experiences of application. *Journal of Gemmology.*, **25**(6), 394–406

Hirata, T., and Zhu, H.-Y., 1992. Identification and vibrational properties of the mixed oxide (1–x) $V_2O_5 + xMoO_3$ ($x \leq 0.3$). *Journal de Physique: Condensed Matter*, **4**(36), 7377–88

Hofmeister, A.M., Hoering, T.C., and Virgo, D., 1987. Vibrational spectroscopy of beryllium aluminosilicates: heat capacity calculations from band assignments. *Physics and Chemistry of Minerals*, **14**(3), 205–24

Iwamoto, N., Umesaki, N., Takahashi, M., Tatsumisago, M., Minami, T., and Matsui, Y., 1987. Molecular dynamics simulation of Li_4SiO_4 melt and glass. *Journal of Non-Crystalline Solids*, **95** and **96** (1), 233–40

Johansson, G., Pettersson, L., and Ingri, N., 1979. On the formation of hepta- and octa-molybdates in aqueous solution. X-ray scattering and Raman measurements. *Acta Chemica Scandinavica*, **A33**, 305–12

Kasprzak, M.S., Leroi, G.E., and Crouch, S.R., 1982. Raman spectroscopic investigation of isomeric and mixed-valence heteropolyanions. *Applied Spectroscopy*, **36**(3), 285–9

Kasuga, Y., 1985a. (Synthesis of single crystal of artificial beryl) [in Japanese]. Japanese Patent Application, Laid-Open No. 60–81084, May 9

Kasuga, Y., 1985b. (Synthesis of single crystal of artificial beryl) [in Japanese]. Japanese Patent Application, Laid-Open No. 60–81097, May 9

Kasuga, Y., 1985c. (Synthesis of single crystal of artificial beryl) [in Japanese]. Japanese Patent Application, Laid-Open No. 60–81098, May 9

Kasuga, Y., 1985d. (Synthesis of single crystal of artificial beryl) [in Japanese]. Japanese Patent Application, Laid-Open No. 60–81099, May 9

Kasuga, Y., 1985e. (Synthesis of single crystal of artificial beryl) [in Japanese]. Japanese Patent Application, Laid-Open No. 60–81100, May 9

Krasser, W., 1969. Die Ramanspektren von MoO_3 and WO_3. *Naturwissenschaften*, **56**(4), 213–14

Kurilenko, L.N., Serebryakova, N.V., Saunin, E.I., Gromov, V.V., and Sokolova, N.P., 1988. IR spectroscopy of the $Li_2O–WO_3$ and $Li_2O–MoO_3$ systems. *Bulletin of the Academy of Sciences of the USSR, Division of Chemical Science*, **37**, 839–44

Landais, E., 1971. Absorption du béryl dans le proche infrarouge. *Revue de Gemmologie a.f.g.*, **28**, 11–15

Landais, E., 1998. Personal communication

Loh, E., 1968. Optical phonons in BeO crystals. *Physical Review*, **166**(3), 673–8

Maaß, J., Ahrens, H., Fröbel, P., and Bärner, K., 1993. Raman spectra and cluster modes of some molybdate- and tungstate-borate glasses. *Solid State Communications*, **87**(6), 567–72

Matson, D.W., Sharma, S.K., and Philpotts, J.A., 1983. The structure of high-silica alkali-silicate glasses. A Raman spectroscopic investigation. *Journal of Non-Crystalline Solids*, **58**(2–3), 323–52

McMillan, P., and Piriou, B., 1982. The structure and vibrational spectra of crystals and glasses in the silica-alumina system. *Journal of Non-Crystalline Solids*, **53**, 279–98

McMillan, P., Piriou, B., and Navrotsky, A., 1982. A Raman spectroscopic study of glasses along the joins silica-calcium aluminate, silica-sodium aluminate, and silica-potassium aluminate. *Geochimica et Cosmochimica Acta*, **46**, 2021–37

Mysen, B.O., 1990. Role of Al in depolymerized, peralkaline aluminosilicate melts in the systems $Li_2O–Al_2O_3–SiO_2$, $Na_2O–Al_2O_3–SiO_2$, and $K_2O–Al_2O_3–SiO_2$. *American Mineralogist*, **75**, 120–34

Mysen, B.O., and Frantz, J.D., 1992. Raman spectroscopy of silicate melts at magmatic temperatures: $Na_2–SiO_2$, $K_2O–SiO_2$ and $Li_2O–SiO_2$ binary compositions in the temperature range 25–1475°C. *Chemical Geology*, **96**, 321–32

Nassau, K., 1976. Synthetic emerald: the confusing history and the current technologies. *Journal of Crystal Growth*, **35**, 211–22

Nassau, K., 1978. Did Professor Nacken ever grow hydrothermal emerald? *Journal of Gemmology*, **16**(1), 36–49

Nassau, K., 1980. *Gems made by man*. Chilton Book Company, Radnor, Pa., USA

Nassau, K., 1998. Personal communication

Nassau, K., and Nassau, J., 1980. The growth of synthetic and imitation gems. In: Freyhart, H.C. (Ed.), *Crystals. Growth, properties and applications. Vol. 2. Growth and properties.* Springer, Berlin, 1–50

Ozeki, T., Kihara, H., and Hikime, S., 1987. Studies of Raman spectra and equilibria of isopolymolybdate ions in aqueous acidic solutions by factor analysis. *Analytical Chemistry*, **59**(7), 945–50

Poe, B.T., McMillian, P.F., Angell, C.A., and Sato, R.K., 1992. Al and Si coordination in $SiO_2–Al_2O_3$ glasses and liquids: a study by NMR and IR spectroscopy and MD simulations. *Chemical Geology*, **96**, 334–49

Pope, S.J.A., and West, Y.D., 1995. Comparison of the FT Raman spectra of inorganic tetrahedral ions over the temperature range 77 to 473 K. *Spectrochimica Acta*, Part A, **51**(12),207–37

Py, M.A., Schmid, Ph.E., and Vallin, J.T., 1997. Raman scattering and structural properties of MoO_3. *Nuovo Cimento*, **38B**(2), 271–9

Riebling, E.F., and Duke, D.A., 1967. $BeO.Al_2O_3.SiO_2$ system: structural relationships of crystalline, glassy and molten beryl. *Journal of Materials Science*, **2**(1), 33–9

Sanchez., C., Livage, J., and Lucazeau, G., 1982. Infrared and Raman study of amorphous V_2O_5. *Journal of Raman Spectroscopy*, **12**(1), 68–72

Schmetzer, K., Bernhardt, H.-J., and Biehler, R., 1991. Emeralds from the Ural mountains, USSR. *Gems & Gemology*, **27**(2), 86–99

Schmetzer, K., and Kiefert, L., 1998. The colour of Igmerald: I.G. Farbenindustrie flux-grown synthetic emerald. *Journal of Gemmology*, **26**(3), 145–55

Schmetzer, K., Kiefert, L., Bernhardt, H-J., and Zhang B.L., 1997. Characterization of Chinese hydrothermal synthetic emerald. *Gems & Gemology*, **33**(4), 276–91

Schwab, S.D., McCreery, R.L., and Cummings, K.D., 1985. Effect of surface chemistry on the morphology, resistance and colloidal behaviour of small silver particles. *Journal of Applied Physics*, **58**(1), 355–60

Sharma, S.K., and Simons, B., 1981. Raman study of crystalline polymorphs and glasses of spodumene composition quenched from various pressures. *American Mineralogist*, **66**, 118–26

Spoliti, M., Cesaro, S.N., Bencivenni, L., D'Alessio, L., Enea, L., and Maltese, M., 1981. The infrared spectra of lithium, sodium, potassium and thallium chromates and lithium and cesium molybdates and tungstates. *High Temperature Science*, **14**, 11–16

Tang, S.H., Shen, Z.X., Ong, C.W., and Kuok, M.H., 1995. Raman spectroscopic study of $LiVO_3$ and $LiVO_3.2H_2O$. *Journal of Molecular Structure*, **354**(1), 29–35

Tatsumisago, M., Takahashi, M., Minami, T., Umesaki, N., and Iwamoto, N., 1987. Raman spectra of rapidly quenched Li_4SiO_4–Li_3BO_3 glasses. *Physics and Chemistry of Glasses*, **28**(2), 95–6

Umesaki, N., Iwamoto, N., Takahashi, M., Tasumisago, M., Minami, T., and Matsui, Y., 1988. Molecular dynamics study of Li_2O–SiO_2 melts and glasses. *Trans. Iron Steel Inst. Japan*, **28**(10), 852–9

Van Praagh, G., 1946. Synthetic emeralds. *Chemical Products and the Chemical News*, **9**, 10–11

Van Praagh, G., 1947. Synthetic quartz crystals. *Geological Magazine*, **84**, 98–100

Walrafen, G.E., and Samanta, S.R., 1979. Raman and infrared spectra of amorphous BeO and $Be(OH)_2.2H_2O$. *Applied Spectroscopy*, **33**(5), 524–5

Webster, R., 1955. The emerald. *Journal of Gemmology*, **5**(4), 185–221

Webster, R., 1958. Synthesis of emerald. *Gemmologist*, **27**(328), 203–6

Weinstock, N., Schulze, H., and Müller, A., 1973. Assignment of ν_2 (E) and ν_4 (F_2) of tetrahedral species by the calculation of the relative Raman intensities: the vibrational spectra of VO_4^{3-}, CrO_4^{2-}, MoO_4^{2-}, WO_4^{2-}, MnO_4^-, TcO_4^-, ReO_4^-, RuO_4, and OsO_4. *Journal of Chemical Physics*, **59**(9), 5063–7

White, W.B., and Minser, D.G., 1984. Raman spectra and structure of natural glasses. *Journal of Non-Crystalline Solids*, **67**(1–3), 45–59

Xu X., Li J., and Yao L., 1989. A study of glass structure in Li_2O–SiO_2 Li_2O–Al_2O_3–SiO_2 and Li–Al–Si–O–N systems. *Journal of Non-Crystalline Solids*, **112**(1–3), 80–4

Zhang, X., and Frech, R., 1997. Vibrational spectroscopic study of lithium vanadium pentoxides. *Electrochimica Acta*, **42**(3), 475–82

Zwaan, J.C., and Burke, E.A.J., 1998. Emeralds from Sandawana, Zimbabwe: the use of Raman microspectroscopy in identification of their solid inclusions. *Journal of Gemmology*, **26**(3), 174–87

Identification of filler substances in emeralds by infrared and Raman spectroscopy

Dr L. Kiefert[1], Professor H.A. Hänni[1], J-P. Chalain[1] and W. Weber[2]

1. SSEF Swiss Gemmological Institute, Falknerstrasse 9, CH-4001 Basel, Switzerland
2. Rainstrasse 4, CH-8330 Pfäffikon, Switzerland

ABSTRACT: For many centuries, fissures in emeralds have been filled with oils and other natural substances to enhance their clarity. For approximately 15 years, the substances used also comprise various artificial resins, mainly epoxy resins. The various substances have different stability, but none of the treatments is permanent. Oils are the most volatile of the fissure filling media used, but the stone can easily be cleaned and refilled. Artificial resins, on the other hand, are much more durable, but they also decompose with time and are then hard to remove. Because of this, some traders require an identification of these substances which can be performed by infrared and/or Raman spectroscopy.

The first step in fissure filler identification is visual observation by the microscope and under long-wave UV-light to estimate the presence or absence of a filler and its position in the stone. Then the filler is identified with one or both of the above-mentioned methods. At the SSEF laboratory, which pioneered the techniques in a complementary way, infrared spectroscopy is used as a macro method and Raman spectroscopy as a micro method. Once a spectrum is obtained with either method, it is compared to the extensive data bank of either infrared or Raman spectra of the pure filler substances. The present paper summarizes common emerald fillers and describes in detail their identification with infrared and Raman spectroscopy.

Keywords: emerald, fissure fillers, infrared, oil, Raman, resin, spectroscopy

Introduction

Most varieties of beryl (aquamarine, yellow beryl, morganite) are generally quite clear and do not contain important inclusions. The clarity of emerald, in contrast, is usually affected by the presence of healed or open fissures. While aquamarines have grown with little interference in pegmatite dykes and pneumatolytic druses, most emeralds were formed in metamorphic rocks and underwent a more agitated geological history. Shearing forces and fluid action due to metamorphic processes led to mineral transitions and any rigid and large gem mineral crystals were prone to crack or break under the pressure with consequent

ISSN: 1355–4565

***Table I:** Selection of filters analysed at SSEF.*

Category	*Trade name*
oil	Universal Oil (paraffin oil); Johnson's Baby oil; 'MAZOLA' pure corn oil; olive oil; Clove oil nat 80–82%; Roth AG; cedar wood oil, Merck; 17196 H.E.Daniel, chinese cedar wood oil; MC153263 H.E. Daniel, 100% nat.cedar wood oil; CE108 Spectrum Quality Products cedar wood oil; 21695 H.E. Daniel 100% nat. Virginian cedar wood oil; 23292 H.E. Daniel 100% nat. cedar wood oil; Merck Cedarwood oil for microscopy; Panreac purified cedar oil; Cedro oil, Colombia; BPC FIG 34 cedarwood oil thick micro
coloured oil	green Joban oil, India
oil/wax	paraffin wax; wax from F.Hakimian, N.Y.; sperm whale oil (hardened)
Canada balsam	hardened; for microscopy; 100% natural, ref M; synthetic, ref Go
artificial resin	Opticon (epoxy resin); Palm oil, Palma (epoxy resin); Permasafe (bisphenole A); 77–309.RM (bisphenole A); Caldofix Struers; Epoxy 330; Scandiplex A 911F; LV 15 (UV-hardening resin)
silicon	'Silicon DC4' silicon fat; Luster's PCJ Nutrientsheen 3 silicon oil

formation of fissures. Should physical and chemical conditions still be favourable to crystal growth after the main destructive event, healing of damaged crystals may take place together with continued growth. If breakage and fissure formation in the gem crystals occurred at a much later period, e.g. during the blasting of the parent rock, the defects stay unhealed and artificial fissure treatment then becomes a commercially attractive step for the miner or stone dealer.

The clarity of an emerald is reduced by the presence of inclusions – guest crystals, internal cavities or negative crystals, healing fissures, structural features and by open fissures. The latter are especially visible in Colombian emeralds because most are otherwise relatively inclusion-free. In emeralds from other countries (e.g. Brazil, Russia, Zambia, Zimbabwe-Sandawana, Afghanistan and India) crystalline inclusions are more frequent, but fissures are still present (see e.g. Gübelin and Koivula, 1986; Epstein, 1989; Kazmi and Snee, 1989; Laskovenko and Zhernakov, 1995; Zimmermann *et al.*, 1997).

To improve the clarity of emerald open fissures may be disguised by impregnating the stones with some more or less permanent colourless substances. Although coloured oils and resins are also used to fill emeralds, we do not focus on these substances in this publication. Effective fillers have refractive properties close to those of emerald. Such substances comprise oils (natural or synthetic), resins (natural or with a natural resin base), glues or artificial resins *(Table I)*. Fissure treatments have been carried out for years – see Ringsrud (1983), Nassau (1984), Hänni (1988), Hurwit, (1989), Themelis (1990), Kane (1990), Kammerling *et al.* (1991), Bosshart (1991a), Shida (1991) and Koivula *et al.* (1994).

The identification of the nature of filler substances in emeralds started to become an issue when artificial resins, commonly epoxy resins, were used as fissure filling substances. When the treatment was performed on rough stones it masked the real appearance of the emerald and inhibited reliable estimation of their true quality. Furthermore, the durability of the new substances was questioned when decomposition of the originally 'invisible' filler was reported in some stones by Kammerling *et al.* (1991) and Federman (1998). The fillers had turned white and totally spoiled the stone it was originally supposed to have improved. Therefore an increasing number of people involved with emeralds wanted to identify epoxy-treated stones, knowing from articles in the gemmological literature that such an identification is possible (e.g. Hänni, 1992; Kammerling *et al.*, 1995; Kiefert and Hänni, 1996; Chalain *et al.*, 1998; Johnson *et al.*, 1998).

The present paper is an attempt to guide laboratories in identification of fissure fillings in emerald, if required. Appropriate optical and spectroscopic properties of emerald filler substances are described. Based on gemmological needs and the results of early analyses of one of the authors (WW), the substances are divided into three major groups, namely oil, Canada balsam, and artificial resin (see *Table I*). Under these headings, methods for the detection and identification of enhancements in emeralds are described in detail. The following two steps are necessary to obtain reliable results: observation by optical means and identification with analytical instruments.

Fissure treatments

Open fissures of emeralds are filled with substances (air, for example) with a refractive index significantly different from that of emerald. Light entering the emerald, even at high angles of incidence to the fracture, is reflected off the surface of the fracture and it behaves as if it were a mirror. When these fractures are filled with substances with a refractive index close to that of the emerald the light can pass through the fractures with almost no reflection. This cancels out the mirror effect and the visibility of the fracture is greatly reduced.

In Colombia, Brazil, and the majority of the other emerald producing countries, treatments of emerald fissures are first carried out on the rough material. If cutting intersects unfilled fissures, further treatment may take place. Fissure fillers usually are heated to reduce their viscosity. The substances are then introduced into emerald fissures using various vacuum or pressure techniques (*Figure 1*). A number of emerald dealers call this technique 'oiling' (Ringsrud, 1983) regardless of the kind of substance used. This causes confusion among inexperienced buyers who think the treatment of emeralds is performed with oil only.

Figure 1: *Vacuum chamber on heating stage. This system is in use at the Institute of Earth Sciences of Basel University for hardening porous rocks to make them workable. For emerald treatment, the cleaned stones are evacuated above the filler, and then lowered into the substance. Normal pressure is admitted when the liquid has penetrated into all open fissures and fractures. © SSEF Swiss Gemmological Institute.*

In the past, the fact that treatments of gemstones have not been communicated or declared has caused considerable damage to the confidence of consumers. Sales figures appear to have gone down directly due to law cases concerning filled emeralds which were reported by the media. Nowadays most trade associations expect dealers to disclose the product that has been used for enhancement. But such disclosures are not always made, and with many older stones it is not clear to the owner whether such stones have been treated. The situation is further complicated by possible multiple treatment with different substances at different trade levels.

The various colourless oils, either natural or synthetic, appear to be well accepted among the trade. Artificial resins, however, which have been used for emerald treatment for about 15 years, are accepted by fewer in the trade. The reasons for this difference in acceptance may be the following.

Oils are mobile to viscous, simple to introduce into fissures, but also prone to escape if in contact with liquid detergent. The fissures are comparatively easy to clean out, and stones are readily re-oiled. The improvement in appearance due to oil is less than with resins since the refractive indices of oils are lower (Chalain *et al.*, 1998). To many jewellers the fact that a customer may recognize the real state of an emerald when the oil drains or dries out may lead him to favour resinous substances.

Artificial resins are more viscous and may possess a solidifying character, which the oils do not have. Fresh artificial resins with higher refractive indices give a better enhancement to a stone. They adhere well in the fissures, but are difficult to dissolve and replace should they have changed their appearance or decomposed.

It is also worth noting that the stability of the treatments with organic substances is difficult to define and depends on the time and temperature specified. When an announcement appears in the trade press that a well known filling product should at the same time be 'permanent' and also 'removable' it casts doubt on its stability. Compared to the durability of an emerald, which can be worn for many centuries without damage, none of the treatments should be considered as stable.

Green fillers are also applied to enhance not only the clarity but also the colour of emerald using green Joban oil, green Opticon etc. This treatment, mainly practised in India, is easily visible under magnification. Emeralds treated in this way must be called 'treated emeralds' according to CIBJO rules (CIBJO, 1991, 1997). This type of treatment is, however, not considered in this article.

Colourless substances in emerald fractures are more difficult to detect than coloured substances. Some substances have a refractive index so close to that of the emerald that when observed with the unaided eye, the fracture disappears almost completely.

Spectroscopic properties of pure filler substances

The organic substances used to fill emeralds either alone or mixed, are commercially available. Therefore, their properties are well known and Fourier transform infrared (FTIR) and Raman spectra are readily available (e.g. Hummel, 1990).

All available organic substances at the SSEF Swiss Gemmological Institute which could be used to fill emerald have had their infrared spectra recorded and the major characteristic peaks related to the chemical bonds (*Figure* 2, see Hummel, 1990). Since 1991, 42 possible filler substances have been characterized at SSEF with FTIR spectroscopy and stored in a reference library for comparison. These include various oils and waxes, among them various natural and synthetic cedarwood oils and Canada balsams, clove oil, olive oil and paraffin oil as well as various epoxy resins such as Opticon, Palma (Palm Oil) and Permasafe which was available in a polymerised state. Initially, use of the term 'Palm Oil' was confusing for those in the trade, until the substance proved to be an epoxy resin made by Shell and marketed under the name 'Epon 828'. The analysed products were supplied by a number of customers, emerald treaters and chemical companies. The technical or trade names of a selection of these substances are listed in *Table I.*

The Raman spectra of the most important filler substances have also been recorded since 1995 at SSEF and stored in a reference library. The spectral area lying between 1200 and

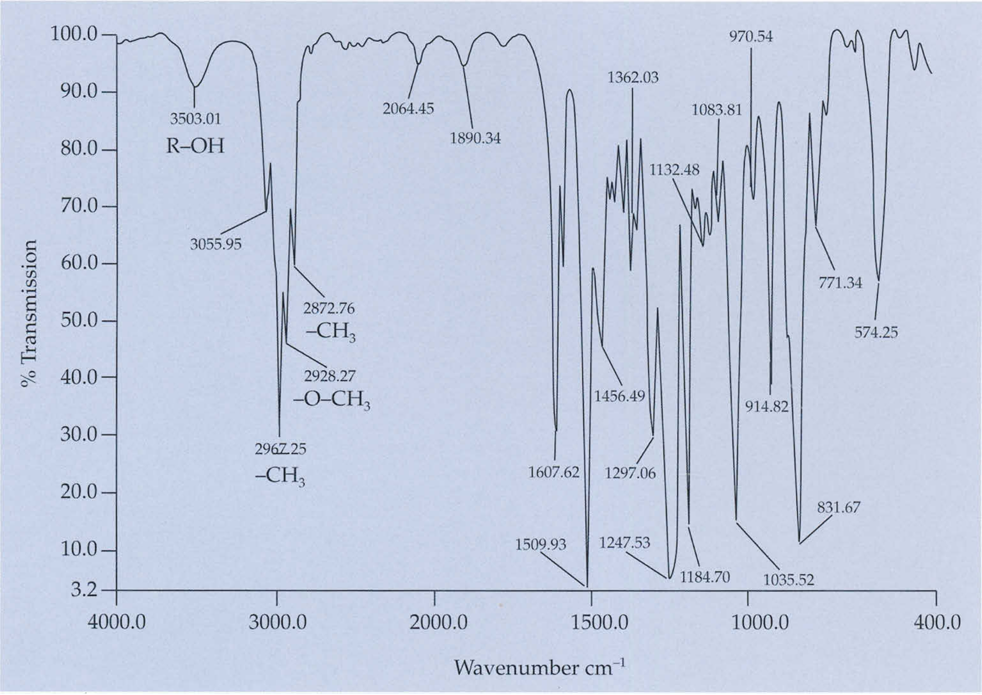

Figure 2: *Infrared spectrum of Epon 828, showing the chemical bonds related to the various peaks. © SSEF Swiss Gemmological Institute.*

3200 cm^{-1} contains the characteristic Raman peaks for the kind of organic substances used for fissure fillers without interference from the Raman peaks of emerald (see below).

According to their spectroscopic properties, which are closely related to their physical properties, the fillers can be divided into three groups: oils, Canada balsam, and artificial resins (see *Table I*). While we could not establish any reliable difference between the spectra of natural and synthetic oils or Canada balsams, distinct differences were observed between the spectra of oils or Canada balsams on the one hand and artificial resins on the other (see below).

FTIR spectra of pure substances

After having verified the identity of the substances in the characteristic spectrum region below 2000 cm^{-1}, we concentrated on the peaks in the 2800–3100 cm^{-1} range which do not suffer interference from emerald absorption.

A comparison of FTIR spectra of oils and artificial resins shows that the general distributions of their absorption peaks are very similar between 2800 and 3000 cm^{-1}. This is not surprising since the peaks in this part of the spectrum are due to C–H vibration bonds which are present in both organic substances. An experienced spectroscopist may, however, note that the relative absorption heights of the peaks at 2870 and 2854 cm^{-1} may differ in oils and artificial resins (*Figure 3a,b*). This difference can be interpreted as giving an indication of one or the other substance, but should not be considered as strictly characteristic, as can be seen in the spectrum of cedar wood oil (*Figure 3c,d*).

In contrast, it appears that none of the analysed oils (natural or synthetic) show significant absorption above 3000 cm^{-1}, while all artificial resins show clear and typical absorption (*Figure 3a–d*). Therefore, the peaks between 3000 and 3100 cm^{-1} are important in distinguishing oils from

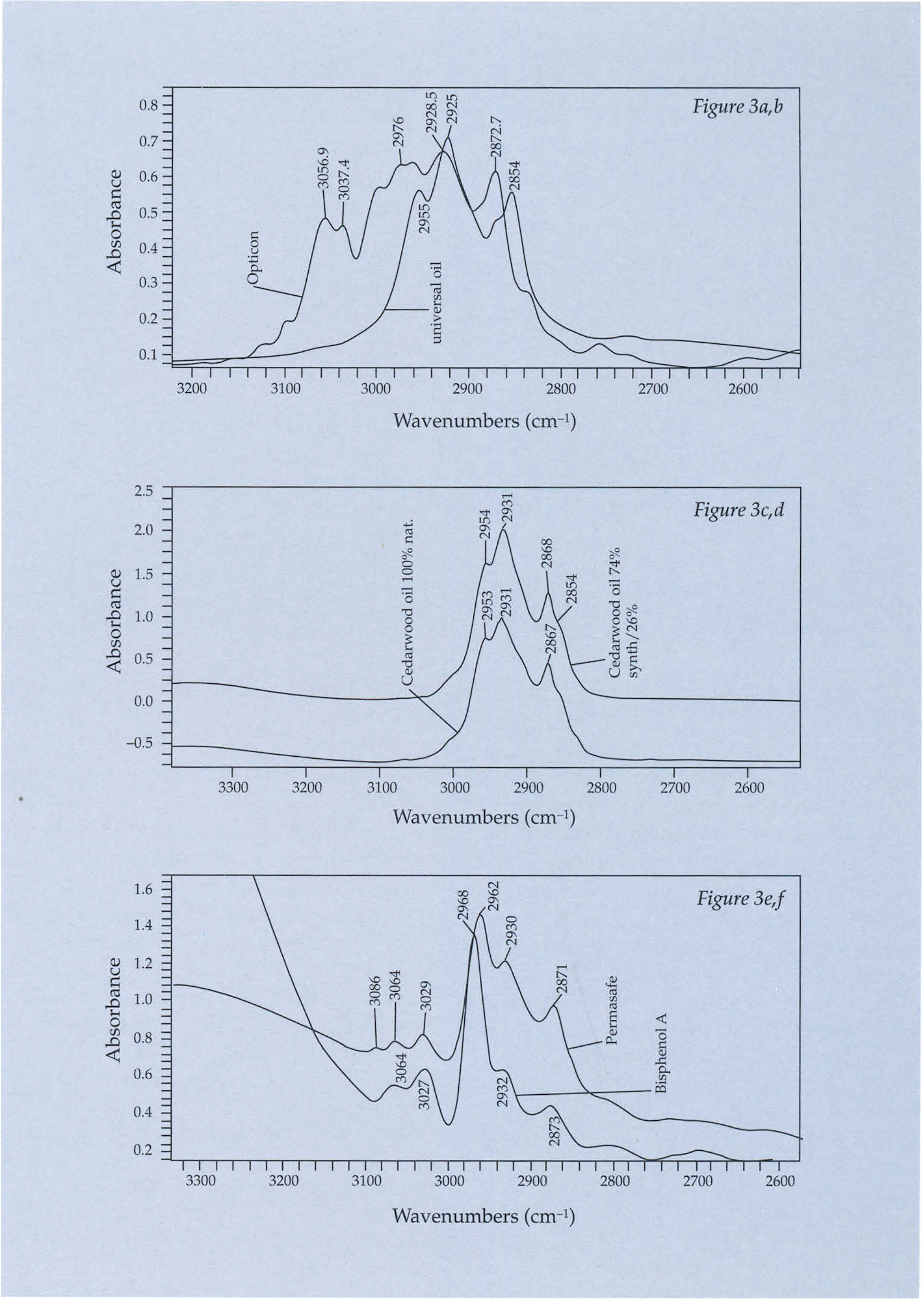

Figure 3: *FTIR spectra of: (a) universal oil; (b) artificial resin (Opticon) showing that the absorption features of the 2854 and 2870 peaks are different in intensity and that absorption features are very different in the 3000–3050 cm^{-1} area; (c) and (d) cedarwood oil; (e) Permasafe; (f) bisphenole A. © SSEF Swiss Gemmological Institute.*

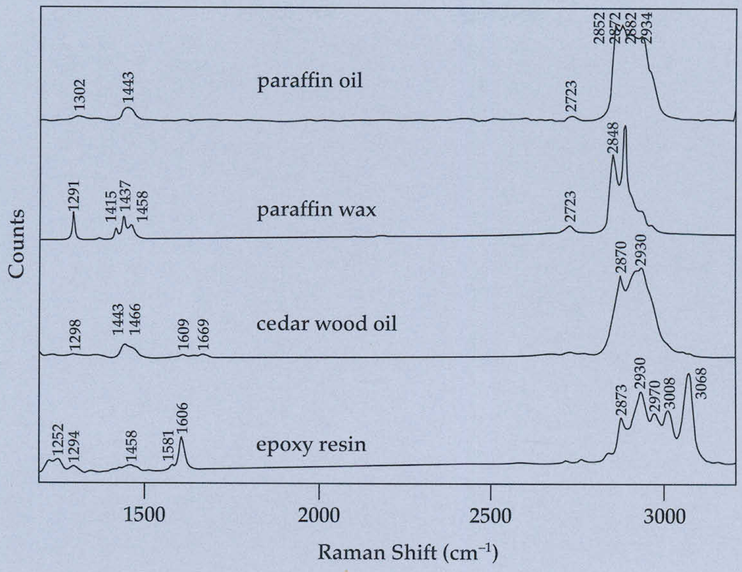

Figure 4: *Part of the SSEF reference collection of Raman spectra of emerald fillers. The four spectra contain peaks at different wavenumbers and an identification of products is possible by comparison. © SSEF Swiss Gemmological Institute.*

Figure 5: *Raman spectra of various cedar wood oils: (a) natural cedar wood oil; (b) synthetic cedar wood oil; (c) 74% synthetic cedar wood oil. © SSEF Swiss Gemmological Institute.*

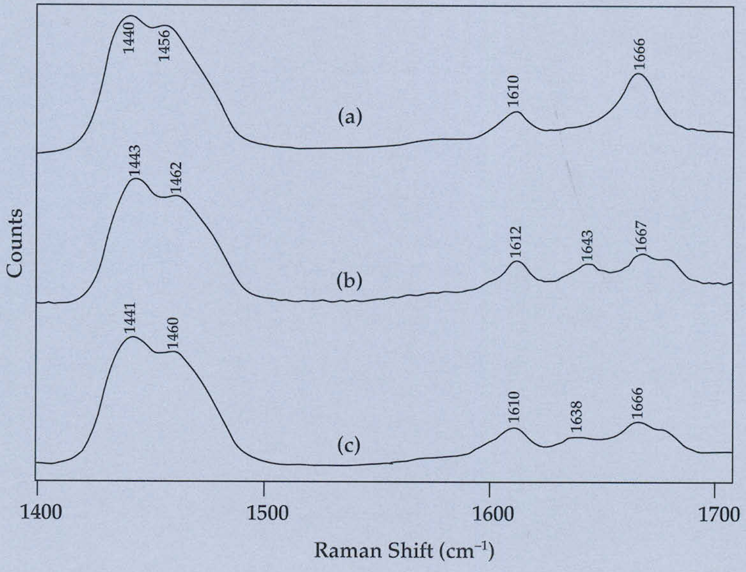

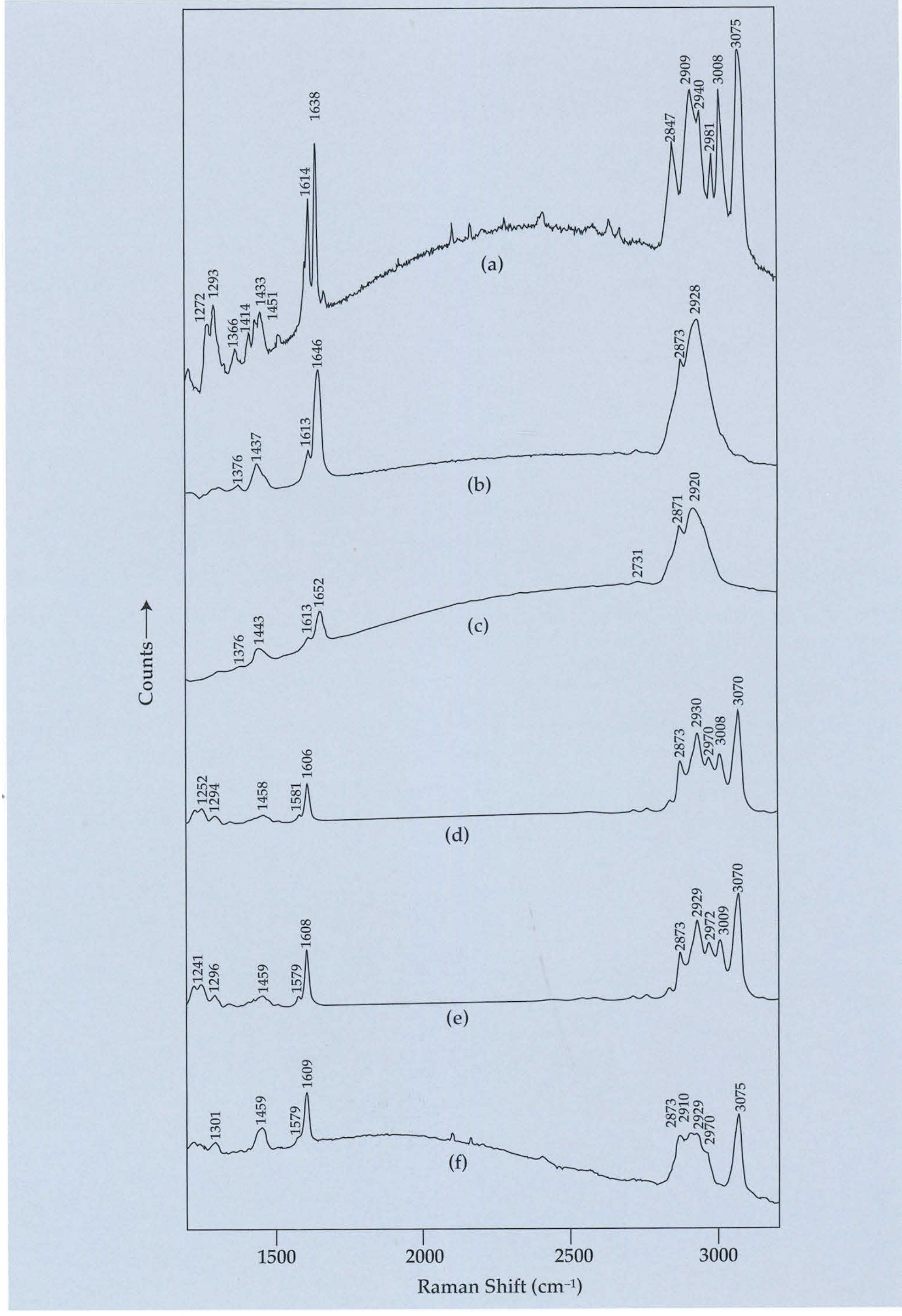

Figure 6: *Raman spectra of (a) clove oil; (b) natural Canada balsam; (c) synthetic Canada balsam; (d) Opticon; (e) Palm oil; (f) Permasafe. (d), (e) and (f) are epoxy resins. © SSEF Swiss Gemmological Institute.*

artificial resins. Some other, less frequently used substances such as Canada balsam or clove oil have other characteristic FTIR spectra which differ from the spectra of oils and artificial resins. A newer artificial resin which is marketed under the name 'Permasafe' has a spectrum very much like the other epoxy resins (*Figure 3e,f*, see also Fritsch *et al.*, 1999) and is also a member of the Bisphenole A family.

Raman spectra of pure substances

In Raman spectroscopy, just as in FTIR spectroscopy, oils and resins show different peaks depending on their chemical composition. Of all the oils identified a distinction can be made between two different types: one type includes oils such as mineral and paraffin oil (*Figure 4*); the other type consists of cedar wood oil (*Figure 4*), which can be natural or produced synthetically. The various cedar wood oils tested in the laboratory show some variation in peak intensity probably due to ageing and oxidation. Their major peaks in the lower region of wavenumbers at 1441 cm^{-1}, 1445 cm^{-1} and 1666 cm^{-1} occur in all tested samples (*Figure 5*). There is a third oil, which may have been used in the past to fill emerald and that is clove oil, but it is identifiable by its strong smell. However, its Raman spectrum differs considerably from the spectra of the other oils (*Figure 6a*), and may be confused with artificial resin if its smell has been undetected and the peak measurements not carefully made (see *Figure 6d,e,f*).

In contrast to FTIR spectroscopy, the Raman spectra of paraffin wax and paraffin oil show similar peak positions, but the peaks of paraffin wax are sharper due to the fact that the molecules in hardened substances are less mobile. Thus, the more liquid substances appear to have a broadening effect on Raman peaks (*Figure 6a*).

One organic substance which is used to fill emerald fissures is Canada balsam which may occur as a natural resin but may also be produced synthetically. The properties of natural and synthetic Canada balsam are alike (*Figure 6b,c*) and just as natural and synthetic cedar wood oil properties are similar, Canada balsam and the oils used to fill emerald have similar chemical properties. They are unable to polymerise, so do not harden as much as epoxy resins and are generally easier to remove from the stone if they start decomposing.

The various epoxy resins marketed under the names Opticon, Palma, Epon 828, have identical spectra with major peaks distinguishing them from the other substances mentioned above (*Figure 6d,e,f*). Permasafe differs slightly from the above-mentioned epoxy resins (*Figure 6f*, see also *Figure 3e,f*).

The spectra presented in *Figures 4 to 6* show that a distinction can be made between oils, Canada balsam, and artificial resins. Other materials such as hardeners for epoxy resin or various polishing materials (diamond powder, chromium oxide) have also been tested and show distinct peak positions.

Storage of the obtained spectra in a reference library file is advisable, so that the spectra of fillers found in emeralds can easily be compared. It is also of advantage to examine the whole possible spectral range of the substance, but to save the detailed spectra only in the range critical for detecting fissure fillings in emerald.

Identification of fissure fillers in emeralds

The aim of this section is to give a detailed description of the methods used at SSEF to identify fissure fillers. In order to enable gemmologists to reproduce these methods, this section is written in the style of a manual describing various steps in identification of fillers, pointing out any difficulties.

The analysis of fissure filling in emerald previously treated with known substances by one of the authors (HH) was carried out with FTIR as well as Raman spectroscopy on several stones and proved that the methods produced spectra comparable with the pure

Instrumentation

For successful identification of fissure fillers in emeralds, thorough analysis with a gemmological microscope, observation under UV light, and identification with FTIR and/or Raman spectroscopy are essential.

At the SSEF laboratory, microscopic observation is performed with a gemmological microscope by Bausch & Lomb, allowing magnification up to 70x. The UV source used is a long-wave (365 nm) UV lamp which is part of the Dialite lamp supplied by System Eickhorst.

The Fourier Transform infrared spectrometer used at the SSEF is a Philips PU9800 instrument with Nicolet software OMNIC. An additional software package from Nicolet which contains a number of IR data collections including Hummel (Polymer), Organics by Raman, Sigma Biological Sample Library, Crime Lab Sample Library, and Aldrich Sample Library allows the direct comparison of a measured spectrum with stored data and its identification.

A Renishaw 1000 Raman system equipped with a CCD Peltier detector and an argon ion laser (514 nm) with a power of 25 mW was used for filler identification. The objective lenses on the microscope are Olympus BH lenses with x5, x10, x20 and x50 magnification. Raman analysis with this system can be performed in two modes. The first is a mode in which data points are collected over a selected range of wavenumbers for a certain time; the range can be chosen by specifying a centre wavelength, and then the system automatically collects data several hundred wave numbers to each side. The second mode, the extended mode, collects data successively over the pre-chosen area. This type of analysis makes it possible to cover any scan range from 100 to 9000 cm^{-1} with a resolution of 2 cm^{-1} (Ostertag, 1996; Hänni *et al.*, 1997). Up to 1999, spectra were collected using Renishaw software, and then translated into the software package GRAMS/386. Since 1999, with the aid of an upgrade of both the Renishaw and the GRAMS software, spectra are directly recorded in GRAMS.

substances. During the last five years, successful identifications have been obtained on more than 500 stones from customers of the laboratory.

Observation

Observation of fissures with the microscope; for the observation of an emerald treatment, a 10x loupe is not always sufficient, while a detailed study with the microscope generally allows the detection of a filler substance in the emerald. It also gives information about the extent of treatment and one may also form an opinion about the nature of the filler. Fractures filled with foreign, artificially-introduced substances commonly appear different from those occupied by natural fluids. Fissures which contain natural fluids (notably aqueous brine) are often oriented parallel to one of the crystal faces, and commonly consist of more than one phase (liquid, vapour or solid).

Trapped individual gas bubbles or extended 'lakes' of air are a reliable indicator for the presence of an artificial filler. Frequently, dendritic to lobular structures can be observed, showing the distribution between the (liquid) filler and a gas phase; the oils or resins have refractive indices close to that of emerald. As a function of the thickness of the fissure, an effect due to the dispersion of light may be observed which resembles the 'flash effect' observed in fissure filled diamonds (Nelson, 1993).

While oil may create an orangy flash effect, flashes which change their colour in different light positions appear to be due only to artificial resins (*Figure 7;* Kammerling *et al.*, 1995). Depending on the orientation of the fibre optic light, the flashes may be orange, violet, or blue, the blue colour being mainly visible when observed almost along the fissure plane. However, multicolour flashes are not always present in fissures treated with artificial resin, and single colour orange flashes are frequently observed.

When fissures are not filled completely, dendritic patterns and worm-like structures may be observed, sometimes with trapped air bubbles (*Figure 8*). The nature of these structures gives an indication of the viscosity of the filler but cannot be used for identification.

On drying, the fillers may become opaque and then the treated fissures are readily visible (*Figure 9*). This is generally the point when identification of the filler becomes a factor of significance for buyers of emeralds.

Before any instrumental analysis is performed, it is important to use the microscope to locate the most easily accessible fillers. The necessary lighting includes reflected light, dark field and/or fibre optic illumination. The latter allows a strong and precise lighting, but, more importantly, easier and more flexible observation in different directions. Holding the emerald with tweezers prevents the surface of the stone becoming greasy from handling and allows light to enter the stone more easily.

Figure 7: *Colour flashes from an epoxy resin treated fissure in an emerald. The resin has a refractive power close to that of emerald and the colours are due to a dispersion effect. © SSEF Swiss Gemmological Institute.*

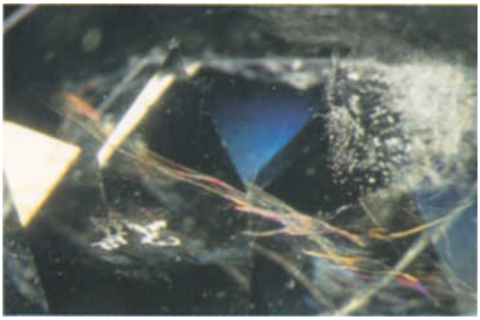

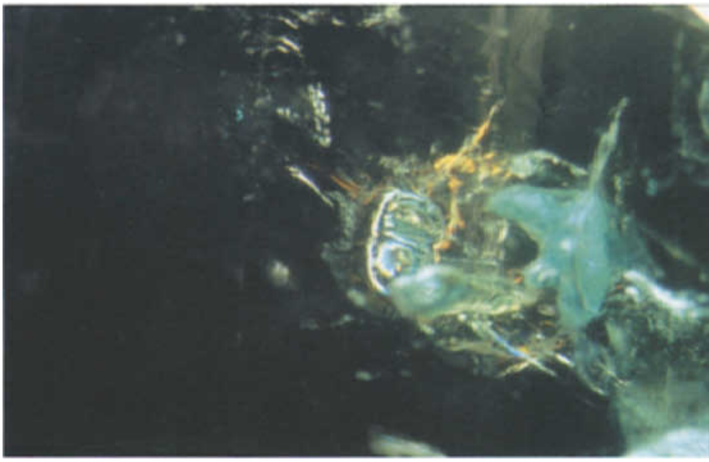

Figure 8: *Trapped air bubbles and dendritic pattern in an epoxy resin-treated emerald. © SSEF Swiss Gemmological Institute.*

Observation of emerald fissures under UV light: The use of long-wave UV light (365 nm) is a convenient tool to observe fissure fillings in emeralds. The stone is placed on top of the UV light source and may be inert or show a reddish colour depending on the amount of Cr and Fe in the stone; but a different fluorescence colour may show in the fissures and can indicate the extent of the treatment by virtue of the spread and number of fluorescing fissure planes (*Figure 10*).

Figure 9: *Decomposed oil on a fissure plane of an emerald. For various reasons it is possible that filling media dry out or may decompose. Heat, solvents, or ultraviolet radiation may contribute to disintegration and lead to a whitish appearance which may be easily visible. © SSEF Swiss Gemmological Institute.*

Figure 10: *Observation under long wave UV radiation (365 nm) can be an effective method for judging the amount of treatment and for finding the best positions to obtain spectra for filler identification. © SSEF Swiss Gemmological Institute.*

Like many organic substances, the majority of substances used to treat fractures in emeralds (oils, balsam, resins) show fluorescence under UV light. In contrast, most natural fluids are inert, although hydrocarbons have been observed and described in Colombian emeralds (Bosshart, 1991b), and it cannot be excluded that they may exhibit a similar fluorescence. Again, artificially filled fissures may not always show fluorescence, especially if the amount is small and the filler fluoresces weakly. Thus, although UV fluorescence may give important information, it should not be considered as a diagnostic test for identification.

Generally speaking, oils show a yellowish fluorescence while many artificial resins that react to UV light show a bluish-white fluorescence. Although not a complete identification tool, this fluorescence allows evaluation of the position and the quantity of filler in the treated fissure (*Figure 10*). When the fissures are readily visible, it is possible to classify the extent of the treatment. At the International Coloured Stone Association (ICA) meeting in Tucson, 1998, the consensus was to use three categories to classify the extent: minor, moderate and significant (SSEF Standard and Applications, 1998). It is emphasized that these grades do not replace a judgement by the dealer who has to evaluate the general quality of the stones. For example, if a small single treated fissure is situated at the centre of the table of an emerald, its extent may be classified as minor. But after the substance decomposes, the visibility of the fracture may have a significant impact on the overall appearance of the stone.

The observation of emerald fissures under UV light combined with microscopic observation, allow location of treated fissures in stones and is an important step in preparation for point analysis with the Raman microprobe or with infrared spectroscopy (see below).

Thus observation of emerald fissures with a microscope and UV light enables the gemmologist to conclude if a foreign substance is present or not, and although some features of emerald fillers such as a certain dendritic pattern or a certain UV fluorescence may give an indication of the type of substance present in the emerald, positive identification of the substance can only be carried out by FTIR or Raman spectroscopy.

Identification by spectroscopic analysis

The identification of individual substances is restricted to laboratory techniques. The first analyses of these substances at SSEF Swiss Gemmological Institute were carried out in 1991 using infrared spectroscopy (*see Figure 11*), and in 1995 SSEF acquired a Raman spectrometer. Since then both FTIR and Raman spectra have been obtained routinely to analyse fissure fillings in emeralds.

It is important to note that the interpretation of spectra obtained with both techniques relies strongly on comparison with known reference spectra stored in a database. Thorough analyses to characterize the chemical nature of the substances were carried out in 1993 by one of the authors (WW) and led to a decision at SSEF to group the substances into three distinct groups; oil, Canada balsam, and artificial resin. Any further distinction (such as that between the different types of oils) is too time consuming and difficult to obtain with the spectroscopic means usually present in a gemmological laboratory to be economically justifiable.

Methods of FTIR analysis: Infrared spectroscopy is one of the most efficient analytical techniques to characterize organic materials. IR spectroscopy is a vibrational spectroscopy, which measures the energies of vibrating molecules in the infrared spectral area. For over fifty years, organic compounds have been studied and their structures explained on the basis of IR spectra. IR spectra are considered as characteristic 'fingerprints' for given compounds. Large catalogues and collections of spectra are available to enable identification and comparison when unknown materials are investigated (Hummel, 1990; Moenke, 1962; Sadtler, 1973).

At SSEF, FTIR spectroscopy is performed in two modes: one is direct transmission, where the analysing beam is transmitted through the sample; the other is measurement in reflection-absorption mode using diffuse reflectance equipment where the analysing beam is directed onto the sample placed on a flat mirror and covered by a hemispherical mirror. Thus the beam is focused through the sample by the mirrors before being collected by the detector. Tests have also been performed in a third mode, with a 5x beam condenser (KBr lens), but the signal obtained with the diffuse reflectance accessory was stronger and the method quicker.

Although the majority of samples are best analysed by the diffuse reflectance method, there are samples in which it is necessary to analyse fissure fillings by *direct transmission*, either because they are too large to fit into the sample chamber for diffuse reflection (more than 40 ct), or because they are mounted in jewellery. To perform analysis by direct transmission, a baseline has to be recorded by measuring the infrared beam in the empty sample chamber. After this, the stone, mounted onto a sample holder, is placed into the beam making sure that it does not contact any masking or plastic. In order to obtain good results with FTIR absorption analysis, either a significant amount of filler substance must be in the stone or the infrared beam must be focused through a fracture which has been located previously (e.g., with UV fluorescence). There are several difficulties using the direct transmission method, the main ones being:

Figure 11: *FTIR spectra from 1991 of untreated emerald (red), of Opticon epoxy resin (blue), and of an Opticon treated emerald (green). Within the transmission area of emerald between 3500 cm*$^{-1}$ *and 2400 cm*$^{-1}$*; the major absorption of the artificial resin is clearly visible. © SSEF Swiss Gemmological Institute.*

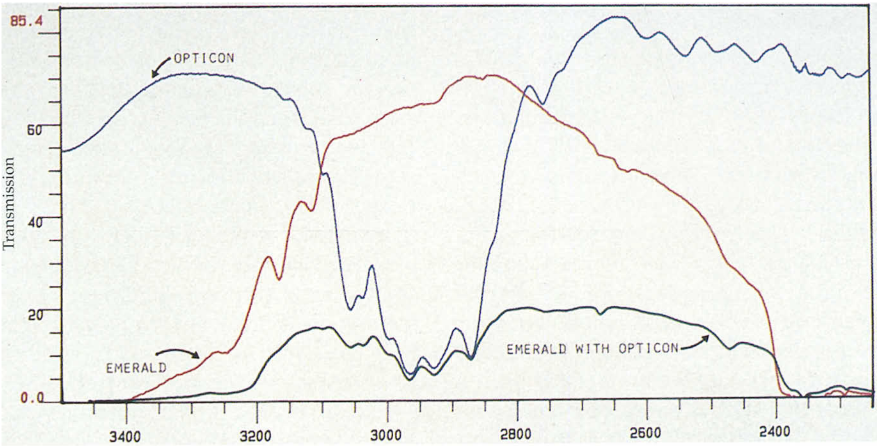

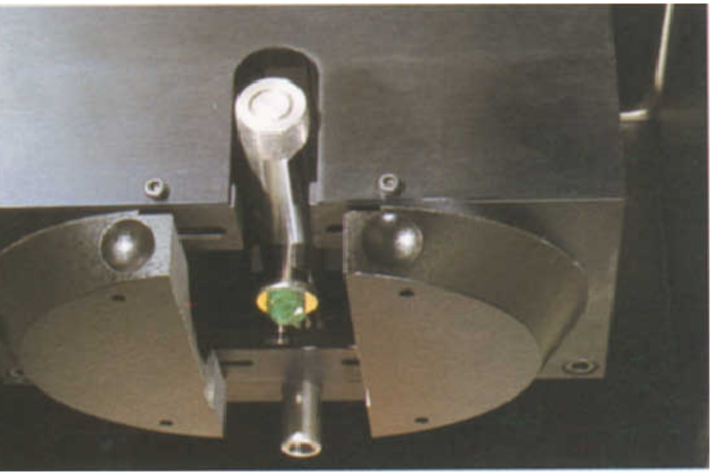

Figure 12: *Diffuse reflectance accessory used at the SSEF fitted to the Philips (PU9800) FTIR spectrometer. In contrast to the micro-method of analysis with Raman spectrometry, this type of FTIR analysis is a macro-method giving an average result. © SSEF Swiss Gemmological Institute.*

- intersecting at least one larger fissure to give a sufficiently strong filler signal;
- selecting an orientation of the stone so that the emerging beam reaches the detector;
- obtaining a transmitted beam of sufficient energy.

It can take a long time to adjust a stone to produce a measurable signal, and since the path of the beam through the stone cannot be exactly monitored, it could well pass beside a treated fracture. The results therefore must be critically assessed.

In *absorption-reflection analysis* the diffuse reflectance accessory tool of FTIR spectrometry (*Figure 12*) has the advantage that the beam can interact with a large volume of the stone. The equipment consists of a flat mirror on which the stone is placed. A baseline spectrum is recorded for the ambient condition in the sample chamber and then the sample is placed into the path of the beam and covered with a hollow mirror which reflects the refracted beam back onto the stone. In this way we are dealing with a macro-method that accumulates analytical information from various fissures in different parts of the stone. Contrary to the analysis of a directly transmitted beam, it is not crucial to look for a special path through the stone (i.e., the beam does not have to be focused on a fracture as precisely as with the direct beam method). The orientation of the stone is, however, important, because the absorption bands of OH-vibrations are close to the spectral area of analysis and cause structural effects which interfere with absorptions of C–H-vibrations of the substance to be analysed (*Figure 13*).

Generally, better results are obtained when the beam interacts with a larger sample, but if the sample is too big, a rather large loss of energy of the reflected beam may occur. If a filler substance located using the microscope cannot be identified with this equipment it is necessary to apply a more localised analysis with micro-FTIR or Raman micro-spectroscopy.

FTIR spectra of fissure fillers in emeralds: Untreated emerald from any natural source shows total absorption below 2400 cm^{-1} and above 3400 cm^{-1} with a transmission window between 2800 and 3100 cm^{-1} (*Figure 11*). The spectra are, however, influenced by the crystal orientation of the emerald (*Figure 13*). Therefore, tests have been carried out to define the best orientation for recording spectra of treated emerald. A more detailed description of the influence of emerald orientation on FTIR spectra will be given in a later article (Chalain *et al.*, in preparation).

As shown with pure substances, the FTIR spectra of emerald fillers present two characteristic areas which can be used for identification. The best absorption region for organic substances such as C–H groups and cyclic aromatic substances is between 1700 and 1600 cm^{-1}. However, the emerald spectrum shows complete absorption in this region and cannot be investigated. The second characteristic region for filler substances lies between 2800 and 3100 cm^{-1}, in which emerald shows an absorption minimum. Therefore, this region is suitable for analysis. When an FTIR analysis is performed on a treated emerald, a combination of the absorption spectrum of the filler substance and the emerald spectrum is obtained (*Figure 11*).

Emeralds treated by one of the authors (HH) with known substances showed that none of the emeralds treated with oil possess any absorption between 3000 and 3100 cm^{-1} (*Figure 14a*), while all emeralds treated with various artificial resins do show characteristic absorption features in this region (*Figures 11,14b,c*). Emerald treated with Canada balsam has yet another typical feature which makes it distinguishable from emeralds treated with other substances. Based on these results, FTIR spectroscopy enables distinction between emeralds treated with oil, with artificial resin, or with Canada balsam. The study was continued by including various treated emeralds with newer substances, which were sent to the laboratory for scientific analysis. Two emeralds were sent to the SSEF laboratory by A. Groom, who promotes emerald treatment with his substance called 'Gematrat'. Unfortunately the pure substance was not supplied. The FTIR spectra of the analysed stones show features similar to those of epoxy resins, so that the substance can be classified in the group of artificial resins (*Figure 14b*). Five emeralds donated by R. Giraldo of Colombia, had been treated with 'Permasafe' and a comparison of the spectrum with the solidified substance shows good agreement with epoxy resin (*Figure 14c*). Due to its spectroscopic features, Permasafe is also classified as artificial resin.

When performing FTIR spectroscopy, care has to be taken that no pollutants adhere to the emerald. When the whole stone is analysed by FTIR spectroscopy, such pollutants may disguise a relatively pure stone and may lead to misinterpretation. Among potential pollution sources are the grease from fingers when handling the stone without tweezers, refractometer fluid when the refractive index has been performed before FTIR analysis, or detergent from the water with which the specific gravity of an emerald has been determined. To avoid such effects, care must be taken to clean the emerald thoroughly prior to analysis, preferably with alcohol or acetone.

Raman micro spectrometry: The Raman spectrometer is equipped with a microscope for selecting the analytical area and targeting the beam to the selected spot. The advantage of this instrument is the ability to focus inside a sample to several millimetres depth. In this way, gemstone inclusions as small as 2 µm can be investigated (see e.g., Dhamelincourt and Schubnel, 1977; Delé-Dubois *et al.*, 1980; Hänni *et al.*, 1997; Koivula and Elen, 1998), and this makes it convenient to focus into the

***Figure 13:** FTIR spectra of ε and ω vibrations of emerald show distinct variations in absorbance of OH-bonds within the 'transmission window' between 3200 cm^{-1} and 2600 cm^{-1}. © SSEF Swiss Gemmological Institute.*

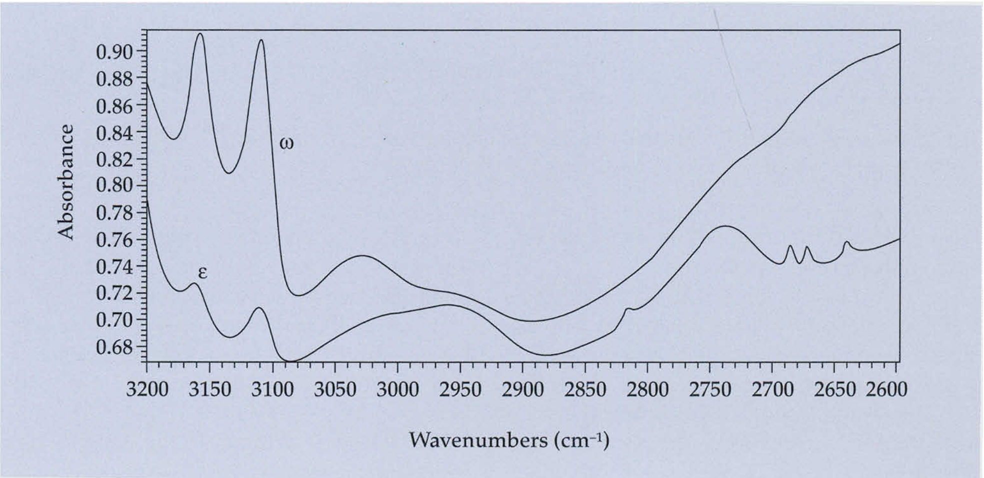

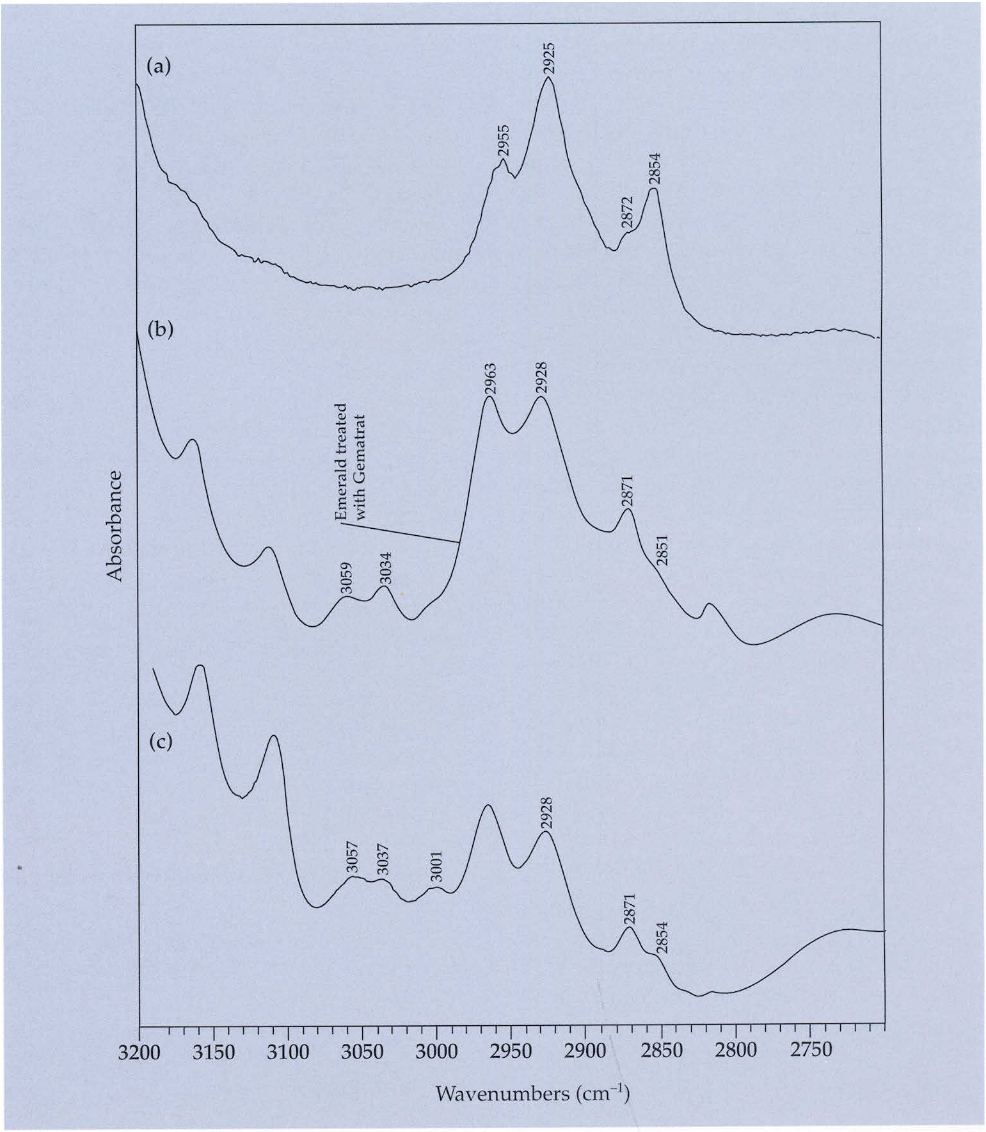

Figure 14: *FTIR spectra: (a) emerald treated with oil; (b) emerald treated with 'Gematrat'; (c) emerald treated with 'Permasafe'. © SSEF Swiss Gemmological Institute.*

fissure of a fracture-filled emerald where spot analysis can be performed.

In comparison with diffuse reflectance FTIR spectroscopy where a large part of the stone is analysed, Raman spectroscopic analysis is applied to a small spot, which has to be chosen first using a microscope. It is very important to perfectly focus the beam onto the area to be analysed. Even then a result is not always obtained and very often several different areas have to be analysed. This may make the method very time consuming.

Fissure fillers have two characteristic regions in their Raman spectra which do not interfere with the emerald peaks: 1200–1700 cm^{-1} (*Figure 15*) and 2800–3100 cm^{-1}. Although the second area generally displays more intense peaks than the

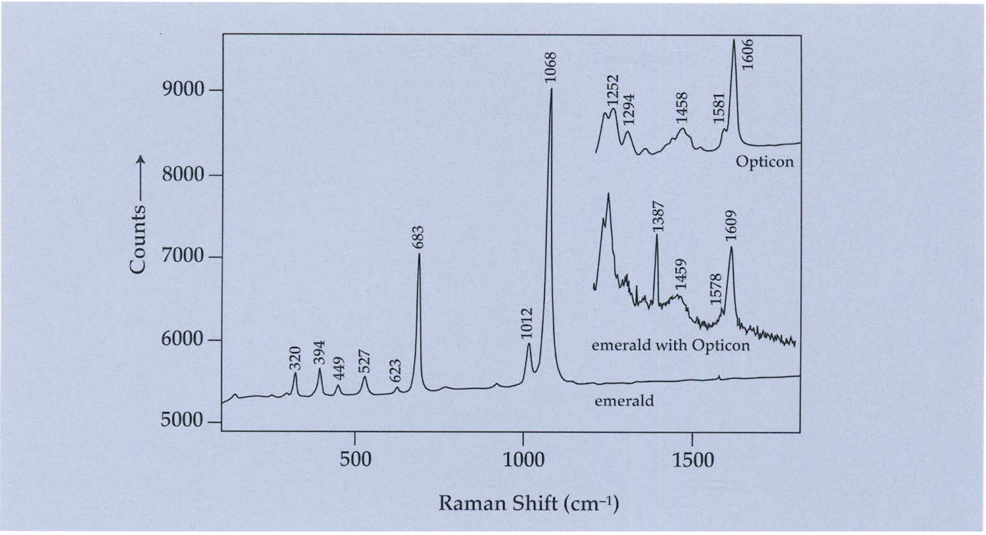

Figure 15: *Raman spectra of Opticon epoxy resin (top), of emerald without treatment (bottom), and of an Opticon-treated emerald (middle). The valuable peaks are in the 1200 to 1800 cm^{-1} area where the vibrations of organic fillers are visible. © SSEF Swiss Gemmological Institute.*

first, it may be masked by a strong Raman fluorescence of the emerald due to the wavelength of the selected laser source. Therefore the first range from 1200 to 1700 cm^{-1} is used routinely for filler identifications by Raman spectroscopy at SSEF (Hänni *et al.* 1996; Kiefert and Hänni, 1996).

The fact that this analysis can be carried out using a finely focused beam on a small area (*Figure 16*; Ostertag, 1996) makes it a much more precise method than non-focused FTIR spectrometry. Therefore, where a treatment is visible with microscopic methods or where FTIR analyses are insufficient for a positive identification, the Raman microprobe often supplies a positive response.

Raman spectra of fissure fillers in emeralds: as mentioned above, the Raman spectrum of emerald itself shows a number of distinct peaks between 100 and 1100 cm^{-1} (*Figure 15*), which are constant for emeralds from many different source areas. Due to the chromium content of an emerald in combination with the selected wavelength of the laser source, the background of the spectrum starts to rise at approximately 2500 cm^{-1} and increases towards higher numbers. This may mask some of the peaks of the filler substances between 2700 and 3100 cm^{-1}. Therefore, when doing Raman analysis on emerald fillers more attention should be given to the spectral area between 1200 and 1800 cm^{-1} where interference with the emerald spectrum is minimized and good spectra of fissure fillers are obtained.

Figure 16: *The laser beam of a Raman spectrometer focused in the middle of a transparent crystal. At the focus the excited volume is a few cubic microns. Photo by Thomas Ostertag.*

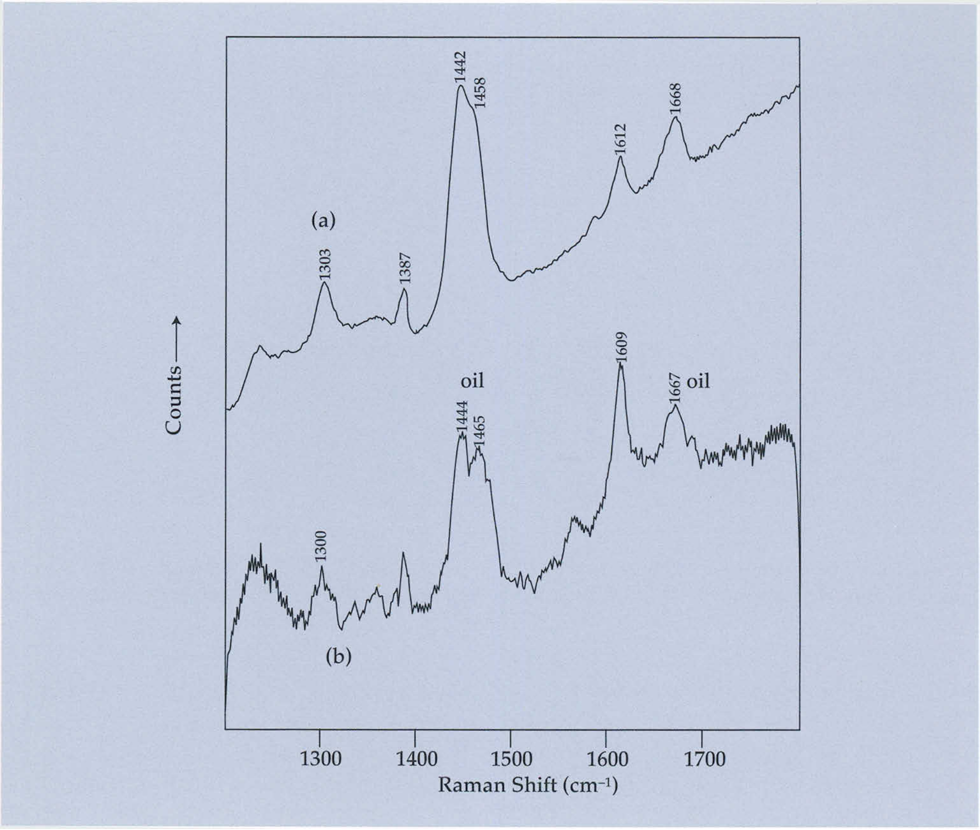

Figure 17: *Raman spectra: (a) emerald fissure with cedar wood oil; (b) emerald fissure with a mixture of cedarwood oil (1440–65 and 1667 cm^{-1}) and artificial resin (1609 cm^{-1}). The peak at 1387 cm^{-1} indicates emerald. © SSEF Swiss Gemmological Institute.*

Figure 15 shows the Raman spectrum of an emerald and the spectrum of a typical epoxy resin, in this case 'Opticon'. When an epoxy resin is encountered in an emerald fissure, the spectrum may vary from a strong signal to a very weak outline of the major peak which, however, is always visible to a certain degree. In contrast, emeralds filled with cedar wood oil show a different spectrum (*Figure 17a*).

Mixtures of various substances are generally also identifiable. Raman spectra of the more recent 'Gematrat' from the United States showed that it possesses spectroscopic properties consistent with a mixture of artificial resin and oil. Multiple fillers which may be the result of incomplete cleaning and refilling with another substance could also show similar mixed substance spectra (*Figure 17b*).

As in FTIR spectroscopy, care must be taken about any pollution from such sources as dop stick glue.

Discussion and conclusions

Experience in day-to-day laboratory routine shows that over the past few years identification of fissure fillers in emeralds has been receiving more and more attention in the trade due to new substances being introduced as fillers. The properties of these new substances such as ageing behaviour and removability are generally not well known and those in the trade are concerned about the reversibility of a filling process when the new filler substances are applied.

The identification of fissure fillers presents a challenge for gemmologists in laboratories, who, up to now have mostly specialised in inorganic chemistry and mineralogy. They have to become familiar with organic chemistry, as the commonly used fillers are organic substances. Therefore, identification of filler substances mainly relies on the comparison of spectra obtained by FTIR or Raman methods from an emerald with those of known substances.

As has been frequently observed in the use of mineralogical techniques the experience of the laboratory shows that FTIR and Raman analyses are complementary. On the one hand, certain substances which cannot be identified with FTIR spectroscopy can easily be identified with Raman spectroscopy. On the other hand there are certain substances which are difficult to identify with Raman spectroscopy but are readily identifiable with FTIR. Oil in emerald fissures, for example, shows a spectrum which is difficult to interpret when the same is analysed with an argon ion laser, but gives good results with FTIR spectroscopy. Which one of the two spectroscopic methods is applied first depends on the position of the fissures and the quantity of substance in the emerald.

The identification techniques are complementary to microscopic observations and results obtained by UV light viewing. For an experienced observer, these two latter methods can be used as an indication of a fissure treatment and an estimation of the quantity of filler(s) present.

Using spectral methods for identification, the analyses of filler substances in emeralds may sometimes be difficult to interpret because:

- there may be variations in infrared absorptions of the emerald due to anisotropy, as a function of its orientation;
- more than one filler substance may be present in the interior of the stone which presents a mixed spectrum;
- the fissures may be filled with artificial resins other than epoxy resins (*Table I*) and may not have aromatic bondings. Continuous research is necessary to keep in contact with developments.

Synthetic or artificial?

To some people in the trade it makes a big difference if a filler substance is natural or synthetic. They think that a synthetic product is worse and less acceptable. As a matter of fact, synthetic substances (by definition of the term) are analogues to their naturally occurring counterparts. Synthetic cedar wood oil or synthetic Canada balsam for example have basically the same properties as the natural ones. They possess chemical compositions and structures that cause the same optical effects and removability from the stone. Therefore, in the context of emerald treatment it is unimportant to differentiate whether a given substance is in its natural state or duplicated by a synthesis. The characteristics as fillers are the same.

In contrast to this, artificial substances do not have a natural counterpart and are newly designed substances with new properties. Epoxy resins possess chemical structures that were invented and designed by chemists and material scientists. Some of the properties are welcome as emerald enhancers, others are not. The ability to form long molecular chains and to polymerise makes them more durable in some respects, but also difficult to remove once applied. Usually epoxy resins have a refractive index closer to emerald than oils. This makes it hard for the jeweller and goldsmith to evaluate the extent and position of the treatment, and damage may occur during setting. The difference should therefore not be made between natural and synthetic, but between natural and synthetic on one side and artificial on the other.

Recent laboratory experience at SSEF indicates that about 5 per cent of emeralds examined contain fillers which cannot be positively identified. These are generally stones in which the filler has decomposed and become opaque, perhaps losing its original homogeneous chemical characteristics.

Acknowledgements

The authors would like to thank Dr Michael Krzemnicki, SSEF, for a critical review of the article and for analysing some of the organic substances with Raman spectroscopy, and Mr Peter Giese, SSEF, for analysing the substances with FTIR. C. Abouchas, L. Decque, R. Naftule, A. Sofiov, Th. Färber, D. Piat, R. Nissani, M. Durlabji, K. Scarratt and R. Giraldo supplied us with various commercial filler substances.

References

Bosshart, G., 1991a. Emeralds from Colombia (Part III). *Journal of Gemmology*, **22**, 500–3

Bosshart, G., 1991b. Emeralds from Colombia (Part II). *Journal of Gemmology*, **22**, 409–25

Chalain, J-P., Hänni, H.A., and Kiefert, L., 1998. Détermination des substances de remplissage dans les émeraudes. In: D. Giard (Ed.)., *L'émeraude*. Association Francaise de Gemmologie, Paris, 107–15

CIBJO, 1991. *Gemstone Book*. UBOS Bern 120 pp

CIBJO, 1997, *Gemstone Book*. UBOS Bern, 119 pp

Delé-Dubois, M.-L., Dhamelincourt, P., and Schubnel, H-J., 1980. Etude par spectroscopie Raman d'inclusions dans les diamants, saphirs et émeraudes. *Rev. de Gemm* a.f.g., **64**, 11–14

Dhamelincourt, P., and Schubnel, H-J., 1977. La microsonde moléculaire à laser et son application à la minéralogie et la gemmologie *Rev. de Gemm* a.f.g., **52**, 4

Epstein, D.S., 1989. The Capoeirana emerald deposit near Nova Era, Minas Gerais, Brazil. *Gems and Gemology*, **25** (3), 150–8

Federman, D., 1998. Emerald on Trial. *Modern Jeweler*, January 1998

Fritsch, E., Maitrallet, P., Hémond, G., Lasnier, B., Notari, F., Froyer, G., and Louarn, G., 1999. Première caractérisation du 'Permasafe', nouveau matériaux de remplissage des fractures utilisé pour les émeraudes. *Rev. de Gemm a.f.g.*, 136, 44–6

Gübelin, E.J., and Koivula, J.I., 1986. *Photoatlas of Inclusions in Gemstones*. ABC Verlag, Zürich

Hänni, H.A., 1988. An oil well in your garden? *Swiss Watch and Jewellery Journal*, March 1988

Hänni, H.A., 1992. Identification of fissure-treated gemstones. *Journal of Gemmology*, **23** (4), 201–5

Hänni, H.A., Kiefert, L., and Chalain, J-P., 1996. How to identify fillings in emeralds using Raman spectroscopy. *Jewellery News Asia, September*

Hänni, H.A., Kiefert, L.Chalain, J-P., and Wilcock, I., 1997. A Raman microscope in the gemmological laboratory. First experiences of application. *Journal of Gemmology*, **25**(6), 394–406

Hummel, D.O., 1990. *Atlas of Polymer and Plastics Analysis*. 2nd edition. Verlag Chemie, Weinheim, Deerfield Beach, Florida, Basel

Hurwit, K.N., 1989. Gem trade lab notes. Emerald with plastic-like filling. *Gems and Gemology*, **25**(2), 104

Johnson, M. *et al.*, 1998. How to detect clarity enhancement in emeralds. *Modern Jeweler* January

Kammerling, R.C., Koivula, J.I, Kane, R.E., Maddison, P., Shigley, J.E. and Fritsch, E., 1991. Fracture filling of emeralds. *Gems and Gemology*, **27** (2), 70–85

Kammerling, R.C., Maddison, P. and Johnson, M.L., 1995. Gem trade lab notes. Emerald with unusual flash-effect colours. *Gems and Gemology*, **31**, 1, 54

Kane, R.E. 1990., Gem trade lab notes. Emerald with filled fractures. *Gems and Gemology*, **26**(1), 95–6

Kazmi, A.H., and Snee, L.W. (eds)., 1989. Emeralds of Pakistan. *Geology, Gemology and Genesis*. Van Nostrand Reinhold, New York

Kiefert, L., and Hänni, H.A., 1996. Detection of fissure fillings in emeralds using a Raman Microscope. Proceedings of Second Australian Conference on vibrational spectroscopy, Queensland University of Technology, 73–4

Koivula, J., Kammerling, R.C., Fritsch, E., Johnson., M.L., and DeGhionno, D., 1994. Gem News. New emerald treatment/polishing systems from Israel. *Gems and Gemology*, **30**(2), 122–32

Koivula, J.I., and Elen, S., 1998. Barite inclusions in fluorite. *Gems and Gemology*, **34**(4), 281–3

Laskovenko, A.F., and Zhernakov, V.I., 1995. An update on the Ural emerald mines. *Gems and Gemology*, **31**(2), 106–13

Moenke, H., 1962. Mineralspektren. (Aufgenommen met dem Jenaer Spektralphotometer UR 10). Akademie-Verlag, Berlin

Nassau, K., 1984. *Gemstone Enhancement*. Butterworths, London 221 pp.

Nelson, J.B., 1993. The glass filling of diamonds. Part 1. An explanation of the colour flashes. *J. Gemm*, **23**, 461–72

Ostertag, T., 1996. Spezielle Anwendung der Raman-Spektroskopie in duen Gebieten der Mineralogie, Petrologie und Gemmologie. Diplomarbeit, Freiburg im Bresgau

Ringsrud, R., 1983. The oil treatment of emeralds in Bogota, Colombia. *Gems and Gemlogy*, **19**, 149–56

Schmetzer, K., Kiefert, L., Bernhardt, H.-J., and Beili, Z., 1997. Characterization of Chinese hydrothermal synthetic emerald. *Gems and Gemology*, **33**(4), 276–91

Sadtler Research Laboratories, Inc., 1973. *Minerals. Infrared Grating Spectra*. Sadtler Research Laboratories Inc., Philadelphia

Shida, J., 1991. Enhanced emeralds: how it must be dealt with. *ICA Gems News*, Hawaii meeting, lecture and abstract

SSEF, 1998. Standards and Applications for Diamond Report, Gemstone Report, Test Report. SSEF Swiss Gemmological Institute Basel. 120 pp

Themelis, T., 1990. Oiling emeralds. *Cornerstone 21*, 24 July

Zimmermann, J.L., Giuliani, G., Cheilletz, A. and Arboleda, C., 1997. Mineralogical significance of fluids in channels of Colombian emeralds: a mass-spectroscopic study. *International Geology Review*, **39**, 425–37

Beryl crystals from pegmatites: morphology and mechanism of crystal growth

Ichiro Sunagawa[1] and Aoi Urano[2]

1. Yamanashi Institute of Gemmology and Jewellery Arts, Tokoji-machi
1955-1, Kofu 400-0808, Japan
2. Nishikawada-cho 880-15, Utsunomiya 321-0151, Japan

ABSTRACT: Surface microtopographs of $\{0001\}$, $\{10\bar{1}0\}$ and $\{11\bar{2}1\}$ faces, growth sectors and growth banding, distribution of inclusions and growth dislocation, and the associated strain fields in single crystals of beryl from four pegmatite localities have been investigated by means of optical microscopy, X-ray topography and etching methods. Based on the observations, the processes of incipient crystal growth, growth fluctuations and partial dissolution of beryl in a pegmatitic environment could be analysed. Single crystals of beryl record clearly multiple changes and fluctuations in growth parameters and directional flow of nutrients during formation of the pegmatites. Entrapment of solid and liquid inclusions, generation of dislocations, and morphological changes have occurred in association with these changes and fluctuations. It has been confirmed that beryl crystals grew by the spiral growth mechanism with elemental step heights on $\{0001\}$ and probably on $\{10\bar{1}0\}$ faces throughout their growth histories, whereas $\{11\bar{2}1\}$ faces only appeared as transitional faces during recovery after periods of partial dissolution.

Keywords: beryl, crystal growth, pegmatite, X-ray topography

Introduction

Pegmatites are major sources of coloured gemstones such as beryl (aquamarine, heliodor, goshenite, etc.), tourmaline, topaz, spodumene (kunzite, hiddenite) and chrysoberyl (cat's-eye). Crystallization of these minerals in pegmatites takes place in supercritical vapour phase conditions or in high temperature hydrothermal solutions which occupy voids in a solidifying magma. In such voids, crystals can grow freely, with little interference from the growth of co-existing crystals. Large, well-developed, transparent and near-perfect crystals can be formed and these are suitable for cutting.

Pegmatite formation represents the latest stage of magmatism, when volatile components such as H_2O, CO_2, Cl_2, F_2 and large cations such as the rare earth elements (REE) and radioactive elements, which cannot find suitable sites in the structures of the rock-forming minerals, are concentrated. Although various magmatic series may develop pegmatites as a result of differential crystallization, those producing gem-quality crystals are principally granitic pegmatites.

ISSN: 1355–4565

Although we know broadly the formation conditions of pegmatites, we do not yet have sufficient knowledge about how the crystals grew or about the nature of changes or fluctuations in growth parameters. To clarify such a problem, the best way is to investigate the constituent minerals and particularly the surface microtopography of their crystal faces, their morphology, and their physical imperfections and chemical inhomogeneities. The external morphology of crystals provides information on growth conditions. The surface microtopographs of crystal faces reflect the growth processes and any partial dissolution processes. The internal morphology of crystals is the record of growth or partial dissolution processes, growth rate anisotropy among different crystallographic orientations, and growth rate fluctuations in one growth sector, or among crystallographically equivalent orientations. The spatial distribution of dislocations and inclusions may be correlated with events that took place during the growth process of the crystal. For successful investigations of this kind, single crystals of high perfection and homogeneity are required to reveal delicate changes in these features.

Despite severe post-growth histories, diamonds are a good example of a mineral species whose growth features have survived and have been investigated to explain growth histories; this knowledge also enables natural and synthetic diamond to be distinguished (Sunagawa, 1995). Therefore, this type of investigation forms an important basis not only for earth sciences but also for gemmology.

The stability field of beryl is the widest among eight Be-containing minerals (behoite, bertrandite, beryl, beryllite, bromellite, chrysoberyl, euclase and phenakite) of 18 minerals belonging to the $BeO–Al_2O_3–SiO_2–H_2O$ (BASH) system (Barton, 1986), and ranges from about 320° to 680°C in pressures up to 10 kbar.

Single crystals of beryl from pegmatites have been investigated using X-ray topography by such investigators as Scandale *et al.* (1979, 1990, 1993), Graziani *et al.* (1981, 1990), and Yoshimura *et al.* (1985). Scandale (1996) has recently reviewed these results, and analysed the growth histories and the relation between optical anomalies and element partitioning during growth. Observations on morphology, growth and etch figures on crystal faces and inclusions have been summarized by Sinkankas (1981).

The purposes of the present study are:

1. to correlate the imperfections and inhomogeneities in single crystals of beryl revealed by polarization microscopy, with those revealed by X-ray topography and etching methods;
2. to analyse the growth mechanism from surface microtopography and spatial distribution of dislocations;
3. to trace the morphological evolution during growth history; and
4. to interpret these results and deduce the growth history of each crystal.

The present study is principally focused on crystal growth phenomena and subtle physical imperfections.

Samples and procedures

We have investigated 19 single crystals of beryl obtained from pegmatites in Australia, Brazil and China. Eleven single crystals from Heffernan's mine, Torrington, New South Wales, Australia, five from Araçuaí and two from unknown localities in Minas Gerais, Brazil, and one from China have been investigated (*Table I*). Crystals are hexagonal prismatic, bounded by basal {0001} and first order prism $\{10\bar{1}0\}$ faces, with some showing second order dipyramidal $\{11\bar{2}1\}$ faces. Some crystals have smooth as-grown surfaces (i.e. they retain growth features), but others have heavily etched surfaces.

The surface microtopographs of {0001}, $\{10\bar{1}0\}$ and $\{11\bar{2}1\}$ faces were observed using reflected light in an optical microscope, a reflection type phase contrast microscope (PCM) and a differential interference contrast microscope (DICM). The surfaces were coated in silver under vacuum to secure high reflectivity, and on such surfaces PCM and DICM microscopy can reveal steps with

Table I: Some details of the beryl crystals investigated

Locality	Sample numbers	Size	Colour	Morphology
Australia:				
Heffernan's mine, Torrington, NSW	1–11	<1 cm – 2 cm	transparent yellowish pale green	hexagonal prism c, m faces present
Minas Gerais, Brazil:				
Araçuaí	12–16	3 cm – 4 cm	transparent pale green	hexagonal prism c, m, s faces present
Unknown	17	1.5 x 5 cm	transparent pale green	hexagonal prism c, m, s faces present corroded
Unknown	18	2 x 2.5 cm	translucent	c, m faces present
China:				
Unknown	19	1 x 7 cm	transparent	hexagonal prism c, m, s faces present corroded

heights of the order of one nanometre (Sunagawa and Bennema, 1982). Both spiral growth steps and etch figures were observed, depending on faces and samples.

Solid and two-phase inclusions, growth banding and growth sectors were investigated under a polarizing microscope by immersion in n-methylaniline solution, with RI 1.5702.

Dislocations were visualized by X-ray topography using the Lang method (Lang, 1978), as well as by chemical etching in HF at 150°C for three hours. X-ray topographs were taken both in prismatic and sectional directions. For the former direction, the natural prism faces of the crystals were used but for the latter direction, sections 2 mm thick were cut perpendicular to the *c*-axis, followed by polishing and weak chemical etching by HF. Dislocations, growth sectors, growth banding, inclusions, and boundaries indicating abrupt growth changes were clearly discernible on X-ray topographs.

Observations

Surface microtopographs

Surface microtopographs of crystal faces (*Figures 1, 2 and 3*) represent the final states of the faces, which may be either as-grown surfaces or weakly dissolved (etched) surfaces, or a combination of both.

Figure 1 is a low magnification reflection photomicrograph of a {0001} face of a representative beryl crystal from Heffernan's mine, and *Figures 2a, b* and *c* are DICM photographs at high magnification of a {0001} face of a crystal obtained in Teofilo Otoni. In *Figure 1*, spiral step patterns originating from a group or an alignment of screw dislocations and, in *Figure 2*, growth spirals originating from isolated dislocations are clearly visible. Spiral steps in *Figure 1* are bunched thick steps and those in *Figure 2* are elemental steps. They are visible, because the steps are decorated by impurities. The height

Figure 1: *Low magnification reflection photomicrograph showing composite growth spirals on (0001) face. Sample No. 6, Heffernan's mine, Torrington, NSW, Australia. Bar 1 mm.*

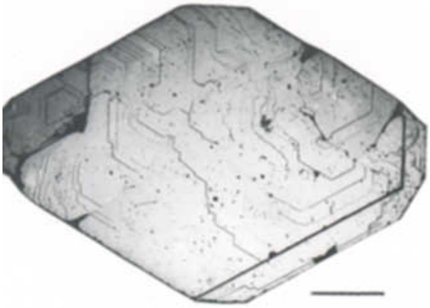

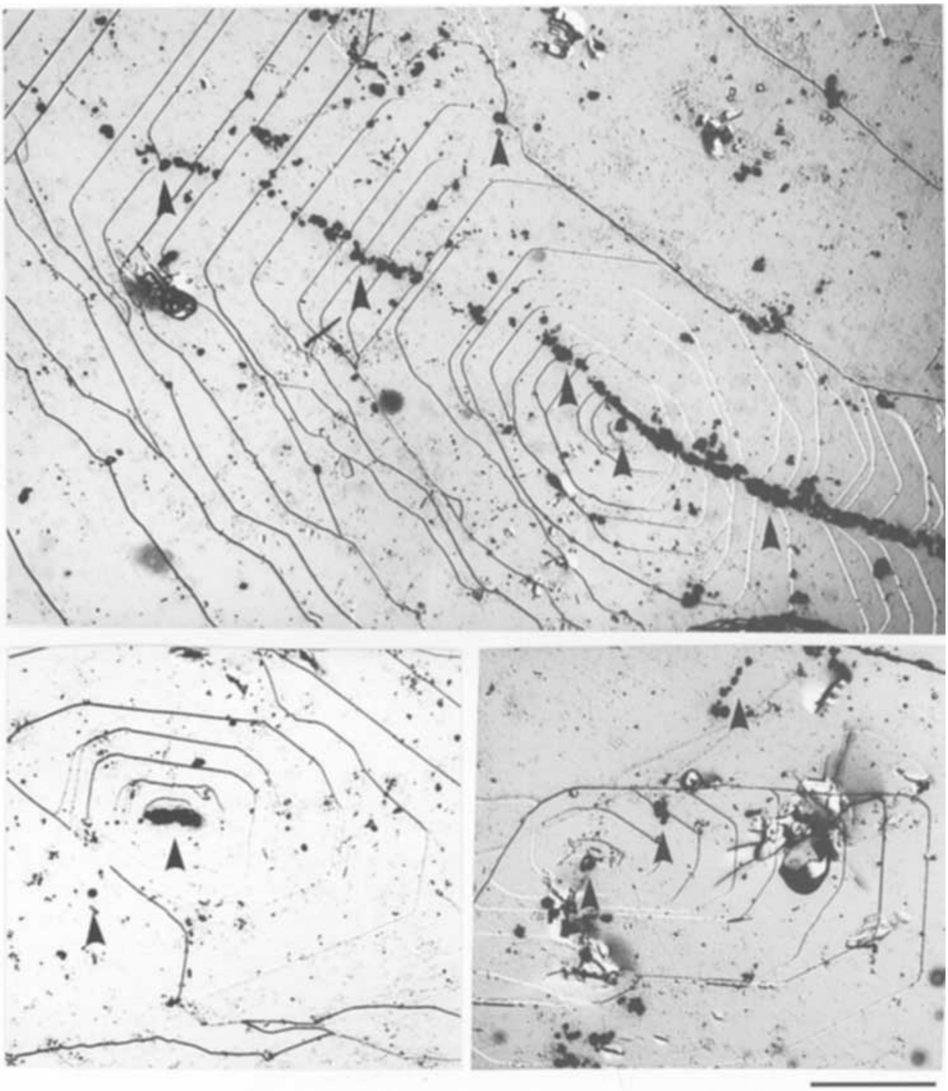

Figure 2a, b and c: *Differential interference contrast microscope (DICM) photographs showing elemental growth spirals on a {0001} face. Arrows indicate typical etch pits at dislocation outcrops. Sample No. 18, Minas Gerais, Brazil. Bar 500 µm.*

of the elemental spiral steps in *Figure 2* has been calculated to be equal to $d_{(0001)}$, i.e. 0.92 nm, whereas that of the bunched steps in *Figure 1* is much higher.

The observed spiral step patterns are essentially hexagonal, following the symmetry of the basal face, although a slight modification is present at the central turns where they show a circular form (*Figure 2*). Step separations between the successive turns of elemental spirals are in the order of 10–200 µm. The average ratio of step separations vs. step height in elemental spirals is 10^{4-6}, topographically comparable with a profile of 10000 to 1000000 metres flat terrace and a cliff of 1 metre.

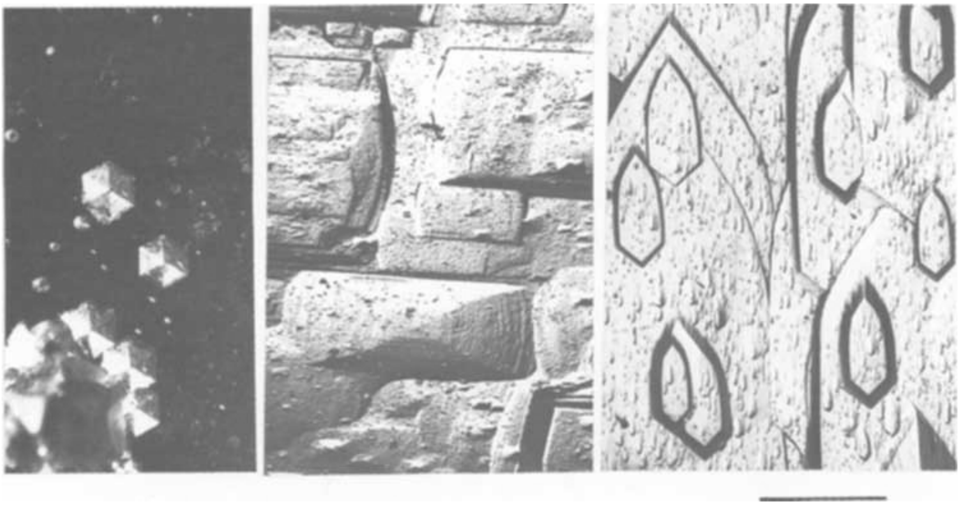

Figure 3: *(a) Deep etch pits on a {0001} face. (b) Rectangular etch figures on a {10$\bar{1}$0} face. (c) Etch pits on a {11$\bar{2}$1} face. All on sample No. 17, Minas Gerais, Brazil. Bar 200 µm.*

The {0001} faces of some samples from Araçuaí, Minas Gerais, and China show corroded surfaces, with a large number of point bottomed hexagonal or circular etch pits about 1 mm across (*Figure 3a*). They occur either isolated or in clusters and growth features are entirely absent from such surfaces. However, on the {0001} surfaces which show spiral growth steps, small etch pits are also visible at the centres of elemental growth spirals (e.g. *Figure 2a, b*), in an alignment (*Figure 2a*), as well as independently (*Figure 2a, c*). Furthermore the advancement of elemental spiral steps is disturbed, either kinked or retarded, along the alignment of these etch pits (*Figure 2a*). All these minute pits are etch pits formed at the outcrops of dislocations on the {0001} surface. Some are edge dislocations, but there should also be some screw or mixed dislocations which did not play an active role as spiral growth centres and only appear as etch pits.

The {10$\bar{1}$0} faces of beryl crystals from Heffernan's mine are characterized by elongated hillocks parallel to the *c*-axis, whereas those from Minas Gerais have hillocks of rectangular form elongated perpendicular to the *c*-axis, with curved shorter edges (*Figure 3b*). The rectangular patterns usually show a summit at the centre and discernible steps on the sloped side faces, suggesting the presence of spiral growth hillocks on the original as-grown surfaces, before they received etching. The {10$\bar{1}$0} faces of most of the samples show weakly or heavily etched surfaces and do not retain any original as-grown surfaces. Thus, elemental growth spirals were not observable on these present surfaces but they must be present on the original as-grown surfaces.

The {11$\bar{2}$1} faces of crystals from Minas Gerais and China are characterized by heavily developed etch pits only (*Figure 3c*) whose symmetry follows strictly that of the face. Step patterns indicative of growth steps were not observed on these faces.

Internal features

Section perpendicular to the c*-axis*

A section cut perpendicular to the *c*-axis of a crystal (No. 12) from Araçuaí is shown in *Figure 4* as an X-ray topograph (a), an optical photomicrograph under crossed polarizers before (b) and after etching (c).

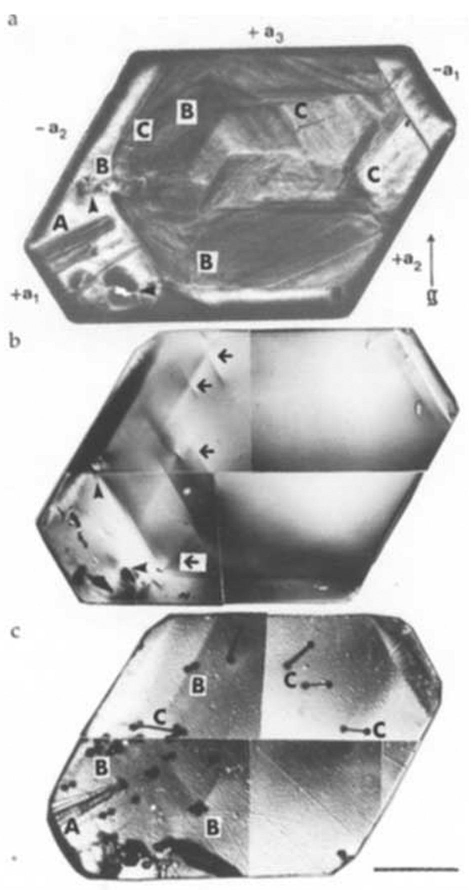

Figure 4: *(a) X-ray topograph; (b) photomicrograph under crossed polarizers before etching of a section cut perpendicular to the c-axis of a crystal (No. 12) from Araçuaí, Minas Gerais, Brazil; (c) same section as (b) after etching. Dislocations parallel (A), perpendicular (B) and inclined (C) to {0001}, and the associated anomalous birefringence (open arrows in b) are indicated. Solid inclusions are indicated by closed arrows. Bar 1 mm.*

Comparing *Figures 4a* and *c*, dislocations parallel, perpendicular and inclined to the section can be clearly distinguished. On the X-ray topograph (*Figure 4a*) and the etched section (*Figure 4c*) dislocations parallel to the section appear as sheaf-like groups of lines, indicated by A. Dislocations perpendicular to the section appear as rounded hexagonal dots indicated by B. On the etched section, they can be seen much more clearly than on the X-ray topograph. The rounded hexagonal dots are etch pits formed at dislocation outcrops. Dislocations inclined to the section appear as short lines connecting two rounded hexagonal dots, as indicated by C. These are dislocation tunnels formed by preferential etching along dislocation lines. Due to the strain fields around dislocations, hexagonal etch pits formed at the outcrops of such dislocations are to some degree rounded, and the associated etch tunnels along the dislocation lines are narrower. Dislocations (B) perpendicular to the section show distinct anomalous birefringence, clearly visible under crossed polarizers (*Figure 4b*, open arrows). Dislocations inclined and parallel to the section do not give distinct anomalous birefringence images. The latter two types of dislocations also appear less clearly on the X-ray topograph (*Figure 4a*). From the thickness of the section it can be deduced that dislocations indicated by C have an inclination of about 30° to the *c*-axis.

Figure 4b shows the distribution of inclusions, which are also visible on the X-ray topograph (*Figure 4a* closed arrowheads). It should be noted that dislocations running perpendicular to the section (parallel to the *c*-axis) are generated from these inclusions.

In *Figure 4a*, an X-ray topograph reveals internal textures more clearly than photographs of unetched (*Figure 4b*) and etched (*Figure 4c*) sections. Three distinct stages (two boundaries) can be seen on *Figure 4a*; the central superimposed double rhombic outlines, surrounded by a slightly rounded hexagonal outline and further by a malformed hexagonal outline. We distinguish three stages – 1, 2 and 3 – during the growth process of this particular crystal.

From the internal textures shown in *Figure 4a*, it is apparent that the widths of the successive stages in crystallographically equivalent directions, i.e. the growth rates, are not the same. The growth rates in the +a_1 direction both between stages 1 and 2, and 2 and 3, are about three times higher than in the $-a_1$ direction. The growth rates in the $+a_2$ direction between stages 1 and 2 are nearly equal to that in the $-a_2$ direction, but decrease to a third of the growth rate in the $-a_2$ direction between stages 2 and 3. There are similar changes in the a_3 direction. The observed variation of growth rates among crystallographically equivalent directions demonstrates that during the period from stage 1 to 2, there was no severe anisotropy involved in the growth environment, except a weak directional flow along the a_1 direction. However, during the period between stages 2 and 3, the presence of a strong directional flow of solutions along the a_1 direction has to be assumed.

A higher growth rate in the $+a_1$ and $-a_2$ directions compared with the $-a_1$, $+a_2$ and a_3 directions should be related firstly to some extent to dislocations parallel to the section which were generated from inclusions at the boundary between stages 2 and 3, and secondly, but to a lesser extent, to dislocations perpendicular to the section which were generated from inclusions trapped at a rounded corner between stages 2 and 3. Entrapment of inclusions should be related to the change in conditions which resulted in the appearance of this boundary, and the dislocations from these inclusions should have accelerated the growth rate in this direction.

By correlating *Figure 4b* with *4a* and *4c*, an anomalous birefringence due to strain fields associated with dislocations is apparent when a section perpendicular to the optic axis is viewed under crossed polarizers. Beryl crystals often exhibit marked optical anomalies under crossed polarizers (*Figure 5*). The present observations have demonstrated that dislocations are one of the main causes of optical anomalies observed in beryl crystals.

Observations parallel to the c-axis

Optical observations were carried out in immersion liquid under crossed polarizers and X-ray topographs were taken parallel to the *c*-axis of uncut prismatic crystals. Since the thicknesses of the crystals are more than a few mm, the quality of the X-ray topographs is poorer than those from the 2 mm section cut perpendicular to the *c*-axis; yet important information was still obtainable.

Figure 5: *An example of commonly observed optical anomalies, most of which are associated with dislocations. Section perpendicular to c-axis. Crossed polarizers. Sample No. 8, Heffernan's mine, Australia. Bar 1 mm.*

In *Figures 6a* (a mosaic photograph of images of internal textures under crossed polarizers) and *6b* (a line drawing of *6a*), the internal textures are most clearly shown in the optical photograph. Also in *Figure 6* the following features can be seen:

1. elongated tube-like inclusions parallel to the *c*-axis, and another type of inclusion concentrated parallel to the {0001} face near the termination of the crystal (F in *Figure 6b*);
2. growth zoning, both strong and faint, parallel to {0001}, {$10\bar{1}0$}, {$11\bar{2}1$} and associated higher order index faces;
3. six growth stages as indicated by labels A to F in *Figure 6b*, where growth zones parallel to {0001} are truncated by rounded boundaries. Starting from the rounded boundaries, growth banding is initially parallel to rounded higher index faces and then to {$11\bar{2}1$} faces, which eventually disappear, and the crystal becomes bounded again only by {0001} and {$10\bar{1}0$};

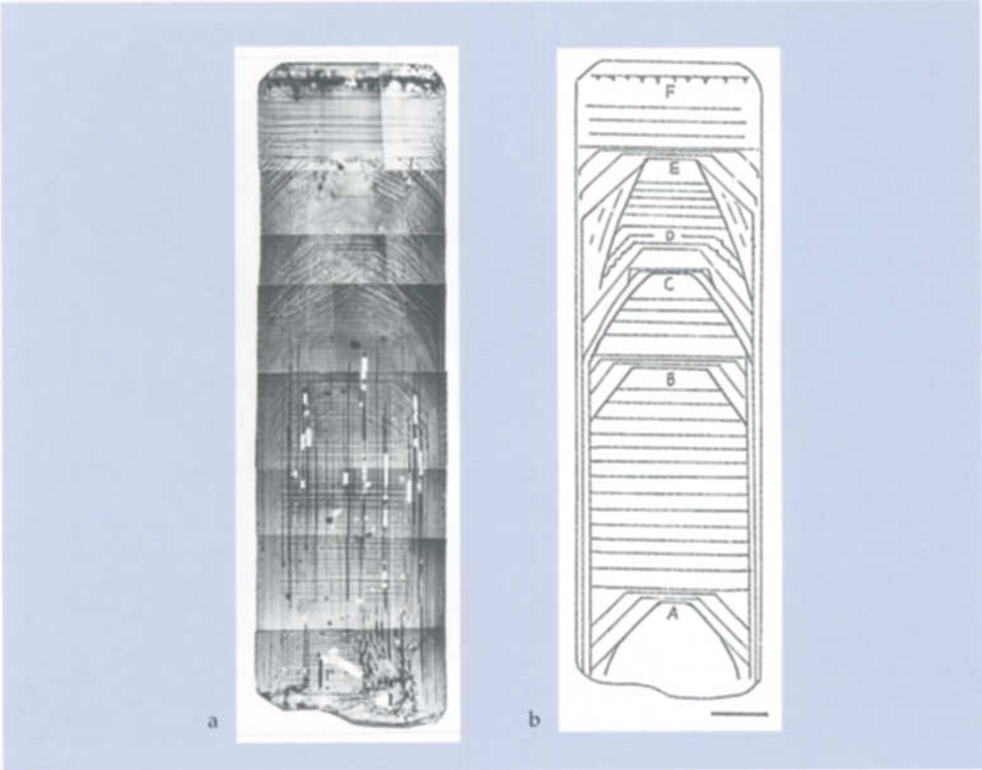

Figure 6: *(a) Mosaic photomicrograph under crossed polarizers and (b) sketch of section in (a) showing the internal texture. Labels A to F in (b) indicate the positions where partial dissolution (A to E) and bubbling (F) took place. Sample No. 10, Heffernan's mine, Australia. Bar 1 mm.*

4. the {0001} growth sector occupies five-sixths of the whole prism in the section, whereas the $\{10\bar{1}0\}$ growth sectors amount to only one-sixth throughout the growth process.

An X-ray topograph of the crystal in *Figure 6* indicated the presence of strain fields. To investigate these strain fields in more detail, another X-ray topograph of another sample from the same locality was taken (*Figure 7*).

Figure 7 clearly shows contrast images parallel and perpendicular to the *c*-axis. A series of bundles of linear contrast images originate from two lines parallel to $\{10\bar{1}0\}$ and nearly perpendicular to the prism surface (indicated by arrows). Their origins are related to faint lines (contrast images) parallel to the *c*-axis in the central zone of the prism.

Figures 8a, b and *c* show higher magnification photographs of tube-like inclusions parallel to the *c*-axis under crossed polarizers. Growth banding, solid and two-phase inclusions, and associated strain fields are discernible. *Figure 8a* clearly shows that the elongated tube-like two-phase inclusions originate from near-platy solid inclusions, either on their own or in clusters. The solid inclusions are, in many cases, inclined to the tube-like inclusions and are located not on the {0001} surface, but on surfaces which are curved or inclined to {0001}. On the basis of their distribution, the starting points of the tube inclusions appear to be closely related to the start of the growth period marked by rounded boundaries, i.e. immediately after the cessation of partial dissolution.

The tube-like inclusions are variable in shape, some with simply tapering tips and others with tips showing crystallographic forms, although all have an aspect ratio (length/breadth) of more than 5. The presence of linear strain fields extending along lines defined by the tubes are visible in *Figure 8c*, indicating that a dislocation is generated from the tip. This is most probably the origin of dislocations running parallel to the c-axis, shown in *Figure 4c*. Negative growth banding is also present (*Figure 8c*). Negative growth banding is due to crystallization of the solution enclosed in the tube-like inclusion, i.e. it constitutes part of the process of formation of a negative crystal.

Both solid and liquid inclusions densely distributed on a plane near and parallel to the {0001} surface (*Figure 6a*) have different properties from the tube-like two-phase inclusions described above. Their distributions in plan and section are shown in *Figures 9a* and *b* respectively. Two-phase inclusions are concentrated below the solid inclusions directly below the plane. The relations between solid and two-phase inclusions are just the reverse of those shown by the first type of inclusions (*Figure 8a*). The two types of inclusions thus cannot have the same origin.

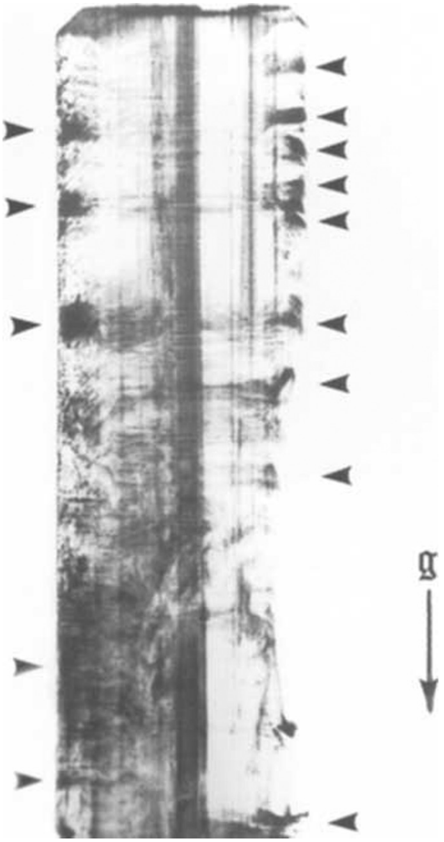

Figure 7: *X-ray topograph of a crystal from Heffernan's mine, Australia. Arrows indicate positions of dislocation bundles perpendicular to the c-axis, 'g' indicates the direction of diffraction plane. Bar 1 mm.*

Discussion

Growth history

At least six stages where partial dissolution took place were distinguished in crystal No. 12 from Heffernan's mine. Similar multiple periods of partial dissolution and re-growth have been observed in beryl crystals from many other localities. We may safely assume that such events took place generally during the formation of many pegmatites. Growth → partial dissolution → re-growth events and morphology changes in association with these events have been encountered in other pegmatitic minerals such as topaz (Isogami and Sunagawa 1975), quartz and tourmaline.

The assumption that pegmatite formation took place under conditions of an open system is confirmed by the fact that directional flow of nutrient solutions during the formation of beryl crystals has been indicated by the growth features in many crystals investigated (*Figure 4*). Similar observations have been reported by Scandale *et al.* (1979, 1990, 1993), and Graziani *et al.* (1981, 1990). In general there is little evidence for directional flow at the early stages of growth, but at the later stages of beryl formation the growth rates on the sides facing the flow of solution were twice as high as on those on the 'lee' side. The increased flow rate resulted in the entrapment of solid inclusions on the interface, which in turn generated dislocations, resulting in further acceleration of the growth rates of the crystal faces facing the flow.

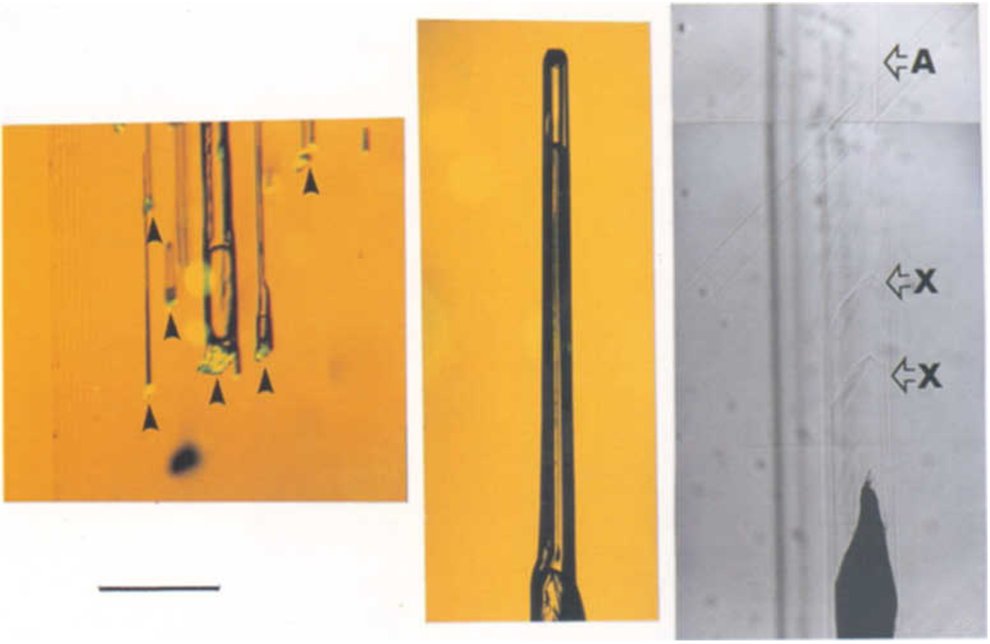

Figure 8: *(a) Photomicrograph of tube-like two-phase inclusions formed adjacent to solid inclusions (indicated by arrows). (b) Negative crystal. (c) Strain field (arrow A) around a dislocation generated from a misfit in the incorporation of the inclusion and negative growth banding (arrows X). Growth banding is also present. Sample No. 10, Heffernan's mine, Australia. Bar 500 µm.*

Based on observations of growth banding in sample No. 10 (*Figure 6*), the morphological evolution of the beryl crystal can be traced, and the morphological importance of the different faces can be evaluated.

At the earliest stage, the crystal developed a hexagonal tabular habit with an aspect ratio (i.e. a ratio of length || c versus width ⊥ c) less than 0.2, and bounded by $\{0001\}$ and $\{10\bar{1}0\}$ faces only. As growth proceeded the aspect ratio increased, and at the final stage the crystal habit became hexagonal prismatic, with a ratio up to 3. The width of the hexagonal prism did not change much and about five-sixths of the width of the prism was already realized during the earliest stage. This implies that the normal growth rate of $\{10\bar{1}0\}$ is much smaller than that of $\{0001\}$. The average ratio of normal growth rates, $\{0001\}$: $\{10\bar{1}0\}$, is about 2 : 1, measured from the widths of concurrently formed growth bands.

Partial dissolution has taken place preferentially and severely at the edges and corners between $\{0001\}$ and $\{10\bar{1}0\}$ faces, resulting in rounded rough hexagonal pyramidal surfaces, with higher $\{hk\bar{i}l\}$ indices than $\{11\bar{2}1\}$. After a period of partial dissolution, regrowth starts and $\{11\bar{2}1\}$ faces start to appear on the partially dissolved rounded surfaces, but eventually completely disappear. The crystal habit changes to a simple hexagonal prism, bounded by $\{0001\}$ and $\{10\bar{1}0\}$ faces only, when the growth conditions are stabilized. The ratio of growth rates of the faces $\{11\bar{2}1\}$ and $\{0001\}$ are around 3.3 to 4.3, and ratio of growth rates of $\{11\bar{2}1\}$ to $\{10\bar{1}0\}$ around 5 to 6.

From the above analysis, it can be concluded that:

1. only $\{0001\}$ and $\{10\bar{1}0\}$ faces are stable and persistent faces in beryl crystals in pegmatitic environments;
2. $\{11\bar{2}1\}$ faces are transient faces which can appear only when certain changes (in the present case, partial dissolution) occur in the growth parameters and which may

disappear when the conditions are stable again; and

3. the order of morphological importance is $\{10\bar{1}0\} > \{0001\} >> \{11\bar{2}1\} >> \{hk\bar{i}l\}$.

Dislocations and inclusions

Two types of inclusions were distinguished: firstly, tube-like two-phase inclusions elongated parallel to the *c*-axis which originate from solid inclusions are common (*Figure 8a*); the second type is shown in *Figure 6a*, where a group of inclusions parallel to {0001} near the termination of a prismatic crystal characteristically show an origin from two-phase inclusions and are capped by solid inclusions.

Most solid inclusions which generate the tube-like inclusions are probably micas distributed principally on partially dissolved beryl faces with their crystal axes inclined to the elongation of the two-phase inclusions. The two-phase inclusions were formed 'behind' the solid inclusion, relative to the direction of crystal growth, where mother liquid was trapped in tubes and normal growth could not proceed. Two-phases appeared in the tube through later cooling and when temperatures had dropped sufficiently. When an inclusion of mother liquid was incorporated, it generated dislocations by mismatch of lattice planes. The dislocations propagate generally along the same direction as the inclusion, parallel to the *c*-axis. The outcrops of these dislocations on the growing {0001} surface acted as growth centres, producing growth spirals. Within the occluded mother liquid, some further growth on the inclusion walls took place, and this resulted in so-called negative crystals (*Figures 8b* and *c*).

The second type of inclusion comprises two-phase inclusions situated beneath the solid inclusions relative to the crystal top (*Figure 9b*). This is the reverse of the relation between solid and liquid inclusions of the first type and may be explained in the following way. If it is assumed that gas bubbles stick on a growing {0001} surface, crystal growth will be retarded underneath, and the bubbles will be surrounded as growth proceeds. This results in the formation of inclusions of the second type, and indicates that gas bubbles were present at this latest stage of beryl formation.

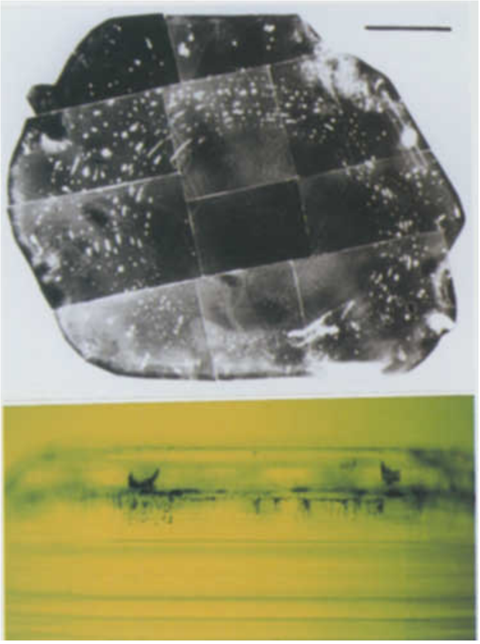

Figure 9: *Cluster of inclusions parallel to (0001), close to the termination of the crystal. Sample No. 10, Heffernan's mine, Australia. (a) Plan view; spiral growth steps on the surface are visible. (b) View perpendicular to {0001} with tube inclusions and growth banding visible. Bar 500 µm.*

In *Figure 4c*, bundles of dislocations parallel to {0001} are visible, i.e. perpendicular to the *c*-axis, and they originate from solid inclusions present along the boundary of two growth stages. In *Figures* 6 and 7, it is obvious that dislocations of this type were generated repeatedly during the whole growth history of the crystal. They originated from a few specific prismatic crystal faces (growth stages), and while some were inherited from earlier dislocations, others were newly generated. There is no doubt that these dislocations acted as sources for growth spirals on $\{10\bar{1}0\}$ faces.

Crystal growth mechanism

Spiral growth on $\{0001\}$ and probably on $\{10\bar{1}0\}$ faces with spiral layers of elemental height, i.e. equal to $d_{(0001)}$ or $d_{(10\bar{1}0)}$ have been confirmed. Both $d_{(0001)}$ and $d_{(10\bar{1}0)}$ are about 0.92 nm, nearly equal. But the normal growth rate of $\{0001\}$ is nearly twice as high as that of $\{10\bar{1}0\}$. To explain this difference, it must be assumed either that the density of dislocation outcrops is twice as high on $\{0001\}$ as on $\{10\bar{1}0\}$ or that the elemental height of spiral steps is a half of $d_{(10\bar{1}0)}$ on $\{10\bar{1}0\}$ faces and equal to $d_{(0001)}$ on $\{0001\}$ faces. Since there is no significant difference in the density of dislocation outcrops on X-ray topographs (e.g. see *Figures 4a* and *c*, or *7*), it is reasonable to assume that the difference in step heights of elemental layers is the probable reason for the growth rate difference between the two faces.

The observed elemental growth spirals on the $\{0001\}$ face are essentially hexagonal, following the symmetry of the face. The step separation normalized by step heights was 10^{4-6}. Although elemental growth spirals were not confirmed on $\{10\bar{1}0\}$ faces in this study because they received natural etching, two types of elongated rectangular patterns are present on these faces. One pattern consists of growth hillocks elongated parallel to the *c*-axis, and the other is a rectangular form with curved steps on the shorter sides parallel to the *c*-axis and straight steps perpendicular to the *c*-axis on the longer sides.

Rectangular growth spirals elongated perpendicular to the *c*-axis, and rhombic growth spirals with the shorter diagonal parallel to the *c*-axis have been reported on $\{10\bar{1}0\}$ faces of beryl and emerald by several workers (Griffin, 1950; Sunagawa, 1964). The first evidence to prove the spiral growth theory (Frank, 1949) was indeed observed on $\{10\bar{1}0\}$ faces of beryl, which exhibited rectangular patterns elongated perpendicular to the *c*-axis, in a form of horseshoe due to co-operation of right-hand and left-hand growth spirals (Griffin, 1950).

The morphology of growth spirals is controlled by the growth parameters. Growth spirals take a circular form when spiral steps are rough, consisting almost entirely of a succession of kinks. They take a polygonal form, with the straight sides in crystallographic directions consistent with the symmetry of the face, when the steps are smooth (low kink density). Thus, in terms of the growth parameters, circular spirals appear when a crystal grows in either higher temperature or higher driving force (supersaturation) conditions.

The step separation between the successive spiral arms is related to the radius of the critical two-dimensional nucleus, which itself is determined by the step free energy and the driving force. This means that for a smaller driving force, i.e. when supersaturation is low, a wider step separation is expected. These relations were theoretically analysed and the ideas were confirmed by observations (see Sunagawa and Bennema, 1982).

Sunagawa (1978) showed that the step separation versus step height ratios are in the order of 10^{4-6} for crystals grown from a vapour phase, and 10^{2-3} for crystals grown from an aqueous solution. The values obtained in this study of 10^{4-6} suggest that the beryls grew from a fluid with a low concentration of nutrients, close to a vapour phase. Hexagonal and rectangular morphologies of observed growth spirals on $\{0001\}$ and $\{10\bar{1}0\}$ faces respectively, imply that the growth temperature was too low to stimulate many kinks and was therefore below the roughening temperature of the respective faces. From both results, a dilute phase for the formation of the pegmatite can be deduced.

Etching effects after the cessation of growth

Etch pits of various sizes were observed on the crystal surfaces. Small etch pits with hexagonal form appear at the outcrops of dislocations. On the surfaces of $\{0001\}$, $\{10\bar{1}0\}$ and $\{11\bar{2}1\}$ faces, much larger and deeper etch pits were formed after the cessation of beryl growth, but the degrees of etching on different crystals differ both within and between localities. Some crystals are not etched, preserving their as-grown surfaces, whereas others are heavily etched and some crystals have been reduced to rounded or irregular forms full of hollows.

Conclusion

From the examination of beryl crystals from four regions by means of polarization microscopy, X-ray topography and etching methods, the following issues have been clarified.

1. The crystallization of hexagonal prismatic beryl crystals in pegmatitic environments is characterized by multiple periods of growth and partial dissolution.
2. The growth rate of $\{10\bar{1}0\}$ is about half that of $\{0001\}$, and about a sixth that of $\{11\bar{2}1\}$. $\{10\bar{1}0\}$ and $\{0001\}$ are stable faces, whereas $\{11\bar{2}1\}$ is a transient face appearing only when growth conditions change.
3. Solid inclusions, principally micas, precipitated on partially dissolved surfaces and were the basis of tube-like two-phase inclusions. These in turn generated dislocations which acted as centres of growth spirals. A second type of two-phase inclusion results from adhesion of gas bubbles in the mother liquid on to the crystal surfaces.
4. The mechanism of spiral growth operated on $\{0001\}$ and $\{10\bar{1}0\}$ faces.
5. Beryl formation in pegmatites probably took place in very dilute liquids, close to vapour phase conditions.
6. After the cessation of growth, some crystals were etched to various degrees with formation of etch pits, whereas other crystals preserved their as-grown surfaces.

Acknowledgements

This work was done at the Institute of Mineralogy, Petrology and Economic Geology, Tohoku University, Sendai, Japan. We acknowledge the help of Dr K. Maiwa, National Research Institute for Metals in X-ray topographic work.

References

Barton, M.D., 1986. Phase equilibria and thermodynamic properties of minerals in the $BeO–Al_2O_3–SiO_2–H_2O$ system with petrologic applications. *Amer. Mineral.*, **71**, 277–300

Frank, F.C., 1949. The influence of dislocations on crystal growth. *Dis. Faraday Soc.*, **5**, 48–54

Graziani, G., Scandale, E., and Zarka, A., 1981. Growth of a beryl single crystal – history of the development and the genetic medium. *J. Appl. Cryst.*, **14**, 241–6

Graziani, G., Lucchesi, S., and Scandale, E., 1990. General and specific growth marks in pegmatite beryl. *Phys. Chem. Mineral.*, **17**, 379–84

Griffin, L.J., 1950. Observation of unimolecular growth steps on crystal surfaces. *Phil. Mag.*, **41**, 196–9

Isogami, M., and Sunagawa, I., 1975. X-ray topographic study of a topaz crystal. *Amer. Mineral.*, **60**, 889–97

Lang, A.R., 1978. Techniques and interpretation in X-ray topography. In: Amelinckx, S., Gevers, R., and van Landuyt, J. (Eds), *Diffraction and imaging techniques in material science,* Vol. 11. North-Holland, Amsterdam. 623–714

Scandale, E., 1996. Growth and sector zoning. Lecture notes of short course on crystal growth in earth sciences, Santa Vittoria d'Alba, Italy, 176–94; X-ray topographic method for minerals, ibid. 361–74

Scandale, E., Scordari, F., and Zarka, A., 1979. Etude des defauts dans des monocristaux de beryl, I. Observations des dislocations, II. Etude de croissance. *J. Appl. Cryst.*, **12**, 70–77, 78–83

Scandale, E., Lucchesi, S., and Graziani, G., 1990. Growth defects and growth marks in pegmatite beryls. *Eur. J. Mineral.*, **2**, 305–11

Scandale, E., Lucchesi, S., and Graziani, G., 1993. Improvements in the growth history reconstruction of a beryl crystal by growth marks. *N. Jb. Miner. Mh.*, H4, 172–84

Sinkankas, J., 1981. *Emerald and other beryls.* Chilton Book Company, Radnor, Pa, USA

Sunagawa, I., 1964. A distinction between natural and synthetic emeralds. *Amer. Mineral.*, **49**, 789–92

Sunagawa, I., 1978. Vapor growth and epitaxy of minerals and synthetic crystals. *J. Crystal Growth*, **45**, 3–12

Sunagawa, I., 1995. The distinction of natural from synthetic diamonds. *J. Gemm.*, **24** (7), 485–99

Sunagawa, I., and Bennema, P., 1982. Morphology of growth spirals: theoretical and experimental. In: Wilcox, W.R. (Ed.), *Preparation and properties of solid state materials,* Vol. 7, Marcel Dekker Inc., New York, 1–129

Yoshimura, J., Koishi, Y., and Suzuki, C.K., 1985. An X-ray topographic study of growth textures of natural beryl crystals. *J. Crystal Growth*, **73**, 275–88

Investigation of the 'haggis rock' from the Scottish Borders

Dr Douglas Nichol

Wrexham, Wales

ABSTRACT: The nature and origin of the peculiar spotted rudite known as 'haggis rock' from the Peebles area of Scotland has long been shrouded in controversy. A re-examination of the rock fragment assemblage indicates that the principal pebble constituents include clayrock, quartz, chert and igneous rocks and that the amount of each varies appreciably even within a single hand specimen. The unusual composition and structure of the rock are attributed to mixing of two independent clast populations; a rounded pebble population resedimented from a shallow water, tidal environment and a matrix population of finer grained material with deep-water affinities associated with oceanic turbidity currents. The 'haggis rock' beds are affected by faulting and appear lensoid in shape. They range up to 5 m thick and are traceable discontinuously for at least 60 km. The 'haggis rock' is amenable to processing using conventional lapidary equipment to produce ornamental pieces but the variations in hardness among the diverse pebbles and between the pebbles and matrix need careful polishing to produce good surfaces.

Keywords: haggis rock, rudite, Scotland

Introduction

The term 'haggis rock' has been used to denote an unusual rudaceous (pebbly) rock that, although dark green coloured, contains sharply contrasting, uniform sized, subrounded to subangular clasts of various colours (*Figure 1*). The striking similarity with Scotland's national culinary dish and ease of working of the rock have resulted in its desultory use in ornaments and costume jewellery. 'Haggis rock' has not been promoted as an ornamental stone and surprisingly has been overlooked by the local tourist industry for the souvenir trade.

Elsewhere in the world, the mining of ornamental rocks has undergone spectacular development during the last 20 years with considerable improvement in both productive processes and the machinery used. Accordingly, a renewed interest in the development potential of 'haggis rock' appears apposite.

The best known occurrences of the rock are restricted to a relatively narrow belt of country in the vicinity of Peebles in the Scottish Borders region of Great Britain (*Figure 2*).

Geological setting

Throughout the Southern Uplands of Scotland, Lower Palaeozoic turbidite sequences predominate. Turbidite is a sedimentary rock inferred to have been deposited from a turbidity flow or

ISSN: 1355–4565

bottom-flowing current laden with suspended sediment. Such a current would be relatively dense and would move swiftly under the influence of gravity down a subaqueous slope and spread over the seabed or the bottom of a lake. Turbidity currents are known to exist at the present day and are believed to have produced the submarine canyons notching the continental slope. They appear to originate in various ways such as by storm waves, tsunamis, earthquake-induced sliding, tectonic movement, over-supply of sediment, and heavily charged rivers in spate. Turbidites are characterised by graded bedding, poor to moderate sorting and well developed sedimentary structures.

The turbidite strata in the Southern Uplands are generally steeply inclined with a consistent northeast-southwest regional strike. They are cut by a series of major northeast-southwest trending strike-parallel faults.

Figure 1: *Samples of the 'haggis rock' illustrating its characteristic texture.*

The principal outcrops of 'haggis rock' lie within thin to thick bedded, sandy and silty turbidite strata which underlie the northern part of the Southern Uplands. The 'haggis rock' forms discontinuous lenses within the Marchburn Formation, a sub-unit of the Leadhill Group of mid-Ordovician age and adjacent to the Southern Upland Fault (SUF) (*Figure 2*). Possible correlatives of the 'haggis

Figure 2: *Sketch map showing location of the 'haggis rock' outcrops. After Ritchie and Eckford (1936).*

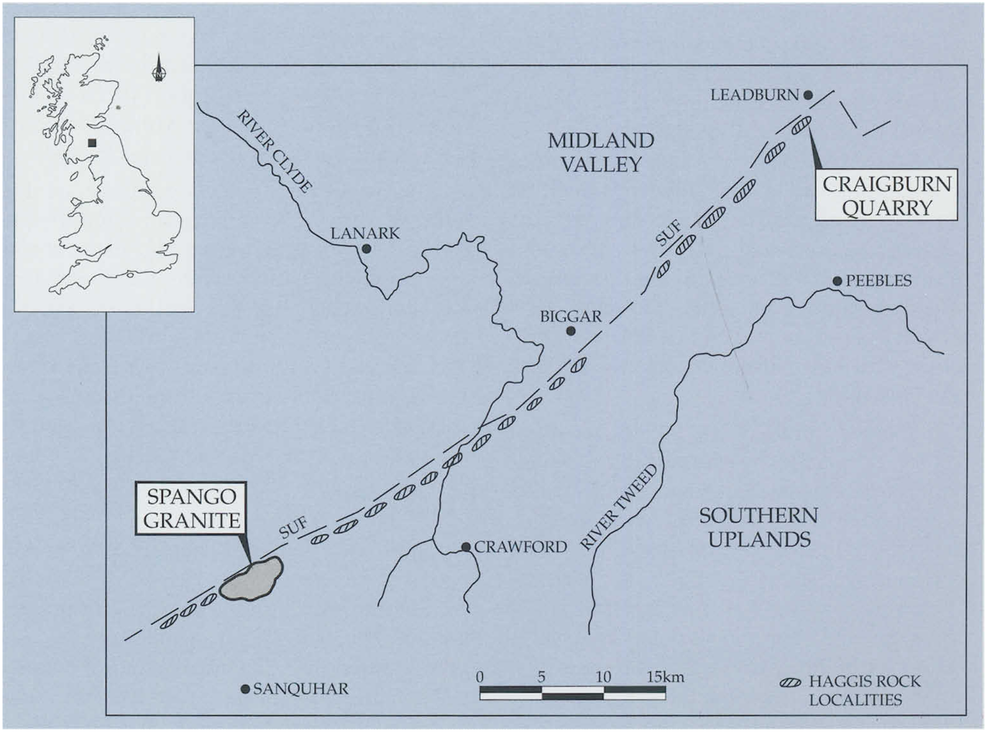

rock' have been recognized by Kelling (1961) in the Portpatrick Formation of southwestern Scotland.

The 'haggis rock' can be most readily examined in the disused Craigburn quarry situated alongside the A703 Edinburgh-Peebles Road, 1.5 km south of Leadburn crossroads (Stone, 1992). National Grid Reference NT 237544 applies. Here, the beds strike northeast and dip at moderate to steep angles northwestwards. Fault-bounded outcrops of 'haggis rock' are observationally accessible at the northeastern end of the quarry.

Historical background

The term 'haggis rock' is acknowledged to be of considerable antiquity having been applied to the rock in olden days by quarrymen. Indeed mention is made of the rock in the explanatory notes of a geological map sheet published in 1871 where the name is stated to be of local origin. Other early accounts of the 'haggis rock' are given by Peach and Horne (1899) who provided hand specimen descriptions and Ritchie and Eckford (1936) who carried out petrographic examination of samples collected from several localities along the outcrop belt. Ritchie & Eckford (*op cit*) matched approximately 80% of the rock-fragment assemblage with older rocks cropping out nearby and concluded that a large part of the material composing the 'haggis rock' is of local derivation. They also considered the narrow grain size distribution and subrounded shape of the pea-sized clasts indicative of sedimentation in a quiet, shallow, inshore, marine environment affected by tidal scour processes.

In marked contrast, the strata associated with the 'haggis rock' are turbidite (greywacke and mudstone) beds that are widely described as accumulations associated with pelagic, open-ocean and deep water environments of deposition (*e.g.* Leggett, 1987, and references therein). In this deep-water setting, the 'haggis rock' apparently represents a deposit of coarse-grained turbidite, perhaps the product of a single turbidity flow instigated by a regional tectonic event during Ordovician time.

Thus two very different settings have been proposed for the depositional environment of the 'haggis rock' and some uncertainty remains. From this brief review of the literature it is evident that the origin of the 'haggis rock' remains a matter of controversy. Conceivably, the 'haggis rock' comprises two independent clastic populations. First, fine grained turbidite material similar to that composing the neighbouring strata and secondly, the pebbly material that originated in a shallow water environment but was subsequently transported from this provenance by turbidity currents and recycled into the deeper waters of the basin of accumulation. This postulated origin accords with the distinctive bimodal grainsize distribution exhibited by the 'haggis rock'. These two clastic populations combine to give a rock which classifies as either a pebbly turbidite or fine conglomerate.

Composition

The most striking feature of 'haggis rock' is the mosaic of colour displayed by the various pebble constituents. Lithologies are listed in *Table I* together with colours quoted with numerical designations based on the Munsell system of colour identification (Rock-Colour Chart Committee, 1963). Munsell colours were determined on polished specimens.

The rock-fragment assemblage of the 'haggis rock' consists predominantly of clayrocks with green, grey and black shales and brown mudstone. White quartz and grey and black chert are subdominant. Igneous rock-fragments constitute a diverse group and the relative abundance of each clast type varies appreciably even within a single hand specimen. The igneous clast types include red jasper, purple volcanic rock, pink felsite and granite and dark green gabbro, dolerite, andesite and spilite.

The matrix material consists of sand, silt and clay sized particles. Following sedimentation and burial, regional metamorphism partially transformed the finer grained detrital matrix material causing minor mineralogical reconstitution. The principal metamorphic mineral is chlorite.

Table I: *Composition and colour of the pebble clasts in the 'haggis rock'.*

Rank No.	*Lithologies*	*Colour*	*Colour designation (Munsell)*
1	Clayrock	Pale brown	5YR 5/2
		Light brown	5YR 5/6
		Light brown	5YR 6/4
		Moderate brown	5YR 4/4
		Moderate brown	5YR 3/4
		Brownish black	5YR 2/1
		Dark greenish grey	5GY 4/1
2	Quartz	White	N9
		Very light grey	N8
3	Chert	Black	N1
		Medium grey	N5
4	Igneous rocks	Medium light grey	N6
		Moderate red	5R 5/4
		Moderate red	5R4/6
		Greyish red	10R 4/2
		Moderate yellowish brown	10YR 5/4
		Dark yellowish brown	10YR 4/2
		Greyish orange	10YR 7/4
		Greyish green	5G 5/2
		Dark greenish grey	5GY 4/1

Physical features

The 'haggis rock' beds range up to 5 m thick and are traceable discontinuously for at least 60 km along the line of strike. They are generally affected by faulting and so outcrops appear lensoid in shape.

Certain samples of 'haggis rock' display a poorly developed foliation associated with the main phase of regional metamorphism and folding. Other structural features include faults, joints, minor fractures, tension cracks, discordant veins and open cavities. In the near surface zone, weathering has affected these tectonic dislocations and rock defects and they commonly feature localised discolouration and a susceptibility to disintegration. Weathered and fresh rock range from moderately weak to weak and strong to very strong respectively.

The known deposits of 'haggis rock' either crop out or are concealed beneath thin overburden and can therefore be worked by opencast methods. Borehole exploration would indicate the subsurface extent and quality of specific 'haggis rock' deposits and provide geotechnical information for quarry design purposes.

Processing

Selected material can be processed satisfactorily using conventional slabbing, trimming, tumbling and polishing equipment.

The textural features and variable grain composition affect the polishing characteristics. The softer matrix material tends to undercut producing an uneven polish. To a much lesser extent, variations in hardness and toughness of the pebble clasts

Figure 3: *'Haggis rock' ornaments.*

also cause irregularities on polished surfaces. Nonetheless, a variety of items have been successfully produced including pendants, paperweights, bookends and costume jewellery pieces (*Figure* 3).

Conclusions

'Haggis rock' formed in a sedimentary environment. It is an unusual pebbly turbidite or fine conglomerate that crops out prominently in the Peebles district of the Scottish Borders. It appears associated with the turbidite strata within the Marchburn Formation which is of Ordovician age.

The 'haggis rock' is characterized by a bimodal grainsize distribution and a mosaic of colour displayed by the pebble constituents. It is suggested that these pebbles were recycled from a shallower water, tidal environment and subsequently combined with finer grained detrital material during turbidite sedimentation in a deep-water ocean basin.

These features confer a visual likeness to Scotland's national culinary dish and prompt considerable interest in the material as an ornamental stone.

The quantity of 'haggis rock' available for extraction appears substantial. It occurs as concordant, lenticular bodies that range up to 5 m thick and which are traceable discontinuously for at least 60 km.

A range of ornaments and jewellery including paperweights, bookends, pendants and brooches can be produced using conventional lapidary equipment. Surprisingly, no recent commercial endeavour has been undertaken to exploit the 'haggis rock' for the ornamental stone market. Further exploration appears warranted to assess the potential for commercial development.

Acknowledgements

Thanks are extended to Miss Angela Hughes for preparing the figures.

References

Kelling, G., 1961. The stratigraphy and structure of the Ordovician rocks of the Rhinns of Galloway. *Quarterly Journal of the Geological Society, London*, **117**, 37–75

Leggett, J.K., 1987. The Southern Uplands as an accretionary prism: the importance of analogues in reconstructing palaeogeography. *Journal of the Geological Society, London*, **144**, 737–52

McAdam, A.D., Clarkson, E.N.K., and Stone, P., 1992. *Scottish borders geology: an excursion guide.* Edinburgh Geological Society, Scottish Academic Press, Edinburgh

Peach, B.N., and Horne, J., 1899. *The Silurian rocks of Britain. Volume 1, Scotland.* Memoir of the Geological Survey, United Kingdom

Ritchie, M., and Eckford, R.J.A., 1936. The 'Haggis Rock' of the Southern Uplands. *Transactions of the Edinburgh Geological Society*, **13**, 371–7

Rock-Colour Chart Committee, 1963. *Rock-Colour Chart.* Geological Society of America, New York

Stone, P., 1992. Noblehouse, Lamancha. In: A.D. McAdam, E.N.K. Clarkson and P. Stone (Eds), *Scottish Borders Geology: an excursion guide*, Scottish Academic Press, Edinburgh, 135–140

A new Brewster-angle meter for gem identification

R.R. Harding,[1] P.G. Read[2] and N.W. Deeks[1]

1. GAGTL, 27 Greville Street, London EC1N 8TN
2. Bournemouth, Dorset

ABSTRACT: A portable, battery-operated meter for determining the Brewster angles of faceted gemstones using polarised laser light is described. The Brewster angle range covered is 54–72°, approximately equivalent to a refractive index range of 1.4–3.1. Birefringence of more than 0.01 can also be measured, and all measurements can be made without the need for contact fluid.

Keywords: Brewster angle, gemstone, laser source, refractive index

Introduction

Brewster's Law states that when an incident monochromatic ray meets the flat surface of an optically denser medium, and the reflected ray from this surface is at 90 degrees to the associated refracted ray in that medium, only those rays polarised in the plane of that surface will be reflected (this is why vertically polarised sun glasses reduce the glare from horizontal reflecting surfaces such as the sea). At the Brewster-angle A in *Figure 1*, the RI of the denser medium is equal to tan A.

The first recorded attempt to use the angle of polarization to measure the RI of a

Figure 1: *Where the reflected and refracted rays are at 90°, angle A is the Brewster angle and the reflected ray is polarised parallel to the reflecting surface.*

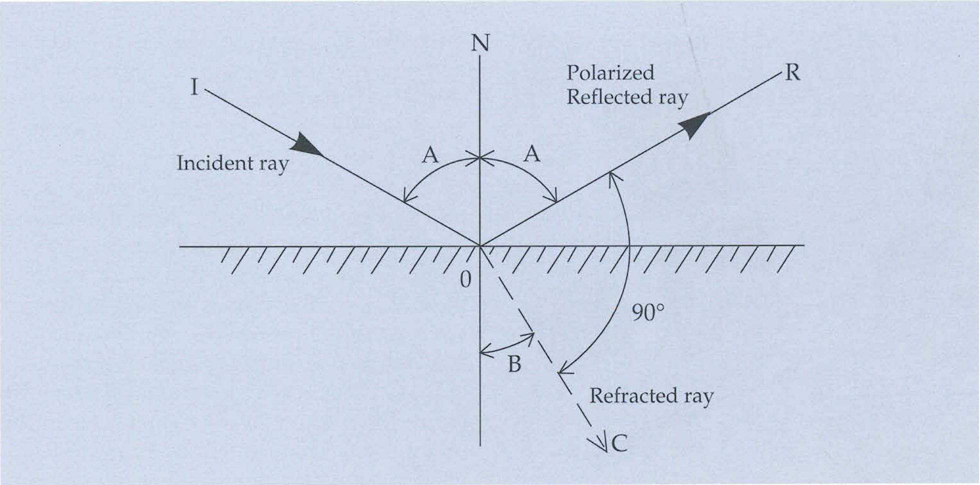

ISSN: 1355–4565

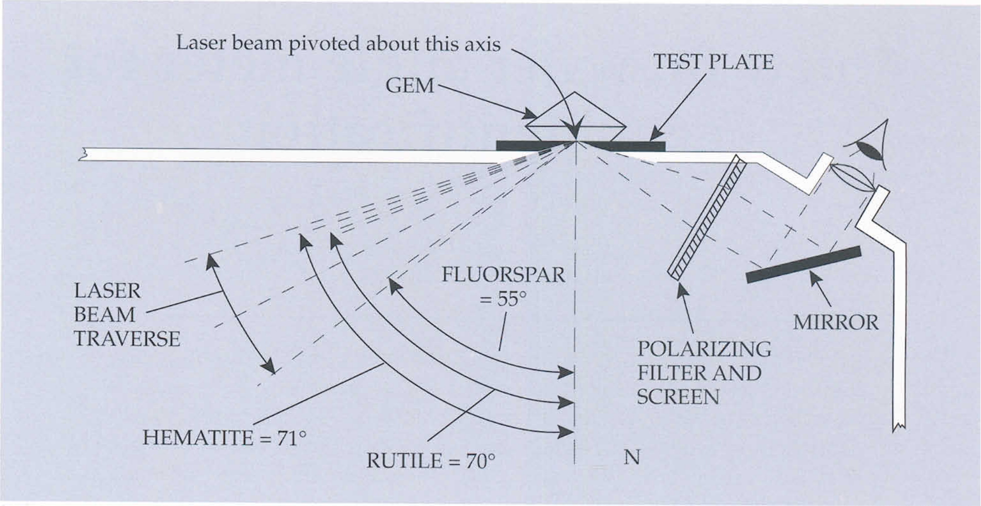

Figure 2: *Schematic diagram showing how a Brewster angle can be measured to identify a gemstone. The reflected ray from the laser beam is passed through a vertically polarised filter and imaged on a translucent screen. At the Brewster angle the reflected light falling on the screen drops to a minimum.*

gemstone was made by B.W. Anderson[1] in 1941 while testing the newly introduced Polaroid polarizing sheet. The method he used involved the construction of a pantograph type mechanism in which one arm was used to rotate a beam of incident light about the surface of a gem while the second arm duplicated this angular movement. An eyepiece, fitted with a sample of the new filter, which was set for vertical polarisation against the horizontally-viewed plane of the gem's surface, was attached to the second arm. This allowed the viewer to follow the movement of the reflected ray as the incident ray was rotated. At the Brewster-angle of the gem the eyepiece filter reduced the intensity of the now horizontally polarized reflected ray to a minimum.

However, the mechanical complication of a pantograph can be avoided by passing the reflected ray through a polarizing filter orientated for vertical polarization and then imaging the result on a translucent screen (*Figure 2*)[2]. Between 1979 and 1994 several experimental Brewster-angle refractometers were developed[3,4,5,6] ranging from fully electronic versions using helium neon lasers, photo-electric detection of the null point, and direct RI readout (in the recession of the late 80s these were considered to be too costly to be commercially viable) to simpler optical screen-imaging versions using miniature solid state lasers. It is this latter method that is used in the GAGTL instrument (*Figure 3*) which, for reasons that will become clearer later in this report, has been called a 'Brewster-angle meter' rather than refractometer.

Figure 3: *Two views of the GAGTL Brewster-angle meter. The operate button on the test plate cover is used to switch on the laser.*

The Brewster-angle meter

The GAGTL Brewster-angle meter uses a solid state laser with a wavelength in the red of 670 nm as the light source. It would have been in many ways desirable to use a low-cost laser having an output at the sodium wavelength of 589.3 nm but one is not yet available. However, using a 670 nm laser does have the advantage of separating the high-dispersion strontium titanate from the lower-dispersion diamond (both having almost identical refractive indices at 589.3 nm).

The laser is mounted in a carriage which is pivoted in an arc around a test aperture by means of a control knob calibrated in Brewster angles from 54 to 72 degrees. The reflected ray from a gemstone placed over the test aperture is passed through a vertically polarized filter and imaged on a translucent screen.

Using the eye as a very sensitive detector to low levels of light intensity, the angle of the laser beam is adjusted until the image of the reflected light falls to a point of minimum brightness. This occurs at the Brewster-angle for that gemstone where the now horizontally-polarized reflected ray is reduced to a minimum by the vertically-polarized filter. This angle is read from the calibrated laser control knob and the gemstone identified from a set of tables.

The reason that the instrument has been designated a meter rather than a refractometer is to avoid confusion with the currently well known refractive indices derived from measurements based on the 589.3 nm wavelength. If Brewster angles obtained at 670 nm were used to derive equivalent refractive indices at 589.3 nm, values of dispersion for each individual gem would have to be assumed. Such assumptions would introduce an element of uncertainty which may be quite significant for gems whose dispersions were not well known and so the simpler procedure of recording the angle was adopted.

Because the reflectivity of a gemstone is related to its refractive index, this can make it difficult to detect the exact angle of minimum brightness for high RI gems. To control image brightness, a polarising filter is inserted behind the eyepiece lens. The eyepiece can then be used as an intensity control and rotated until there is just enough light to detect the minimum intensity Brewster-angle. Normal focusing of the image is by push-pull adjustment.

Identification of gems

The refractive index range covered by the meter is 1.40 to 3.1. Brewster angles can be measured to an accuracy of 0.2° at the lower end of its range and to an accuracy of 0.4° at the top end. Double refraction can be measured by rotating the stone in 30 degree increments on the test platform, but becomes increasingly difficult to detect for values around and below 0.2° (equivalent to birefringence of 0.01). If not detectable by the meter, the presence or absence of double refraction can be verified by using a polariscope. The method is particularly relevant in identifying gems of high RI and a selection, in ascending order of Brewster angle, is given in *Table I.* The range of angles

Table I: *Brewster angles of a selection of gems.*

Brewster angle	*Gem*
55.0-55.3	*Fire opal*
57.0, 57.1	Quartz
58.2, 58.5	Tourmaline
59.5-59.8	Spinel (natural)
60.3, 60.4	Sapphire, ruby
60.6-61.4	Zircon (low)
60.8-61.0	Spessartine garnet
61.2	YAG
61.8	Demantoid garnet
61.4, 63.0	Titanite (sphene)
62.0, 63.0	Zircon (high)
62.3, 62.4	Scheelite
62.9	GGG
64.8-65.1	CZ (colourless)
65.6, 66.2	Lithium niobate
66.5-66.9	Strontium titanate
67.4	Diamond
69.0, 69.3	Synthetic moissanite
68.2, 70.2	Synthetic rutile

N.B.: Readings from birefringent stones separated by a comma; a dash indicates a range of readings possible from an isotropic stone because of compositional variation.

given for some gems reflects both theoretical (birefringence) variation and that found from practical measurement.

Compared to the standard refractometer, the Brewster-angle meter has the advantage of providing a wide measurement range without the need for a contact fluid. Compared to the reflectance meter, it is less sensitive to the surface condition of the gem, a less than perfect polish simply diminishing the sharpness of the minimum brightness setting of the laser angle rather than giving a misleading low reading. However, a clean grease-free gemstone test surface will, with most gemstones, produce an improved image of the reflected beam in which the precise Brewster-angle is indicated by a dark horizontal band bisecting the viewed image.

If one wishes to obtain the RI of a gem at 589.3 nm from its Brewster angle at 670 nm, this can be estimated if one assumes that the gem's dispersion varies in a linear way with wavelength. The RI can be obtained using the following formula:

$$\text{RI at 589.3 nm} = \text{Tan } A_G + \frac{670.0 - 589.3}{686.7 - 430.8} \times D_G$$

$$= \text{Tan } A_G + 0.3154 \times D_G$$

where A_G = Brewster angle of gem; D_G = dispersion of gem as measured between the wavelengths 686.7 and 430.8 nm.

Safety features

The instrument is powered by two standard AA batteries. For safety, and to give maximum battery life, the laser can only be switched on (by means of a push button) when the test platform cover is in position. The laser used in this instrument is a Class IIIa device (rated at 5 mW) and, like pen-type laser pointers, its beam can be harmful to the eyes if viewed directly. When in use, the meter's laser beam is reflected by the surface of the gemstone under test and imaged via a polarising filter onto a translucent screen. It is this diffused and much weaker image of the gemstone surface, and not the direct laser beam, which is viewed, via a mirror, through the instrument's eyepiece.

References

1. Anderson, B.W., Brewster Angle, *Gemmologist*, 1941, X, 61–3
2. Read, P.G., An experimental Brewster-angle refractometer, *J. Gemm.*, 1979, XVI, **8**, 537–41
3. Yu, R.M., The Brewster-angle refractometer, *Gems & Gemology*, Winter 1979, 245–7
4. Read, P.G., Further development of the Brewster-angle refracometer, *J. Gemm.*, 1988, **21**, 1, 36–9
5. Landais, E., A universal automatic refractometer – the Dialsan, *Revue de Gemmologie a.f.g.*, 1988, **96**, 7–8
6. Read, P.G., An experimental optical Brewster-angle refractometer, *Gemm. Assoc. of New Zealand Newsletter*, Nov. 1994, 5–7

Abstracts

Diamonds

Gems and Minerals

Diamonds

He, Ar and C isotopes in coated and polycrystalline diamonds.

R. Burgess, L.H. Johnson, D.P. Mattey, J.W. Harris and G. Turner. *Chemical Geology*, **146**(3–4), 1998, pp 205–17.

Helium, Ar and C isotopic measurements were carried out on different qualities of industrial grade and polycrystalline diamonds from Africa and Brazil, including coated and cloudy diamonds, which contain abundant volatile-rich micro-inclusions, and framesites and carbonados, which consist of aggregates of micron-sized diamond crystals interspersed with mineral inclusions. In order to selectively release the primary trapped He, the diamonds were analysed using an *in vacuo* crushing technique. The He data were combined with Ar, K and U data, obtained from ^{40}Ar–^{39}Ar stepped-heating studies of irradiated fractions of the diamonds, and bulk C isotope data obtained from crushed residues. Results indicate that coated and cloudy diamonds best preserve a mantle signature, with ^{3}He/^{4}He values of 1–7 Ra and δ^{13}C of –5 to –6 ‰. Coated diamonds have high He and Ar concentration of $10^{-6} – 10^{-5}$ cm^3/g. Framesites have ^{3}He/^{4}He values 0.1–3 Ra and bimodal δ^{13}C, with modes at –6 and –20 ‰. Carbonados have the lowest δ^{13}C values ≤ –25 ‰ and ^{3}He/^{4}He of < 0.1 Ra. U and K concentrations increase progressively from coats to framesites to carbonados. Whilst it is tempting to attribute low C, low δ^{13}C and high U to the influence of subducted crustal material, it is likely that implantation of ^{4}He by U- and Th-rich minerals adjacent to the micro-diamonds is also a possible cause of low He isotope ratios. J.F.

Twinning in natural diamond. II. Interpenetrant cubes.

W.G. Machado, M. Moore and A. Yacoot. *Journal of Applied Crystallography*, **31**, 1998, pp 777–82.

Single crystals of natural diamond which exhibit an approximately cubic morphology are known to have grown either: (a) by non-faceted cuboid growth or (b) by fibrous growth branching in a multiplicity of (111) columns, to give a mean surface orientation of {100}. Interpenetrant twins of diamond are uncommon; when they occur they are usually coloured and appear (by X-ray topography) to have been formed by fibrous growth on a twin origin, with the 14 growth sectors adequately filled by fibres, without the necessity of branching. R.A.H.

Behandlung natürlicher Diamanten zur Reduzierung der Gelb-oder Braunsättigung.

K. Schmetzer. *Goldschmiede Zeitung*, **97**(5), 1999, pp 47–8.

An announcement by the firm of Lazare Kaplan International of a stated new process of improving the colour of natural diamond has agitated the trade. The statement by LKI announces an irreversible process of decreasing yellow and brown tones in natural stones. The method of treatment was developed by the General Electric Company and according to the statement made by LKI was undetectable. More than one hundred stones treated by this method have been passed by workers without the artificially induced colour being noticed. The treated stones have come specifically from the Antwerp firm of Pegasus Overseas Limited. Pegasus OL alone is selling the treated stones. Despite this limited outlet the arrival on the market of these stones is not merely a rumour and it is serious when diamonds pass freely into the market with certification.

The available technical literature has had to be searched and in particular the literature of patents, to see whether previously published reports bear on the question in any way. Two reports describing the reduction of yellow colouration in diamond have so far been found, one involving a high-pressure/high temperature method, the other involving irradiation/high pressure/high temperature. M.O'D.

A noble gas study of cubic diamonds from Zaire: constraints on their mantle source.

N. Wada and J.I. Matsuda. *Geochimica et Cosmochimica Acta*, **62**(13), 1998, pp 2335–45.

Analyses are presented of 16 diamond samples for their isotopic compositions and concentrations of He, Ne, Ar and Xe. The results show slight but significant

Abstractors

J. Flinders	J.F.	R.A. Howie	R.A.H.	P.G. Read	P.G.R.
R.K. Harrison	R.K.H.	M. O'Donoghue	M.O'D.	G.W. Robinson	G.W.R.

For further information on many of the topics referred to, consult *Mineralogical Abstracts*

ISSN: 1355-4565

differences from the noble gases and their isotopes in MORB, which are discussed. A nucleogenic origin for excess ^{21}Ne in the diamonds relative to MORB is consistent with their lower ^{3}He/^{4}He ratios. Positively correlated excesses of ^{129}Xe and $^{131-136}$Xe of ≤ 10 % relative to atmospheric Xe ratios, are attributed to the decay of extinct ^{129}I and spontaneous fission of extinct ^{244}Pu and/or extinct ^{238}U, respectively. From the ^{3}He/^{4}He ratios and ^{40}Ar/^{36}Ar ratios, it is suggested that the cubic diamonds crystallized in a fluid which separated from a mantle source previously enriched in incompatible elements. R.K.H.

Formation of diamond with mineral inclusions of 'mixed' eclogite and peridotite paragenesis.

W. Wang. *Earth & Planetary Science Letters*, **106**(3–4), 1998, pp 831–43.

Two diamonds which contain both ultramafic and eclogitic mineral inclusions in the same diamond hosts were studied. Diamond L32 contains seven Fe-rich garnets, four omphacites and one olivine inclusion, whilst diamond S32 contains four olivine, one sanidine and one coesite inclusion. Both garnet and omphacite inclusions have a basaltic bulk composition, similar to those from other localities. All the garnet and omphacite inclusions in diamond L32 have positive Eu anomalies (Eu/Eu* 1.64–1.79). These observations imply that mantle eclogite is the metamorphic product of subducted ancient oceanic crust. Olivine inclusions from both diamonds have *mg* values (91–92) lower than normal olivine inclusions in diamonds from the same kimberlite pipe (92–95). A suggested model for formation of diamonds with mixed mineral inclusions invokes ascending diamond-bearing eclogite (recycled oceanic crust) entrained in mantle plumes, undergoing extensive partial melting, whereas the ambient peridotite matrix remains subsolidus in the diamond stable field. This provides a mechanism for transporting diamond from an eclogitic to an ultramafic host. Subsequent regrowth of diamond captures mineral inclusions of different lithological suites. Partial melts of basaltic sources interact with the surrounding peridotite, producing lower *mg* values of the coexisting olivine inclusions in the studied diamonds. Diamonds with 'mixed' mineral inclusions demonstrate that plume activity occurred in Archaean cratons. J.F.

Twinning in natural diamond. I. Contact twins.

A. Yacoot, M. Moore and W.G. Machado. *Journal of Applied Crystallography*, **31**, 1998, pp 767–76.

Growth histories of contact twins of natural diamonds have been elucidated by non-destructive techniques of X-ray topography, using both conventional and synchrotron sources. The common 'triangular' contact twin (macle) results from {111} faceted growth from a central nucleation site, sometimes marked by an inclusion. If this period of growth is followed by one of dissolution, then the twinned rhombic dodecahedron may result; the dissolution shape of a twinned octahedron is the same as the twin of the dissolution shape of the octahedron. A peritropic twin consists of two macles fortuitously joined on their common (111) facets in only approximate twin orientation. In all these variants, the composition 'plane' may be far from planar, resulting from intergrowth of one twin component into the other. R.A.H.

Gems and Minerals

Australian Chinese writing stone.

A. Bevan, P. Downes and J. Bevan. *Australian Gemmologist*, **20**(5), pp 178–81, illus. 3 black-and- white, 1 map.

This appraisal of a decorative porphyritic basaltic rock from the Pilbara region of Western Australia details its geological occurrence and its mineralogy, petrology and physical characteristics. Also known as Chinese writing stone (some groups and sprays of lath-like crystals look like characters in Chinese writing), and, in Australia, as 'chook's foot rock' (the laths resembling chicken's feet), this material is an attractive carving rock which could be fashioned into a variety of items. P.G.R.

[Mineralogy of rhodonite deposits of the Middle Urals.] (Russian with English abstract)

A.I. Brusnitsyn. *Proceedings of the Russian Mineralogical Society*, **127**(3), 1998, pp 1–11.

Mineralogical details are presented for the minerals of the rhodonite deposits at Malosedelnikovskoye, Kurganovskoye and Borodulinskoye, all of which are worked out of decorative material. Analyses are tabulated for rhodonite, pyroxmangite, tephroite and spessartine, and a list of 30 other associated species is presented. R.A.H.

Occurrence and distribution of 'moganite' in agate/chalcedony: a combined micro-Raman, Rietveld, and cathodoluminescence study.

J. Götze, L. Nasdala, R. Kleeberg and M. Wenzel. *Contributions to Mineralogy & Petrology*, **133**(1–2), 1998, pp 96–105.

Raman, XRD (using Rietveld refinement), and CL techniques were used to measure the content and spatial distribution of the silica polymorph moganite, considered to represent periodic Brazil-law twinning of α-quartz at the unit-cell scale, in agate/chalcedony samples of different origin. Homogeneous standard samples, which included the nearly α-quartz-free moganite type material from Gran Canaria, were analysed by XRD and Raman spectroscopy to compare results from these techniques, and provide a calibration curve for the Raman results. However, because different length scales were analysed by each technique, the 'moganite content' in microcrystalline SiO_2 samples measured by Raman spectroscopy (short range order) was considerably higher than when measured by XRD (long-range order). The low XRD values result from the presence of moganite nanocrystals, nano-range moganite lamellae and single Brazil-law twin-planes, that are detected by vibrational spectroscopy but too small to be detected by XRD. High-resolution Raman analysis can measure moganite content, and its spatial variation in microcrystalline silica samples, with a lateral resolution in the µm-range. Variations in the moganite-to-quartz ratio are revealed by varying intensity ratios of the main symmetric stretching-bending vibrations (A_1 modes) of α-quartz ($465\ cm^{-1}$) and moganite ($502\ cm^{-1}$), respectively. Traces of Raman microprobe analyses ⊥ the rhythmic zoning of agates showed that the moganite-to-quartz ratio is often not uniform; exhibiting a cyclic pattern that correlates with the observed CL pattern (colour and intensity). Variations of C1 and Raman data between single bands in agates suggest alternating formation of fine-grained, highly defective chalcedony intergrown with moganite, and coarse-grained low-defect quartz. Multiple zones indicate dynamic internal growth during self-organizational crystallization from silica-rich fluids. J.F.

Neolithic jadeitite axe from Sobotište (western Slovakia).

D. Hovorka, Z. Farkaš and J. Spišiak. *Geologica Carpathica,* **49**(4), 1998, pp 301–4.

Numerous archaeological artefacts suggest the presence of a Neolithic population in the area between the villages of Kunov-Sobotište-Podbranc, W Slovakia. Early linear pottery of the Baden culture, together with polished stone artefacts, constrain the time period as early Neolithic to middle Aeneolithic. Among the polished stone artefacts one, an axe, is unique for its use of jadeitite. EPMA of the axe (Na_2O 9.86–14.91 wt. %) as well as results of detailed studies from N Italy and the W Alps, showed the rock had a complicated geological history. Since the use of jadeitite as a raw material has not been previously recorded for finds from either the E Alps, Bohemian Massif or W Carpathians, it is inferred that the finished product was imported from a distant area, such as NW Italy. J.F.

Mineralien aus der Reisseckgruppe (Kärnten).

G. Kandutsch. *Lapis,* **23**(6), 1998, pp 27–45, illus. in colour.

Gem-quality crystals of aquamarine, scheelite, smoky quartz and amethyst are found in the Reisseck group of mountains of the Hohe Tauern, Carinthia, Austria. Examples are described and illustrated. M.O'D.

Il ghiaccaio di Argentière.

G. Monistier. *Rivista mineralogica italiana,* **22**(2), 1998, pp 30–7.

Exceptional and gem-quality crystals of smoky quartz with some fine pink fluorite and reddish-brown sphene, occur in the area of the Argentiere glacier, Chamonix, France. Specimens can be found in the mineral shows held at Chamonix. M.O'D.

The Rozná pegmatite field, western Moravia (Czech Republic).

D. Nemec. *Chemie der Erde: Geochemistry,* **58**(3), 1998, pp 233–46.

Further investigation of the area surrounding the late Variscan Li-bearing pegmatite dyke, on the Hradisko hill at Rozná, has revealed a coarse-grained muscovite-pegmatite dyke swarm, with the same geochemistry as the main dyke, and which together represent a pegmatite field. Li mineralization is confined to the quartz zone, and mostly consists of lepidolite of variable composition. A sky-blue, low-Fe, low-Mn elbaite is typical of the Rozná pegmatite field. Hydrozircon, cassiterite, monazite, goyazite and eosphorite (the last two from alteration of amblygonite-montebrasite) were examined in detail; EPMA results are given. J.F.

Blue quartz from the Antequera-Olvera ophite, Málaga, Spain.

J.C. Romero Silva. *Mineralogical Record,* **27**(2), 1996, pp 99–103.

Crystals of blue quartz occur as fracture fillings and in vugs in altered ophite in gypsum near Antequera, Malaga, Spain. The colour is due to inclusions of the rare mineral aerinite. Laser ablation MS show a high iron content for the aerinite. G.W.R.

Rubine und verschiedenfarbige Saphire aus Ilakaka, Madagascar.

K. Schmetzer. *Lapis,* **24**(6), 1999, pp 46–7.

Gem-quality ruby and variously-coloured sapphires are reported from Ilakaka, Madagascar, in an area close to the Isalo National Park. Crystals ranging between 0.5 and 2 ct occur as rubies or as sapphires coloured blue-violet, violet, reddish-violet, yellow or orange. Twinning lamellae have been observed as inclusions. Details of the absorption spectra are given. M.O'D.

Die wundervollen Achate von Ojo Laguna, Chihuahua, Mexiko.

J. Zenz. *Mineralien Welt,* **10**(4), 1999, pp 58–63.

Exceptional and highly-coloured specimens of agate are described from Ojo Laguna, Chihuahua, Mexico. The location borders Highway no 45 and is about 230 km from the Texan city of El Paso. M.O'D.

BOOK REVIEWS

The Koh-i-Noor diamond

I. Amini, 1994. Roli Books, New Delhi. pp 257, softcover. £6.95. ISBN 81 7436 003 4.

Very readable mixture of legend and fact with the Koh-i-Noor diamond as a theme. M.O'D.

Chanel joaillerie

F. Baudot, 1998. Editions Assouline, Paris. pp 78, illus. in colour. Price on application.

Short history of the life of Gabrielle 'Coco' Chanel and of her innovative jewellery designs. Very well illustrated. M.O'D.

Diamonds

M. Dundek, 1999. Noble Gems International, London. pp 31, £7.00. ISBN 0 9535371 0 2.

Short but well-produced coverage of the production, grading and valuation of gem diamonds aimed at the student or trade beginner. Quite a lot of information is included and there are some good photographs, including one showing a laser-inscribed brilliant. Well worth the very reasonable price. M.O'D.

The optical papers of Sir Isaac Newton. Vol 1. The optical lectures, 1670–1672

I. Newton and A. E. Shapiro (Ed.), 1984. University Press, Cambridge. pp xix, 627, hardcover. £135.00. ISBN 0 521 25248 2.

Though this book was published some time ago it is so relevant to our studies that I make no apology for bringing it to readers' notice. The original high price is down to £30.00 (in Cambridge bookshops, at least, in mid-1999) so anyone who wishes to read about the multitude of experiments conducted by Newton on the nature and production of colour, with accompanying commentary of high scholarship, should be able to secure a copy. The book presents the text of two versions of the *Optical lectures* with accompanying diagrams: the original Latin is translated and there are many illuminating notes. Cambridge University Library is the major centre of Newton scholarship and most of his MSS are housed there. M.O'D.

Royal Insignia: British and foreign orders of chivalry from the Royal Collection

S. Patterson, 1996. The Royal Collection, Windsor. pp 208, illus. in colour, softcover. £14.95.

The Royal Collection contains a wide variety of artefacts, not least among which are many classes of material of interest to the jewellery historian. Badges of British and foreign orders of knighthood and their equivalents have been exchanged between royal families for several generations and the collection, housed in the Royal Library at Windsor Castle, has not been widely publicized in the past. Fortunately escaping the fire of 1992, the insignia are beautifully illustrated in the most reasonably priced book: catalogue descriptions are authoritative and both notes and bibliography match the text in quality. The book usefully complements the recent great survey of the crown jewels and readers should try to get a copy as soon as possible, since there seem to be few about. M.O'D.

Falize: A dynasty of jewellers

K. Purcell, 1999. Thames and Hudson, London. pp 320, illus. in colour, hardcover. £55.00. ISBN 0 500 01911 8.

As the author is a director of a leading London firm which specializes in antique jewellery, 18th century gold boxes and in Fabergé items, she is almost uniquely fitted for the task of describing the history and products of the firm of Falize which began life in 1840 and continued in business until 1936. An interesting brief note on the last years of the firm is provided by Robert Falize, who well remembers the last members of the three generations of the family to work in the jewellery trade. The products of the firm attracted crowned heads and many other celebrated people at the turn of the century and the Paris shop must have been beautiful to see in those days.

The book begins with family biographies: the author has looked very carefully into them, the impetus given by a chance noting of a Falize gravestone near Fontainebleu in 1988. The works and designs of each generation are given together with their biographies and this conjunction works very well. Another most interesting section deals with sources of inspiration – the artefacts produced varied greatly in design but with all showing prodigies of ornament which make them recognizable to the connoisseur of today. Materials and techniques are described in another chapter and the book concludes with notes on writings, lectures and travels undertaken by the Falizes and with comprehensive notes to the text and bibliography.

As always, books by this publisher are excellently illustrated and we find the same high standard with this one. The small but elegant exhibition shown with the launch of the book showed the public the beauties of this particular style of jewellery and the present author has further helped to ensure the immortality of this most interesting firm. M.O'D.

Perlen & Perlmutter

J. Schlüter and C. Rätsch, 1999. Hamburg [Friedensallee 7–9, D-22765, Hamburg], pp 175, illus. in colour, hardcover. DM 19.80. ISBN 3 89234 832 4.

Forming a very attractive small book on pearl and mother-of-pearl, this study describes the formation and use of the two materials from the earliest times, the text being supplemented by well-chosen illustrations depicting the use of pearl in art as well as in ornament. Together with the historical survey are notes on the testing of pearls: gemmology students will need more than these notes provide but German readers could not do much better if they need an introduction to this beautiful material as a starter for their studies. An English version would be welcome. M.O'D.

Science in the micro-cosmos: gemstones

J. Shida, Gemmological Association of all Japan, Tokyo. pp 520, illus. in colour, hardcover, in slip case. £122.00 approx.

Described on the dust-jacket as 'volume 2', this superbly illustrated book in fact is the author's second book on gemstones, the first one dealing with inclusions. The majority of the photographs in the present book are of inclusions too, but there are some illustrations of gemstones in various fashioned states. Despite possible language difficulties it is easy for the experienced gemmologist to work out what is being shown by the photographs and for the keen photographer details of the cameras and films used are noted at the end of the book which also carries a short bibliography. Readers in the west should try to keep up with Far Eastern gem and mineral book publishing as the standard is so high. The paper used here is heavy so handle the book with respect for the binding. M.O'D.

The arts of the Sikh kingdoms

S. Strong, 1999. V & A Publications, London. pp 256, illus. in colour, softcover. £19.95 ISBN 1 85177 262 6.

A catalogue of an exhibition held at the Victoria and Albert Museum, London, during the Summer of 1999, this celebration of the 300th anniversary of the formation of the sacred Sikh brotherhood describes a variety of artefacts, some of which are set with magnificent examples of rough fashioned gemstones. Surely pride of place among these is taken by the Timur ruby (a rough red spinel) set on a necklace of gold, diamonds and spinels and lent by Her Majesty The Queen: nevertheless other examples rival it, especially another royal loan, the belt of Maharaja Sher Singh. This was made in Lahore around 1840 and is set with 19 large faceted emeralds, some of which are carved. It is possible that all or at least some of the emeralds were fashioned from the same crystal which may have come from the Urals or from the general area of Afghanistan. The book describes these items not only in captions to the excellent photographs but also in the catalogue at the end of the main text.

While a relatively small section of the whole book is devoted to gem-set pieces, the reader should carefully study the whole of the text to gain some idea of why such items were made and for whom. The development of the Sikh religion is very important for the study of civilizations in general and the decorative arts play a significant part in it. Many of the items shown come from British collections and so can be pursued after the exhibition has closed. The whole work is a study in the best traditions of national museum scholarship with many references to major sources and with a leavening of informed conjecture. M.O'D.

Gemstones: quality and value (2nd edn.)

Y. Suwa, 1999. Sekai Bunka Publishing Inc, Tokyo. pp 143, Illus. in colour, hardcover. £120.00 approx. ISBN 4 418 99902 7

The previous edition of this book appeared in Japanese with a separate supplement in English. There are two main sections: the first deals with 24 classic gemstones: in each case a 'beauty grade' is allocated and different shades of colour (or general appearance in the case of opal) are shown on a grid as photographs of fashioned stones. Details, including properties, variations and producing locations of the stones are given as well as an overall guide to values. Photographs by the well-known team of Harold and Erica Van Pelt make for a most beautiful first part and the second, dealing with the mining, fashioning and manufacturing of gem-set jewellery, is equally attractive and full of useful information which is not too easy to find quickly elsewhere. There is a short bibliography and a glossary. I strongly recommend this book which will be particularly appropriate on the counter. M.O'D.

Türkis: der Edelstein mit der Farbe des Himmels

extraLapis no 16, 1999. Christian Weise Verlag, Munich. pp 96, illus. in colour, softcover. DM 38.92. ISBN 3 921656 48 6 (series ISSN 0945 8492).

Turquoise is one of the most difficult of gemstones to illustrate adequately. So many specimens have a somewhat pale and unfeatured blue while the darker and finer examples are usually set in ways which demand the best of the photographer's ingenuity. I was keenly anticipating the appearance of this number of the beautiful *extraLapis* series so that I could experience turquoise at its best. The publishers have not disappointed (they never do!) and this study, cast like the others into a single chapterless sequence by a number of authors, will be found immediately essential to the many gemmologists and others who handle this fairly common gemstone.

The text introduces turquoise and how it occurs and then proceeds to list and briefly describe major world sources, the south-western United States, China, Persia/Iran, Sinai and Cornwall being singled out for particular attention. Handling and pricing, followed by a bibliography, complete an excellent and very reasonable priced book. *ExtraLapis* issues are even now becoming hard to find and readers should buy them as soon as they appear. M.O'D.

Proceedings of the Gemmological Association and Gem Testing Laboratory of Great Britain and Notices

MEMBERS' MEETINGS

London

On 14 July 1999 at the Gem Tutorial Centre, 27 Greville Street, London EC1N 8TN, Professor Peter R. Simpson gave a talk entitled *Demantoid garnet and other new gems and minerals from Namibia.*

On 22 September 1999 at the Gem Tutorial Centre, Ian Mercer illustrated gemmological activities in China, Hong Kong and Idar-Oberstein.

Midlands Branch

On 4 July 1999 the first of a series of practical 'Play Groups' was held at Barnt Green. The session included an enquiry into the properties and spectrum characteristics of all colours of gem garnets, including new garnets from Tanzania and colour-change varieties.

On 24 September 1999 at the Earth Sciences Building, University of Birmingham, Edgbaston, a three-fold presentation was given. Gwyn Green lead a discussion on the findings of the first Play Group session. Doug Morgan and Denis Price spoke on various facets of gem cutting.

A second Play Group was held on 26 September.

North West Branch

On 15 September at Church House, Hanover Street, Liverpool 1, John Harris gave a talk entitled *Photographing gems and their inclusions.*

Scottish Branch

A field trip was held on 4 and 5 July to Aberdeenshire, a source of tourmaline and other minerals.

On 5 August in Edinburgh, Art Grant gave a talk entitled *An apatite for faceting.*

ANNUAL GENERAL MEETING

The Annual General Meeting of the GAGTL was held on Monday 28 June 1999 at 27 Greville Street, London EC1N 8TN. Ian Thomson chaired the meeting and welcomed those present. The Annual Report and Accounts were approved and signed.

Ian Mercer, Jeffrey Monnickendam, Michael O'Donoghue and Evelyne Stern were elected, and Terry Davidson and Noel Deeks re-elected to the Council of Management. It was reported that Christopher Cavey had resigned from the Council in January 1999.

Peter Dwyer-Hickey, John Greatwood, Laurence Music, Dr Jamie Nelson and Peter Read were re-elected to the Members' Council. John Kessler and Jeffrey Monnickendam did not seek re-election to the Members' Council, and it was reported that Robert Fuller had resigned from the Council in February 1999. Hazlems Fenton were re-appointed Auditors.

The comment was made from the floor that despite repeated requests, the accounts did not contain any more detail than in previous years. Discussion followed and it was agreed that the Council of Management would consider providing additional information in the 2000 figures.

Responding to a question from the floor, Noel Deeks reported that the website had proved very popular and was attracting approximately 20,000 hits a month.

Following the Annual General Meeting, a Reunion of Members and Bring and Buy Sale were held, at which the winners of the 1999 Photographic Competition were announced and entries displayed.

ISSN: 1355–4565

GIFTS TO THE ASSOCIATION

The Association is most grateful to the following for their gifts for research and teaching purposes:

Daniel Dower of Dower & Hall, London, for four salt crystals from the Salt Lake, Tunisia.

Alex Farn, Vice President of the GAGTL, for a photograph of a 'Bombay Bunch' strung with silver wire tassels (published in *Gem & Jewellery News*, September 1999) and an envelope containing many of the silver wire tassels; two freak sectioned cultured pearsl; an X-ray of a cultured pearl necklet with interesting nuclei; the name plate from an early endoscope in mother-of-pearl; an X-ray of a single line diamond bracelet showing that the diamonds are transparent to X-rays; and an X-ray of two sections of natural pearls joined together and mounted in a ring with the join hidden by the mount.

Luc Genot, Brussels, Belgium, for his diploma thesis *Les pierres de lune bleues de Meethiyagoda.*

Martin Guptill, California, for six pieces of sunstone, two in matrix, three rough pieces and a faceted sample.

Holts of London for 211 crystals and gem materials comprising a wide range of teaching specimens.

Beverly Mitchell of the Signet Group, London for 40 bags of various fashioned gem materials including chalcedony, quartz, opal, garnet, moonstone, sapphire, emerald, ruby and zircon.

NEWS OF FELLOWS

Michael O'Donoghue arranged an exhibition *Gemstones of the 20th century* for the London Guildhall University Summer Show in June 1999. Specimens of species discovered from 1900–1999 were shown as well as examples of established gemstones found in new locations. He also gave a talk on synthetic and treated gemstones to the staff of Chanel Joaillerie, London, on 5 July 1999.

On 8 September 1999 Tony French and Michael O'Donoghue conducted a one-day course for the Wessex Branch of the National Association of Goldsmiths at Wimborne, Dorset. Gemmological techniques were explained and rehearsed, with some emphasis on synthetic and treated specimens.

GEM DIAMOND EXAMINATIONS

In June 1999, 90 candidates sat the Gem Diamond Examination, 65 of whom qualified, including two with Distinction. The Bruton Medal was not awarded on this occasion. The names of the successful candidates are listed below:

Qualified with Distinction:

Cunningham, DeeDee C., Toronto, Ont., Canada
Dong Cheng Yu, Beijing, P.R. China

Qualified

Arrowsmith-Katada, Jodie, Lower Plenty, Victoria, Australia
Barbarovich, Peter M., North Crawley, Buckinghamshire
Beattie, Rosamund C., Chiswick, London
Bhatia, Umesh K., Faridabad, Haryana, India
Bin Luo, Wuhan, Hubei, P.R. China
Burgoyne, Sheila, Totteridge, London
Chan Lai Lai Lily, Hong Kong
Chen Geng, Beijing, P.R. China
Chongjie Pan, Wuhan, Hubei, P.R. China
Cooksey, Brian D., Bures St. Mary, Suffolk
Cubbins, Graham, Blackpool, Lancashire
Dai Ru, Beijing, P.R. China
Edery, Gabrielle J., Hither Green, London
Englezos, Antonios, Lescos, Geece
Farrell, Terry, Cambridge
Finlay, Louden B., London
Furze, Cindy, Cheshunt, Hertfordshire
Ge Wang, Wuhan, Hubei, P.R. China
Hardiman, Julie, Eastleigh, Hampshire
Hering, Peter, Cambridge
Hodgson, Jane E., Watford, Hertfordshire
Huaxia Lin, Wuhan, Hubei, P.R. China
Hui Zhang, Wuhan, Hubei, P.R. China
Iconomou, Politimi, Kallithea, Athens, Greece
Kalha, Mahmoud A.M., Linstock, Carlisle
Kam Siu Tong John, Hong Kong
Konstandopoulou, Garoufallia, Athens, Greece
Koukou, Katerina, Athens, Greece
Kwok Emily Yee-Man, Hong Kong
Lam, Jill, Rochester, Kent
Lan Wang, Wuhan, Hubei, P.R. China
Liang Cai, Wuhan, Hubei, P.R. China
Liu Kai Lin, Beijing, P.R. China

Ma Guoqiang, Beijing, P.R. China
Ma Zhen, Beijing, P.R. China
Marshall, Andrew P., Gravesend, Kent
McCabe, Marianne C., London
McCarthy, Kieran, London
Mi Zhou, Wuhan, Hubei, P.R. China
Murase, Yuka, Chiba, Japan
Nakazawa, Haruyo, London
Ngala, Dabou K., Forest Gate, London
Parnell, Alexander J., Brighton, Sussex
Polette, Anne-Sophie, London
Qu Shang, Beijing, P.R. China
Saunders, Ian, Worksop, Nottinghamshire
Selant, Sabbir, Manchester
Shah, Varsheet, Kingston-upon-Thames, Surrey
Shan, Kuang, Wuhan, Hubei, P.R. China
Siyu Geng, Wuhan, Hubei, P.R. China
Smits, Cyntha, Alphen aan den Rijn, The Netherlands
Thackrah, Merle, Great Horkesley, Essex
Tupper, Michael I., South Holmwood, Surrey
Walls, Karen, New Malden, Surrey
Wenhong, Tian, Wuhan, Hubei, P.R. China
Woolland, Natalie K.A., Seaton, Devon
Worters, Fleur, Sevenoaks, Kent
Yan Zhang, Wuhan, Hubei, P.R. China
Yee Loo Andrew Shun, Hong Kong
Yu Chaofan, Beijing, P.R. China
Zhang Cheng, Beijing, P.R. China
Zhang Chufen, Guangzhou, P.R. China
Zhao Jun, Wuhan, Hubei, P.R. China

EXAMINATIONS IN GEMMOLOGY

In the Examinations in Gemmology held worldwide in June 1999, 206 candidates sat the Preliminary Examination of whom 156 qualified. In the Diploma Examination 231 sat of whom 116 qualified, including four with Distinction.

The **Anderson Bank Prize** for the best non-trade candidate of the year in the Diploma Examination was awarded to Jie Yang of Wuhan, Hubei, P.R. China.

The **Diploma Trade Prize** for the best candidate of the year who derives her main income from activities essentially connected with the jewellery trade was awarded to Miss Yurika Tachibana of Tokyo, Japan.

The **Anderson Medal** for the best candidate of the year in the Preliminary Examination was awarded to Miss Liu Jie Wen, Guilin, Guangxi, P.R. China.

The **Preliminary Trade Prize** for the best candidate of the year who derives her main income from activities essentially connected with the jewellery trade was awarded to Miss Yan Wei of Shanghai, P.R. China.

The Tully Medal was not awarded on this occasion.

The names of the successful candidates are as follows:

Diploma

Qualified with Distinction

Chan Wai Mang Eva, Montreal, Quebec, Canada
Jie Yang, Wuhan, Hubei, P.R. China
Tachibana, Yurika, Tokyo, Japan
Yan Wei, Shanghai, P.R. China

Qualifed

Adcock, Graham D., Lutterworth Leicestershire
Arrowsmith-Katada, Jodie, Lower Plenty, Victoria, Australia
Aung, Tin Lei Lei, Yangon, Myanmar
Bell-Burrow, Briony, London
Camroux-Oliver, Jessica, Edinburgh
Cheng Mu-Sen, Taipei, Taiwan, R.O. China
Chun Min-Jun, Seoul, Korea
Clouder, Carol, Southampton, Hampshire
Daniel, Eliena, London
Dapergolas, Stavroula, Toronto, Ontario, Canada
de Vries, Marius L., London
Dines, Rachel S., London
Domercq, Sandrine, London
Dower, Dan, London
Englezos, Antonios, Lescos, Greece
Flynn, Matthew, Amersham, Buckinghamshire
Freakley, Sharon A.M., Bangkok, Thailand
Fris, Arnold, Goedereede, The Netherlands
Fujiwara, Yuka, Kobe Hyogo, Japan
Galdeano, Nerea, Basauri-Bizkaia, Spain
Haden, Claire L., Birmingham, West Midlands
Haiyu Wen, Wuhan, Hubei, P.R. China
Harrison, Tarn J., Leamington Spa, Warwickshire
Hengyi Zheng, Wuhan, Hubei, P.R. China
Hill, Stephen E., Rickmansworth, Hertfordshire
Hsu Hui May, Taipei, Taiwan, R.O. China
Hu Yiqing, Shenzhen, P.R. China
Huaxia Lin, Wuhan, Hubei, P.R. China
Isacsson, Johanna, Stockholm, Sweden
Jamal-Jetha, Nimet, Dollard des Ormeaux, Quebec, Canada
Jingshi Wu, Wuhan, Hubei, P.R. China
Jinsenji, Osamu, Saitama Pref., Japan
Kamil, Ruzwain, Colombo, Sri Lanka
Kataoka, Satomi, Osaka, Japan
Kerger, Michele L., Sutton Coldfield, West Midlands
Keung Lam Ho, Hong Kong

Koukou, Katerina, Athens, Greece
Lam King Nam, Hong Kong
Lan Jiang, Wuhan, Hubei, P.R. China
Lee, Seung-Jun, Taegu, Korea
Lee, Martin, South Croydon, Surrey
Lewinsohn, Lisa, Sharpthorne, Sussex
Li Yat Choi Johnson, Hong Kong
Liang-Chin Wu, Taipei, Taiwan, R.O. China
Lin Chung-Jung, Taipei, Taiwan, R.O. China
Lin Wanxia, Guilin, P.R. China
Liu Jie Wen, Guilin, P.R. China
Liu Kaixin, Shenzen, P.R. China
Lopez Perez, Jose M., Valencia, Spain
Lu Jeng-Ven, Taipei, Taiwan, R.O. China
McFarlin, Patrick M., Amarillo, Texas, U.S.A.
McKeown, Nicola, Plymouth, Devon
Morton, Heather D., Vancouver, BC, Canada
Murase, Yuka, Chiba, Japan
Osborne-Shaw, Lisa, London
Oya, Kenichi, Niigata City, Niigata Pref., Japan
Parikh, Purnima, Vancouver, BC, Canada
Perez-Dorao, Carlos, Bilbao-Bizkaia, Spain
Petropoulos, Andreas, Athens, Greece
Qin Bin, Guilin, P.R. China
Raniga, Dhanesh G., Vancouver, BC, Canada
Rythen, Carolina, Stockholm, Sweden
Sakai, Junko, Otsu City, Shiga Pref., Japan
Saminpanya, Seriwat, Singapore
San-San Chen, Taipei, Taiwan, R.O. China
Schepers, Reinhold M., Limbricht, The Netherlands
Scholtes, Wanda, Schagk, The Netherlands
Shah, Monica, Manchester
Shahdadpuri, Neeta D., Hong Kong
Sherman, Gregory E., New York, NY, U.S.A.
Sietsma, Talke, Breda, The Netherlands
Smith, Peggy E.J., Rochester, Kent
Soe Moe Naing, Yangon, Myanmar
Sopers, Margarita B.M., Den Haag, The Netherlands

FORTHCOMING EVENTS

31 October	**London.** Annual Conference: *New Developments in the Gem World.* The Barbican Centre, London
3 November	**Scottish Branch.** *New gemstones from East Africa.* Campbell Bridges
17 November	**North West Branch.** AGM followed by talks on diamonds and simulants
26 November	**Midlands Branch.** *The Crown Jewels.* Alan Jobbins
4 December	**Midlands Branch.** 47th Annual Dinner
8 December	**London.** *Jewellery and silverware today.* Chris Walton
28 January	**Midlands Branch.** Bring and Buy followed by a quiz
30 January	**Midlands Branch.** Gem Play Group
15 February	**London.** *Some sites of precious minerals in England.* Dr R.F. Symes
25 February	**Midlands Branch.** *Gem trails from the Orient to Germany.* Ian Mercer
27 February	**Midlands Branch.** Gem Play Group
15 March	**London.** *Chalcedony – 21st century girl's best friend.* Stephen Webster
31 March	**Midlands Branch.** *All that glisters is not gold.* Dr Rob Ixer

For further information on the above events contact:

London:	Mary Burland on 020 7404 3334
Midlands Branch:	Gwyn Green on 0121 445 5359
North West Branch:	Deanna Brady on 0151 648 4266
Scottish Branch:	Catriona McInnes on 0131 667 2199

GAGTL WEB SITE

For up-to-the-minute information on GAGTL events visit our web site on www.gagtl.ac.uk/gagtl

Speake, Malcolm F., Birmingham, West Midlands
Stewart, Michelle, Stourport-on-Severn, Worcestershire
Susitha, Pothmulla, Kankanamge, Colombo, Sri Lanka
Tamaki, Yosuke, Sakurai City, Nara Pref., Japan
Tanaka, Nariko, Tokyo, Japan
Tang Yu-Lung, Taipei, Taiwan, R.O. China
Tang Tak Chuen, Hong Kong
Tezapsidou, Eleni K., Thessaloniki, Greece
Thomas, Allyson R., Harborne, West Midlands
Tianyang Zhang, Wuhan, Hubei, P.R. China
Tsutsumi, Masao, Higashi-Hiroshima City, Hiroshima Pref., Japan
van der Have, Ciska A., Amsterdam, The Netherlands
Van Spaendonck, Anouk D., Oegstgeest, The Netherlands
Vanderburgh, Amy E., Nobleton, Ontario, Canada
Vidoni, Tanya M., Toronto, Ontario, Canada
Wang Yan-Ping, Shanghai, P.R. China
Wang Dongmei, Shanghai, P.R. China
Wangchun Liao, Wuhan, Hubei, P.R. China
Ward-Jones, Ann, London
Warren, C., Donald, Weston, Ontario, Canada
Warrington, Jennifer L., Auckland, New Zealand
Waterfall, Mary C., Ely, Cambridgeshire
Wen Jiang, Wuhan, Hubei, P.R. China
Westbury, Vikki L.H., Woking, Surrey
Wheeler, Nick, Sudbury, Suffolk
Xiaoling Huang, Wuhan, Hubei, P.R. China
Xinping Li, Wuhan, Hubei, P.R. China
Xueqian Cheng, Wuhan, Hubei, P.R. China
Yang Hui-Ning, Taipei, Taiwan, R.O. China
Yi Zhou, Wuhan, Hubei, P.R. China
Yili You, Wuhan, Hubei, P.R. China
Zaw, Thiha, Yangon, Myanmar
Zhang Chunyan, Shanghai, P.R. China
Zhou Weiqi, Shantou, P.R. China
Zhu Jian-Qing, Shanghai, P.R. China
Zhuang Yilin, Shantou, P.R. China
Zimmermann, Bettina E., Zunzgen, Switzerland
Zin Win Mon, Yangon, Myanmar

Preliminary Examination

Qualified

Abdulrazzaq, Anwar A.H., Myharraq, Bahrain
Ahari, Roshanak, Tehran, Iran
Al-Alawi, Abeer S.T., Manama, Bahrain
Alcenius, Jim, Espoo, Finland
Ascot, Leon, Urdorf, Switzerland
Bakker, Jeroen, Apeldoorn, The Netherlands
Balzan, Cortney, Fairfax, Calif., U.S.A.
Bashore, Kerri A., Hayes End, Middlesex
Basile, Appadoure, London
Bass, Adrienne K., Preston, Lancashire
Bergmann, Eleanor, London
Blairs, Lawrence I.J., Llanrwst, Conwy, North Wales
Blomquist, Eva, Jonkoping, Sweden
Boardman, Adrian, Warrington, Cheshire
Bonac, Lia, Stechford, West Midlands
Bonnet, Christian, La Chaux-de-Fonds, Switzerland
Brown, Mary J., Mayangone Township, Myanmar
Burton, Mark Greig, London
Chan Ying Fong Bianca, Hong Kong
Chan, Rebecca, Hong Kong
Chan Wai Mang Eva, Montreal, Quebec, Canada
Chang Keng Ti, Taichung, Taiwan, R.O. China
Checkley, Emma, Hockley, West Midlands
Chen Hsi Hung, Taichung, Taiwan, R.O. China
Cheng Sze Man, Hong Kong
Cheng Kin-Nor Anne, Hong Kong
Cheng Po Lam, Hong Kong
Cheung Lai Yee Joey, Hong Kong
Choksi, Shivang R., Gujarat, India
Chow Suet Lai, Hong Kong
Chung Ju Ching, Taichung, Taiwan, R.O. China
Cubbins, Graham, Blackpool, Lancashire
Delpachitra, Samadara, Kandy, Sri Lanka
Deng, Luyang, Shanghai, P.R. China
Diyaljee, Dalida I., Berbice, Guyana
Dowling, Siobhan L., London
Dunn-Lwin, Simon B., London
Dupuy, Harold A., Los Angeles, Calif., U.S.A.
Eensaar, Karin, Tallinn, Estonia
Fu Sheng, Shanghai, P.R. China
Fujita, Takashi, Osaka City, Osaka, Japan
Galdeano, Nerea, Basauri-Bizkaia, Spain
Gravier, Denis M., St. Jean le Vieux, France
Gray, Christopher, Glasgow
Gschwend, Heinz, Rorschach, Switzerland
Gunston, Rosa M., London
Haddow, Jane E., Hockley, West Midlands
Hagen, Bente, Oslo, Norway
Haider, Hamayou Yousafzai, Islamabad, Pakistan
Hashimoto, Megumi, Kyoto City, Kyoto, Japan
Hirano, Kiyomi, Kawanishi City, Hyogo Pref., Japan
Ho Wing Hung, Anthony, Hong Kong
Ho, Anna, Hong Kong
Ho See Wai, Celia, Hong Kong
Ho Siu Kei, Paulie, Hong Kong
Ho Sau Wa, Hong Kong
Ho Sau Lan, Hong Kong
Ho Wing Cheung, Hong Kong
Hoksbergen, Edward C., Schoonhoven, The Netherlands
Holgate, Martin R., Doncaster, Yorks
Holt, Jason B.A., London
Htay Than Than, Yangon, Myanmar
Hui Po Lung, Hong Kong
Hung Tin Man, Hong Kong
Hynes, Lola A., London

Jamal-Jethra, Nimet, Dollard des Ormeaux, Quebec, Canada
Julkunen, Maarit, Savukoski, Sweden
Kassotakis, Dimitris, Xaidari, Greece
Kauppinen, Minna K., Varkaus, Finland
Kause, Nora M., Tampere, Finland
Khan, Mariyam Z., London
Klingspor, Pontus A., Oslo, Norway
Knight, Jennifer J., Selby, N. Yorks
Kong Bei, Guilin, P.R. China
Kumagai, Hiromi, Sendai City, Miyogi Pref., Japan
Ladak, Nelina, London
Lam Chi Hing, Hong Kong
Lam Chuk Yi, Winnie, Hong Kong
Langton, Ronnie, Blackpool, Lancashire
Lauttanen, Tero T., Helsinki, Finland
Lee Ching, Hong Kong
Leung Kin On, Hong Kong
Leung Shun Lok, Hong Kong
Leverington, Michael C., Bexhill-on-Sea, Sussex
Lichtsteiner, Patrick, Ormalingen, Switzerland
Lin Yeong Leh, Taipei, Taiwan, R.O. China
Liu Jie Wen, Guilin, Guangxi, P.R. China
Liu Jun, Shanghai, P.R. China
Liu Kwok Kwan, Hong Kong
Lo Chau Heung, Hong Kong
Loxton, Sam C., London
McAuley, Mary, Harmondsworth, Middlesex
Matos, Maria, Ericeira, Portugal
Maulave, Xavier R.L., Yangon, Myanmar
Min Zin, Yangon, Myanmar
Mitch, Alexandra, Atlanta, Georgia, U.S.A.
Momosaki, Nobuko, Hirikata City, Osaka, Japan
Morris, Julie, Tadcaster, N. Yorks
Murai, Shinobu, Minamikawachi Gun, Osaka, Japan
Nakazaki, Tomoko, Higashikurume City, Tokyo, Japan
Nassar, Shareen, Nairobi, Kenya
Ndirangu, Joseph K., Hong Kong
Ng Wing Yee, Rachel, Hong Kong
Odugleh, Ahmed, London
Oksanen, Tarja K., Helsinki, Finland
Pace, Michael, Elk Grove, Calif., U.S.A.
Pala, Sunil, Coventry, West Midlands
Pan Dejuan, Guangzhou, P.R. China
Phillips, Andrew T., Penang, West Malaysia
Poon Sau Man, Hong Kong
Poon Pik Wan, Sandy, Hong Kong
Qu Han, Guilin, P.R. China
Roberts, Jennifer L., York

Rweyemamu, Edward J., London
Sakajo, Hiroko, Yao City, Osaka, Japan
Salmela, Riikka J., Vantaa, Finland
Schafroth, Thomas, Bern, Switzerland
Seitanidis, Nikolaos, Katerini, Greece
Shah, Sarju M., Nairobi, Kenya
Shahdadpuri, Neeta D., Hong Kong
Shi Yinghong, Shanghai, P.R. China
Shin Min-A., Seoul, Korea
Sidiropoyloy, Maria-Theresa, Thessaloniki, Greece
Sin Ling Karen Lam, Hong Kong
Sin Yee Chow, Hong Kong
Smith, Wendy, London
Stamatakis, Zoe, Athens, Greece
Strachan, Melanie E., Glasgow
Takayama, Rie, Kyoto City, Kyoto, Japan
Tang Chi Wai, Hong Kong
Terrell, Celia-Jane W., Atherstone, Warwickshire
Thompson, Mary T., Stockport, Cheshire
Thurston, Louise J., Doncaster, Yorkshire
To Yuen Shan, Naomi, Hong Kong
To Lai Ha, Flora, Hong Kong
Tsang, Judy, Hong Kong
Tsoha, Theodore, Volos, Greece
Tuckwell, Alice E., Newcastle-under-Lyme, Staffordshire
Uhlin, Christophe R., Leystonstone, London
Verganelakis, Vassilis, Athens, Greece
Wang Xuan, Guilin, P.R. China
Ward, Joanna K., Leicester
Whelan, Craig R., Liverpool, Lancashire
Williams, Johanna L.M., London
Williams, Lorraine, London
Win Zaw, Stanmore, Middlesex
Win Win Khaing, Yangon, Myanmar
Winter, Nicola K., London
Wong Kwok Man, Hong Kong
Wong Kuen Kuen, Hong Kong
Wong, Sandy, Hong Kong
Woolland, Natalie K.A., Seaton, Devon
Yeung Chin Pang, Hong Kong
Yan Wei, Shanghai, P.R. China.
Yeung Ling Ling, Hong Kong
Zhang Chunyan, Xiamen, P.R. China

MEMBERSHIP

The following have been elected to membership during the period June to September 1999:

Fellowship and Diamond Membership (FGA DGA)

Shaikh, Leela, Hendon, London. 1978, 1985

Fellowship (FGA)

Adcock, Graham D., Lutterworth, Leicestershire. 1999
Bagri, Abhishek, Bombay, India. 1999
Haden, Claire L., Halesowen, West Midlands. 1999
Harrison, Tarn J., Leamington Spa, Warwickshire. 1999
Hsiao Chin-Kang, Taipei, Taiwan, R.O. China. 1998
Inoue, Yoshie, Tokyo, Japan. 1983
Jamal-Jetha, Nimet, Dollard des Ormeaux, Quebec, Canada. 1999
Lin Yi Hwa, Yangon, Myanmar. 1999
McFarlin, Patrick M., Amarillo, Texas, U.S.A. 1999
Parikka, Pekka J., Helsinki, Finland. 1989
Shah, Monica, Cheadle, Cheshire. 1999
Sherman, Gregory E., New York, NY, USA. 1999
Smith, Perry E.J., Rochester, Kent. 1999
Stewart, Michelle, Stourport-on-Severn, Worcestershire. 1999
Thomas, Allyson, Birmingham, West Midlands. 1999
Townsend, Rachel E., Kingsland, Herefordshire. 1999
Triossi, Amanda, London. 1988
Tun, Win Myint, Yangon, Myanmar. 1992
Westbury, Vikki L.H., Woking, Surrey. 1999

Diamond Membership (DGA)

Furze, Cindy J., Cheshunt, Hertfordshire. 1999
Saunders, Ian R., Worksop, Nottinghamshire. 1999
Selant, Sabbir, Preston, Lancashire. 1999
Walls, Karen L., New Malden, Surrey. 1999

Ordinary Membership

Agarwal, Anubhav, Lucknow, India
Anderson, Meredith, Chertsey, Surrey
Ayukawa, Yasuyo, London
Blachier, Helene M.A., Ponsonnas, France
Bolissian, Inge, London
Bosi, Martin, Edinburgh
Bruce-Lockhart, Simon D., London
Chatt, Julian P., Glastonbury, Somerset
Coan, Michael, Yonkers, New York, U.S.A.
Cohen, Vanessa, Conte Carlo, Monaco
Collins, Gabrielle, Radlett, Hertfordshire
Comar, Ankush, Bushey, Hertfordshire
Cooke, Caroline M., St. Margarets, Middlesex
Douglas, Christianne E.M., London
Everington, Therese, Lincoln
Gandusio, Susanna, Paradiso, Switzerland
Garcia-Monzón, Patricia, Madrid, Spain
Giurgiu-Cairney, Anda, Acton, London.
Gomez de Kondserovsky, Alexandre, Creteil, France
Gondwe, Magoli M., Chelsea, London
Graham, Roderick S., London
Greslin-Michel, Valerie, London
Hamano, Yumi, London
Hammond, Ian, Muir of Ord, Scotland
Harrison, Robert, Miami, Florida, U.S.A.
Harvey, Kirsty L., Witney, Oxfordshire

Hatton, Paul M., London
Ito, Eiko, New Southgate, London
Jang, Yunsil, Staines, Middlesex
Jo, Midori, Ikoma shi Nara, Japan
Joyner, Louise, London
Katz, Joslynne F., Edgware, Middlesex
King, Kumi, London
Kote, Satomi, London
Langdale, Jason, Southampton, Hampshire
Maisey, Anthony P., Croydon, Surrey
Morton, Aude A., London
Nakagawa, Eriko, Putney, London
Nyirenda, Arnold S., Cricklewood, London
Osman, A. Noorani, Mount Lavinia, Sri Lanka
Pattni, Dilip, Belmont, Surrey
Pennington, Susan E., Bickerstaffe, Lancs.
Perez, Sergio, Egham, Surrey
Pratt, Jonathan J., Guildford, Surrey
Resnick, Theodore, San Antonio, Texas, U.S.A.
Rila, Mohamed Lafir, Galle, Sri Lanka
Roberts, Jennifer L., York
Rose, Annette, London
Sanai, Sayceda A., Hyderabad, India
Saxon, Michael B., Chardon, Ohio, U.S.A.
Sperry, Lynn, London
Squires, Caroline, Tring, Hertfordshire
Sun, I-Ching Tracey, Harrow, Middlesex
Thompson, Mary T., Offerton, Stockport, Cheshire
Ward, Joanna, Leicester
Williams, Lorraine A., London
Yue, Louisa, Bushey, Hertfordshire
Zancanella, Raffaele, Cavalese, Italy
Zin Win Mon, Yangon, Myanmar

Laboratory Membership

Development and Promotion Comercial Center of Parana/Brasil for Golf Arabian and Middle East, Brasilia, Brazil.
Emdico (London) Ltd., London EC1N 8AN
Jon Gems Ltd., London EC1N 8AT
Nabil Mouzannar FGA, London EC1N 8NX
Tel Aviv Jewellers Ltd, London EC1N 8BQ

Transfers

The following members, having qualified in the 1999 Gemmology and/or Gem Diamond Examinations, have been transferred to Fellowship and Diamond Membership as appropriate:

Ordinary Membership to Fellowship (FGA)

Domercq, Sandrine, London
Dower, Daniel G., London
Freakley, Sharon, A.M., Bangkok, Thailand
Fujiwara, Yuka, Kobe Hyogo, Japan
Jinsenji, Osamu, Toda City, Saitama Pref., Japan
Kamil, Mohammed R., Colombo, Sri Lanka
Kataoka, Satomi, Osaka City, Osaka, Japan
Oya, Kenichi, Niigata City, Niigata Pref., Japan
Rythen, L.A. Carolina, Stockholm, Sweden
Sakai, Junko, Otsu City, Shiga Pref., Japan
Saminpanya, Seriwat, Manchester
San-San Chen, Taipei, Taiwan, R.O. China.
Shahdadpuri, Neeta D., London
Speake, Malcolm F., Ladywood, Birmingham
Tachibana, Yurika, Tokyo, Japan
Tamaki, Yosuke, Sakurai City, Nara Pref., Japan
Tanaka, Nariko, Tachikawa City, Tokyo, Japan
Tsutsumi, Masao, Higashi-Hiroshima City, Hiroshima Pref., Japan
Ward-Jones, Ann, London
Waterfall, Mary C., Ely, Cambridgeshire
Wheeler, Nick, Sudbury, Suffolk
Zin Win Mon, Yangon, Myanmar

Ordinary Membership to Fellowship and Diamond Membership (FGA, DGA)

Arrowsmith, Jodie, Kyoto City, Japan
Englezos, Antonios, Lescos, Greece
Koukou, Katerina, Athens, Greece
Murase, Yuka, Chiba, Japan

Ordinary Membership to Diamond Membership (DGA)

Farrell, Terry, Cambridge, Cambridgeshire
Hardiman, Julie C., Eastleigh, Hampshire
Kalha, Mahmoud A.M., Linstock, Carlisle
Thackrah, Merle, Great Horkesley, Essex
Woolland, Natalie K.A., Seaton, Devon

Diamond Membership to Diamond Membership and Fellowship (FGA, DGA)

Bell-Burrow, Briony, London
Daniel, Eliena, London
de Vries, Marius, London
Flynn, Matthew, Amersham, Buckinghamshire
Galdeano, Nerea, Basauri-Bizkaia, Spain
Lee, Martin, South Croydon, Surrey
Liang-Chin Wu, Tainan, Taiwan, R.O.China.
Perez-Dorao, Carlos, Bilbao-Bizkaia, Spain

Fellowship to Fellowship and Diamond Membership (FGA, DGA)

Burgoyne, Sheila, Totteridge, London
Cooksey, Brian D., Bures St. Mary, Suffolk
Cunningham, DeeDee, Toronto, Ontario, Canada
Edery, Gabrielle, Hither Green, London
Finlay, Louden B., London
Hering, Peter J., Cambridge, Cambridgeshire
Hodgson, Jane E., Watford, Hertfordshire
Kam Siu Tong John, Hong Kong
Konstandopoulou, Garoufallia, Athens, Greece

Letter to the Editor

From Susan Stocklmayer, FGA

Dear Sir

Chrome chalcedony

It is generally recognized that the first modern discovery of chrome chalcedony was from Zimbabwe (Rhodesia). As a former mineralogist for the Geological Survey of Zimbabwe, I read with interest the recent article by Dr Jaroslav Hyrsl in the April 1999 volume of the *Journal*. However, it was disappointing to note that Dr Hyrsl, in quoting the date of the discovery as 1955, has propagated an error first introduced in 1989 by Philips and Brown (*Australian Gemmologist*, **17**, 205–7).

To set the record straight the discovery of chrome chalcedony ('mtorolite'), as reported in three articles published in the *Chamber of Mines Journal* of Rhodesia in 1967, is attributed to a Mr M.J. Maclean in 1965. One of these articles written by C.C. Smith (former Curator of Geology, Bulawayo Museum) also contains comments by Dr Gübelin and provides a full gemmological description of the material including spectrographic analyses.

Whilst it may be difficult to access original articles published in somewhat obscure journals, I could supply copies of the three mentioned for anyone interested.

Yours etc.
Susan M. Stocklmayer
Lesmurdie, Perth, WA 6076, Australia

Lam, Jill, Rochester, Kent
Marshall, Andrew P., Gravesend, Kent
McCabe, Marianne C., London
McCarthy, Kieran, London
Nakazawa, Haruyo, London
Shah, Varsheet, Kingston, Surrey
Smits, Cyntha A.N., Alphen a/d Ryn, The Netherlands
Tupper, Michael I., South Holmwood, Surrey

SUBSCRIPTIONS 2000

The following are the membership subscription rates for 2000. Existing Fellows, Diamond Members and Ordinary Members will be entitled to a £5.00 discount for subscriptions paid before 31 January 2000.

	Fellows, Diamond Members and Ordinary Members	*Laboratory Members*
UK	£59.00	£250.00 plus VAT
Europe	£64.00	£250.00
Overseas	£74.00	£250.00

ISLAND OF GEMS

For the fourth successive year, the *Island of Gems* exhibition is to be held in London. The exhibition, on the gems and gem industry of Sri Lanka, is to be held on 13 and 14 November at the Resource Centre, 356 Holloway Road, London N7 6PA. There will be displays and demonstrations on the geology of Sri Lanka, gem mining, gem cutting and polishing, gemstones and education.

The entrance fee, which includes a free gemstone and a souvenir brochure, is £3.00 for adults and £1.50 for children under 12 and OAPs.

For further information contact D.H. Ariyaratna on 020 8514 8250 or visit the website at www.lankagems.freeserve.co.uk.

GEMMOLOGICAL ASSOCIATION AND GEM TESTING LABORATORY OF GREAT BRITAIN


F.M. JEWELLERY

The Journal of
Gemmology

Current issue £12.00
(including postage UK and Europe
Overseas: £15.70 to include airmail postage)

Back issues

Back issues may be purchased as follows:

Vol. 25 and 26 – £10.00 per issue
Up to and including Vol. 24 – £4.00 per issue

Members of the GAGTL are eligible for a 10% discount

A proforma invoice including postage and packing will be issued on receipt of orders.

*Subject to availability

For details of issues in print and an order form contact
Mary Burland at the GAGTL
27 Greville Street, London EC1N 8TN
Tel: 020 7404 3334   Fax: 020 7404 8843
e-mail: gagtl@btinternet.com

Museums, Educational Establishments, Collectors & Students

I have what is probably the largest range of genuinely rare stones in the UK, from Analcime to Wulfenite. Also rare and modern synthetics, and inexpensive crystals and stones for students. New computerised lists available with even more detail. Please send £2 in 1st class stamps refundable on first order (overseas free).

Two special offers for students:
New Teach/Buy service and free stones on an order.

A.J. French, FGA
82 Brookley Road, Brockenhurst,
Hants SO42 7RA
Telephone: 01590 623214

Pearls
Gemstones

Lapidary Equipment

GENOT L
Since 1953

CH. De Wavre, 850
B-1040 Bxl – Belgium

Tel : 32-2-647.38.16
Fax : 32-2-648.20.26
E-mail : gama@skynet.be

www.gemline.org
www.geofana.net

PROMPT LAPIDARY SERVICE!

Gemstones and diamonds cut to your specification and repaired on our premises.
Large selection of gemstones including rare items and mineral specimens in stock.
Valuations and gem testing carried out.
Mail order service available.

R. HOLT & CO. LTD

98 Hatton Garden, London EC1N 8NX
Telephone 020-7405 0197/5286
Fax 020-7430 1279

Guide to the preparation of typescripts for publication in *The Journal of Gemmology*

The Editor is glad to consider original articles shedding new light on subjects of gemmological interest for publication in *The Journal*. Articles are not normally accepted which have already been published elsewhere in English, and an article is accepted only on the understanding that (1) full information as to any previous publication (whether in English or another language) has been given, (2) it is not under consideration for publication elsewhere and (3) it will not be published elsewhere without the consent of the Editor.

Typescripts Two copies of all papers should be submitted on A4 paper (or USA equivalent) to the Editor. Typescripts should be double spaced with margins of at least 25 mm. They should be set out in the manner of recent issues of *The Journal* and in conformity with the information set out below. Papers may be of any length, but long papers of more than 10 000 words (unless capable of division into parts or of exceptional importance) are unlikely to be acceptable, whereas a short paper of 400–500 words may achieve early publication.

The abstract, references, notes, captions and tables should be typed double spaced on separate sheets.

On matters of style and rendering, please consult *The Oxford dictionary for writers and editors* (Oxford University Press, 1981).

Title page The title should be as brief as is consistent with clear indication of the content of the paper. It should be followed by the names (with initials) of the authors and by their addresses.

Abstract A short abstract of 50-100 words is required.

Key Words Up to six key words indicating the subject matter of the article should be supplied.

Headings In all headings only the first letter and proper names are capitalized.

A **This is a first level heading**

First level headings are in bold and are flush left on a separate line. The first text line following is flush left.

B *This is a second level heading*

Second level headings are in italics and are flush left on a separate line. The first text line following is flush left.

Illustrations Either transparencies or photographs of good quality can be submitted for both coloured and black-and-white illustrations. It is recommended that authors retain copies of all illustrations because of the risk of loss or damage either during the printing process or in transit.

Diagrams must be of a professional quality and prepared in dense black ink on a good quality surface. Original illustrations will not be returned unless specifically requested.

All illustrations (maps, diagrams and pictures) are numbered consecutively with Arabic numerals and labelled Figure 1, Figure 2, etc. All illustrations are referred to as 'Figures'.

Tables Must be typed double spaced, using few horizontal rules and no vertical rules. They are numbered consecutively with Roman numerals (Table IV, etc.). Titles should be concise, but as independently informative as possible. The approximate position of the Table in the text should be marked in the margin of the typescript.

Notes and References Authors may choose one of two systems:

(1) The Harvard system in which authors' names (no initials) and dates (and specific pages, only in the case of quotations) are given in the main body of the text, e.g. (Gübelin and Koivula, 1986, 29). References are listed alphabetically at the end of the paper under the heading References.

(2) The system in which superscript numbers are inserted in the text (e.g. ... to which Gübelin refers.^{3}) and referred to in numerical order at the end of the paper under the heading Notes. Informational notes must be restricted to the minimum; usually the material can be incorporated in the text. If absolutely necessary both systems may be used.

References in both systems should be set out as follows, with *double spacing* for all lines.

Papers Hurwit, K., 1991. Gem Trade Lab notes. *Gems & Gemology*, **27**, 2, 110–11

Books Hughes, R.W., 1990. *Corundum*. Butterworth-Heinemann, London. p. 162

Abbreviations for titles of periodicals are those sanctioned by the *World List of scientific periodicals* 4th edn. The place of publication should always be given when books are referred to.

Volume 26 No. 8 October 1999

Contents

The Journal of Gemmology

Cover Picture

Vacuum and heating equipment used to harden porous rocks and to fill fractures in emeralds (see 'Identification of filler substances in emeralds by infrared and Raman spectroscopy' pp.501–520)

Registered Office: Palladium House, 1–4 Argyll Street, London W1V 2LD

ISSN: 1355–4565

Designed & Printed by Quadrant Offset Limited, Hertford, England

Volume 26 Numbers 1–8 1998–1999

The Journal of Gemmology

VOLUME 26
NUMBERS 1–8
1998–1999
INDEX

THE GEMMOLOGICAL ASSOCIATION AND GEM
TESTING LABORATORY OF GREAT BRITAIN

The Journal of
Gemmology

VOLUME 26
NUMBERS 1–8 1998–1999

CONTENTS

[No. 1, January 1998]

[No. 2, April 1998]

[No. 3, July 1998]

[No. 4, October 1998]

[No. 5, January 1999]

[No. 6, April 1999]

[No. 7, July 1999]

[No. 8, October 1999]

INDEX

Compiled by Robin W. Sanderson

Alphabetical arrangement is letter-by-letter.
Names of authors are printed in capitals, pages of abstracts and book reviews in italics.

Special usages:
above and *below* in cross-references indicate that the reference is to another subheading under the same heading, not a separate heading.
A number in brackets following a page number indicates that there is more than one reference to the subject on the page.

Registered Office: Palladium House, 1–4 Argyll Street, London W1V 2LD

ISSN: 1355-4565

Produced and printed by Stephen Austin & Sons Ltd, Hertford, England